

Faculty of Engineering and Materials Sciences
German University in Cairo



Field-Oriented Control of Permanent Magnet Synchronous Motors

A thesis submitted in partial fulfilment of the University's
requirements for the degree of Bachelor of Science (B.Sc.) in
Mechatronics Engineering

Author: Nabil H. Hassan

Supervisor: Assoc Prof.Dr.Walid Hafez Omran

June 2024

Declaration

This is to certify that:

- (i) the thesis comprises only my original work toward the Bachelor of Science (B.Sc.) at the German University in Cairo (GUC),
- (ii) due acknowledgement has been made in the text to all other material used

Nabil H. Hassan
19 May, 2024

Acknowledgement

I hereby realize the praise and grace of Allah, the almighty god; his mercy paved the path to complete this thesis. I am eternally thankful to all of the people with whom I have had the pleasure to work during this thesis and other related projects. I would like to express my sincere gratitude to my supervisor, Prof. Dr. Walid Hafez Omran, for his patience, motivation, continuous support, and guidance during my research. In addition to my advisor, I thank M.Sc. Eng. Mahmoud Hamdy Abdelaziz for his tireless commitment and guidance throughout the whole research. Special thanks to my friend Amr Wael Mahgoub for his help throughout the semester. I am also deeply grateful to my friends Mina Domadous , Ahmed Daw, Mohamed Gamal,Abdullah Rashad and Mohamed EL-Salahawy, whose companionship and support have been invaluable. Their understanding, patience, and encouragement have helped me persevere through the challenges of this thesis. Their friendship has been a source of strength and joy, and I am thankful for the countless ways they have contributed to my personal and academic growth. In addition, I express my heartfelt gratitude to my family, especially my father, Geologist Hesham Rashad., for his continuous support and encouragement, and to my mother for her endless love and support. A special thanks to my older brother, Eng. Mohamed H. Hassan for his support and help. His encouragement have been crucial in the completion of this work.

Abstract

This thesis explores the field-oriented control (FOC) of permanent magnet synchronous motors (PMSMs) for electric vehicles, encompassing theoretical principles and practical applications. Beginning with meticulous modeling of PMSMs in the ABC frame, the study transitions to transforming these models into the dq frame using reference frame theory, simplifying motor control, and enhancing efficiency.

Various tuning methods for PI controllers are investigated, ranging from manual tuning to systematic approaches such as symmetric and magnitude optimum methods. Through rigorous analysis, their effectiveness in achieving the desired motor performance is evaluated.

Modulation techniques, including sinusoidal pulse width modulation (SPWM) and space vector pulse width modulation (SVPWM), are compared to analyze their impact on motor performance, focusing on total harmonic distortion (THD) and DC voltage utilization.

Extensive simulations using MATLAB/SIMULINK validate theoretical models and control strategies, providing a comprehensive evaluation of different modulation techniques and PI controller tuning methods across various operating conditions.

Results highlight the superiority of SVPWM over SPWM in harmonic performance and voltage utilization. Moreover, systematic tuning methods for PI controllers demonstrate performance comparable to manual tuning, offering valuable insights for enhancing PMSM efficiency and reliability in electric vehicle applications.

Contents

1 INTRODUCTION	1
1.1 Motivation	4
1.2 Aims and Objectives	4
1.3 Summary	4
2 LITERATURE REVIEW	5
2.1 Permanent Magnet Synchronous Motor	5
2.1.1 History of Permanent Magnet Synchronous Motors (PMSMs)	5
2.1.2 Rise of PMSMs in Electric Vehicles (EVs)	5
2.2 Field Oriented Control (FOC)	6
2.3 Power Electronics and Inverter	7
2.4 Modulation Techniques	8
2.5 FOC Applications	9
3 PERMANENT MAGNET SYNCHRONOUS MOTOR	10
3.1 Permanent Magnet Synchronous Motor	10
3.2 Structure of PMSM Stator	10
3.3 Structure of PMSM Rotor	11
3.3.1 Surface Mount PMSM (SM-PMSM)	12
3.3.2 Surface-Inset PMSM (SIPM)	13
3.3.3 Interior PMSM (IPMSM)	14
3.4 Theory of Operation	15
3.4.1 Rotating Magnetic Field of a three phase motor	15
3.4.2 Starting of Synchronous Motor	18
4 MATHEMATICAL MODELING OF PMSM	20
4.1 Mathematical Derivation of Electrical and Mechanical equations in "abc" stationary Frame	21
4.1.1 Electrical equations of PMSM	21
4.1.2 Mechanical Equations of PMSM	25
4.2 Reference Frame Theory	26
4.2.1 Clarke's Transformation	26
4.2.2 Rotational Park's Transformation	28
4.3 Mathematical Derivation of Electrical equations in "dq" coordinate Frame	30

4.3.1	" $\alpha\beta\theta$ " Coordinate Frame Model of Permanent Magnet Synchronous Motor	31
4.3.2	" dq " Coordinate Frame Model of Permanent Magnet Synchronous Motor	34
5	FIELD-ORIENTED CONTROL AND INVERTERS	38
5.1	Derivation of FOC	39
5.1.1	Electromagnetic Torque	41
5.1.2	Mutual Flux Linkages	43
5.1.3	Key Results	43
5.2	Control Strategies	44
5.2.1	$i_d = 0$ Control Strategy	44
5.2.2	Maximum Torque Per Ampere Control (MTPA)	45
5.2.3	Flux-Weakening Control	47
5.3	PI Controllers	50
5.3.1	The Current Controller	51
5.3.2	The Speed Controller	52
5.3.3	Controllers Design	53
5.4	Inverters and Modulation Techniques	59
5.4.1	Inverters	59
5.4.2	Modulation Techniques	65
6	SIMULATIONS AND RESULTS	78
6.1	Open-loop Response	78
6.1.1	No Load Torque Response	79
6.1.2	With Load Torque Response	79
6.2	Closed-loop Response with FOC	82
6.2.1	FOC Using Ideal Converter	82
6.2.2	FOC Using Inverter	94
6.2.3	MTPA and Flux Weakening	108
7	Conclusion and Future Work	113
7.1	Conclusion	113
7.2	Future Work	113
Appendices		118
A	SIMULINK Models	119
B	MATLAB Codes	128

List of Tables

6.1	Parameters of SM-PMSM	79
6.2	Current Controllers parameters	82
6.3	Speed Controllers parameters	82
6.4	Parameters of IPMSM	109

List of Figures

1.1	Electric Vehicle System	1
1.2	PMSM of an EV	2
1.3	Basic Structure of PMSM	2
1.4	Basic FOC Diagram	3
3.1	PMSM simplified structure	11
3.2	PMSM exploded diagram	12
3.3	SM-PMSM Structure	13
3.4	SIPM Structure	13
3.5	IPMSM Structure	14
3.6	Winding arrangement of a three-phase two-pole induction motor. .	15
3.7	The current waveforms in the stator windings of a three-phase motor.	16
3.8	RMF direction at different positions	16
3.9	MMF Distribution by phase as current in the four-pole motor.	17
3.10	Starting of synchronous motor by auxiliary motor diagram	19
3.11	A squirrel-cage damper winding.	19
4.1	The per-phase equivalent circuit of synchronous motor	21
4.2	Self-inductance of phase as winding with respect to rotor positions.	24
4.3	mutual-inductance between the phase as and bs stator windings. .	24
4.4	Clarke Transformation	27
4.5	Clarke's Transformation demonstration in SIMULINK	28
4.6	Park's Transformation	29
4.7	Rotational Park's Transformation from $\alpha\beta$ frame to dq frame in SIMULINK	29
4.8	The three reference frames	30
4.9	Equivalent Circuits in dq-frame	37
5.1	Phasor Diagram of PMSM. [16]	41
5.2	Torque graph of PMSM. [11]	42
5.3	Space vector diagram of $i_d = 0$ control. [9]	44
5.4	FOC Block diagram of $i_d = 0$ control. [20]	45
5.5	MTPA operating points and the constant torque loci in the current plane. [9]	45
5.6	Locus of the constant torque in the current vector plane [9]	46
5.7	FOC Block diagram of MTPA control strategy [4]	47
5.8	Schematic diagram of voltage and current boundary [9]	48

5.9	Block diagram of the voltage closed-loop flux-weakening scheme[9]	49
5.10	Block diagram of the voltage closed-loop flux-weakening control and MTPA control[9]	49
5.11	Block diagram of the PI controller[31]	50
5.12	Dynamic Cross-Axis Decoupling Control[1]	52
5.13	Bode plot of closed current controller loop	56
5.14	Step response of the closed loop function	57
5.15	Bode plot of closed Speed controller loop	58
5.16	Full-wave single-phase inverter [16]	60
5.17	IGBT symbol [16]	60
5.18	Three phase inverter [16]	61
5.19	120° conduction mode Line to Neutral Voltage and Line to Line voltage [1]	62
5.20	120° conduction mode Line to Neutral Voltage	63
5.21	120° conduction mode line to line Voltage	63
5.22	180° conduction mode Line to Neutral Voltage and Line to Line voltage [1]	64
5.23	180° conduction mode where T1, T6 and T2 are ON and the rest are OFF	64
5.24	180° conduction mode Line to Neutral Voltage	65
5.25	180° conduction mode line to line Voltage	65
5.26	Square Wave Modulation.[7]	66
5.27	Sinusoidal PWM technique.[14]	67
5.28	Voltage modulation range for SPWM.[14]	68
5.29	SPWM technique for a three-phase inverter.[14]	68
5.30	Over-modulation in the SPWM technique.[14]	69
5.31	Principle of THIPWM.[14]	70
5.32	Output voltage vectors in the complex plane (or dq axes stationary frame).[14]	71
5.33	Rotation of voltage vector.[14]	72
5.34	Modulation process for voltage generation.[14]	73
5.35	Possible range of the reference vector voltage in the SVPWM.[14]	74
5.36	Switching sequence.[14]	74
5.37	Alternate switching sequence.[14]	75
5.38	Switching sequences in six sectors.[14]	75
5.39	Voltages for equivalent SVPWM by using the offset voltage ($MI=0.9$).[14]	76
5.40	Modulation waveforms of popular Discontinuous PWM methods.[21]	77
6.1	Open-loop response of simscape machine with no load torque	80
6.2	Open-loop response of Modeled machine based on equations with no load torque	80
6.3	Open-loop response of simscape machine with load torque	81
6.4	Open-loop response of Modeled machine based on equations with load torque	81
6.5	Step response of speed with Manual tuning and Optimum criterion	83
6.6	The response of torque with Manual tuning and Optimum criterion	83

6.7	The currents I_{dq}	84
6.8	The currents I_{abc}	84
6.9	Step response of speed with Manual tuning and Optimum criterion	85
6.10	The response of torque with Manual tuning and Optimum criterion	85
6.11	The currents I_{dq}	86
6.12	The currents I_{abc}	86
6.13	Step response of speed	88
6.14	The response of torque	88
6.15	The currents I_{dq}	89
6.16	The currents I_{abc}	89
6.17	Step response of speed With Varying speed and Load Torque	90
6.18	The response of torque With Varying speed and Load Torque	90
6.19	The currents I_{dq} With Varying speed and Load Torque	91
6.20	The currents I_{abc} With Varying speed and Load Torque	91
6.21	The Speed With Varying speed and Load Torque	92
6.22	The torque With Varying speed and Load Torque	93
6.23	The I_{dq} currents With Varying speed and Load Torque	93
6.24	One of the sixth pulse signals generated from SPWM modulation	94
6.25	Speed and torque responses using SPWM with no load	95
6.26	The three phase currents I_{abc} responses using SPWM with no load	95
6.27	The Line to Line voltage V_{ab} produced from the inverter	96
6.28	Speed and torque responses using SPWM with load torque of 30 N.m	97
6.29	The three phase currents I_{abc} responses using SPWM with load torque of 30 N.m	97
6.30	The I_{dq} responses using SPWM with load torque of 30 N.m	98
6.31	The I_{abc} responses using SPWM with varying speed and load torque	98
6.32	Speed and torque responses using SPWM with varying speed and load torque	99
6.33	The I_{dq} responses using SPWM with varying speed and load torque	99
6.34	The line-to-line voltages V_{ab} using SVPWM	100
6.35	The modulating signal generated from SVPWM associated with phase A	101
6.36	Speed and torque responses using SVPWM with load torque of 30 N.m	101
6.37	The three phase currents I_{abc} responses using SVPWM with load torque of 30 N.m	102
6.38	The I_{dq} responses using SVPWM with load torque of 30 N.m	102
6.39	Speed and torque responses using SVPWM with varying speed and load torque	103
6.40	The three phase currents I_{abc} responses using SVPWM with varying speed and load torque	104
6.41	The I_{dq} responses using SVPWM with varying speed and load torque	104
6.42	The speed and torque responses	105
6.43	The I_{dq} currents	106
6.44	The FFT analysis of the current waveforms	107
6.45	The FFT analysis of the voltage waveforms	107
6.46	The FFT analysis of the voltage waveforms	108

6.47 The speed and torque response	109
6.48 The speed and torque response	110
6.49 The I_{dq} currents	110
6.50 The I_{abc} currents	111
6.51 The speed and torque response	111
6.52 The I_{dq} currents	112
A.1 Open-loop response of Modeled machine based on equations with load torque	119
A.2 PMSM Dynamic Model in SIMULINK	120
A.3 PMSM Mechanical System	120
A.4 PMSM Mechanical Equation	121
A.5 PMSM Electrical Equations	121
A.6 I_d Equation	122
A.7 I_q Equation	122
A.8 Torque Equation	123
A.9 Cross-axes Dynamic Decoupling Control	123
A.10 FOC comparison of the manual tuning and Optimum Criteria methods	124
A.11 FOC with SPWM modulation technique and Inverter	125
A.12 FOC with SVPWM modulation technique and Inverter	126
A.13 FOC with SVPWM	127

List of Symbols

The next list describes several symbols that will be later used within the body of the document

- Δv_d^* The change in voltage associated with d arbitrary axis.
- Δv_q^* The change in voltage associated with q arbitrary axis.
- δ The torque angle.
- γ An arbitrary angle of "dq" coordinate frame.
- λ_a The flux linkage associated with phase a.
- λ_b The flux linkage associated with phase b.
- λ_c The flux linkage associated with phase c.
- λ_m The flux established flux on the stator winding by the permanent magnet.
- Λ_0 The flux linkage associated with 0arbitrary axis.
- $\Lambda_{\alpha\beta 0}$ The flux linkage associated with $\alpha\beta 0$ arbitrary reference frame.
- Λ_α The flux linkage associated with α arbitrary axis.
- Λ_β The flux linkage associated with β arbitrary axis.
- Λ_{abc} The flux linkage associated with three phases abc.
- Λ_{dq} The flux linkage associated with the "dq" arbitrary reference frame.
- Λ_d The flux linkage associated with d arbitrary axis.
- $\Lambda_{m\alpha\beta 0}$ The flux established flux on the stator winding by the permanent magnet associated with the $\alpha\beta 0$ arbitrary reference frame.
- $\Lambda_{m\alpha\beta}$ The flux established flux on the stator winding by the permanent magnet associated with the $\alpha\beta$ arbitrary axes.
- Λ_{mabc} The flux established flux on the stator winding by the permanent magnet associated with the three phases abc.

- λ_{ma} The flux established flux on the stator winding by the permanent magnet associated with phase a.
- λ_{mb} The flux established flux on the stator winding by the permanent magnet associated with phase b.
- λ_{mc} The flux established flux on the stator winding by the permanent magnet associated with phase c.
- Λ_q The flux linkage associated with q arbitrary axis.
- μ_0 The is the permeability of air.
- Ω The normalized frequency.
- ω The angular frequency of the system in rad/sec.
- ω_r^* The reference or desired rotor angular speed.
- ω_0 The arbitrary angular speed associated with the "dq" arbitrary reference frame.
- ω_e The electrical angular frequency of the system.
- ω_m The mechanical angular frequency of the system.
- Ω_n The natural frequency of the system.
- ω_r The rotor angular speed.
- $\Omega_{B\phi}$ The normalized bandwidth.
- ϕ The phase angle between voltage and stator current phasor.
- Φ_a The instantaneous flux at a given time t associated with phase a.
- Φ_b The instantaneous flux at a given time t associated with phase b.
- Φ_c The instantaneous flux at a given time t associated with phase c.
- Φ_m The maximum or peak flux.
- Φ_r The resultant flux.
- ϕ_r The phase margin.
- \mathbf{C} The Clarke's transformation matrix.
- \mathbf{C}^{-1} The inverse Clarke's transformation matrix.
- \mathbf{Q} The rotational Park's transformation matrix.
- \mathbf{Q}^{-1} The inverse rotational Park's transformation matrix.

θ	The angular position.
θ_e	The electrical angle of the system.
θ_m	The mechanical angle of the system.
ζ	The damping coefficient of the system.
A	The cross-sectional area of solenoid coil.
B	The viscous friction (or damping) coefficient.
D_g	The inner diameter of the stator winding.
f	The frequency of the system in Hz.
f_a	An arbitrary variable associated with phase a.
f_b	An arbitrary variable associated with phase b.
$f_{\alpha\beta 0}$	An arbitrary three-phase variable in " $\alpha\beta 0$ " reference frame.
$f_{\alpha\beta}$	An arbitrary three-phase variable in " $\alpha\beta$ " reference frame.
f_α	An arbitrary variable associated with α -axis.
f_β	An arbitrary variable associated with β -axis.
f_{abc}	An arbitrary three-phase variable in " abc " reference frame.
$f_{B\phi}$	The bandwidth frequency.
f_{dq}	An arbitrary three phase variable in " dq " reference frame.
$G_C(s)$	The transfer function of the PI controller.
$G_{ci}(s)$	The current controller transfer function.
$G_s(s)$	The transfer function of a system plant.
i_d^*	The reference current associated with d arbitrary axis.
i_q^*	The reference current variable associated with q arbitrary axis.
i_a	The current associated with phase a.
i_b	The current associated with phase b.
i_c	The current associated with phase c.
i_f	The flux component current.
I_m	The magnitude of the maximum or peak current.
i_s	The resultant current vector in the " dq " reference frame.

i_T	The torque component current.
i_0	The current variable in the 0 arbitrary $\alpha\beta0$ arbitrary reference frame.
$i_{\alpha\beta0}$	The three phase current associated with $\alpha\beta0$ arbitrary reference frame.
i_α	The current associated with α arbitrary axis.
i_β	The current variable associated with β arbitrary axis.
i_{abc}	The three-phase current associated with phases abc.
i_{dq}	The current associated with the "dq" arbitrary reference frame.
i_d	The current associated with d arbitrary axis.
i_q	The current associated with q arbitrary axis.
I_{smax}	The maximum current.
J	The inertia of the rotor.
K_i	The integral gain.
K_n	The normalized gain.
K_p	The proportional gain.
K_s	The reciprocal of stator resistance constant.
L_A	The average value of the magnetizing inductance.
L_B	The variation in value of the magnetizing inductance.
l_g	The axial length of one solenoid coil in the phase winding.
L_s	The self-inductance of the stator winding.
$L_{\alpha\beta0}$	The self inductance of the stator winding associated with the $\alpha\beta0$ arbitrary reference frame.
L_{aa}	The self-inductance of the stator winding associated with phase a.
L_{Ad}	The average value of the magnetizing inductance associated with d arbitrary axis.
L_{Aq}	The average value of the magnetizing inductance associated with q arbitrary axis.
L_{bb}	The self-inductance of the stator winding associated with phase b.
L_{cc}	The self-inductance of the stator winding associated with phase c.
L_d	The self-inductance associated with d arbitrary axis.

L_{ls}	The leakage inductance.
L_q	The self-inductance associated with q arbitrary axis.
$L_{s\alpha\beta 0}$	The constant self inductance matrix of the stator winding associated with the $\alpha\beta 0$ arbitrary reference frame.
M_{ab}	The Mutual inductance of the stator winding associated with phase a and phase b.
M_{ac}	The Mutual inductance of the stator winding associated with phase a and phase c.
M_{ba}	The Mutual inductance of the stator winding associated with phase b and phase a.
M_{bc}	The Mutual inductance of the stator winding associated with phase b and phase c.
M_{ca}	The Mutual inductance of the stator winding associated with phase c and phase a.
M_{cb}	The Mutual inductance of the stator winding associated with phase c and phase b.
MI	The Modulation Index.
N_s	The synchronous speed in rpm.
N_T	The total number of turns in a phase winding.
P	Number of poles of the motor.
r_a	The stator resistance associated with phase a.
r_b	The stator resistance associated with phase b.
r_c	The stator resistance associated with phase c.
R_s	The stator resistance matrix.
r_s	The stator resistance in each phase.
t	time.
T_e^*	The reference or desired electromagnetic torque.
T_0	The switching time associated with the zero vector in a sector.
T_1	The switching time associated with the first vector in a sector.
T_2	The switching time associated with the second vector in a sector.
T_e	The developed electromagnetic torque.

T_i	The integral time constant.
T_L	The load torque.
T_s	Total switching time.
$T_{\sigma I}$	The total delay time constants of the inner control loop.
T_{cs}	The stator time constant.
U_{smax}	The maximum voltage.
v^*	The Voltage reference vector.
v_d^*	The reference voltage associated with d arbitrary axis.
v_q^*	The reference voltage variable associated with q arbitrary axis.
v_d^f	The initial voltage level associated with d arbitrary axis.
v_q^f	The initial voltage level variable associated with q arbitrary axis.
v_a	The voltage associated with phase a.
v_b	The voltage associated with phase b.
v_c	The voltage associated with phase c.
$v_{\alpha\beta 0}$	The three phase voltage associated with $\alpha\beta 0$ arbitrary reference frame.
v_α	The voltage associated with α arbitrary axis.
v_β	The voltage variable associated with β arbitrary axis.
v_{abc}	The three-phase voltage associated with phases abc.
v_{ab}	The line to line voltage associated with phase a and phase b.
v_{an}	The line to neutral voltage associated with phase a.
v_{bc}	The line to line voltage associated with phase b and phase c.
v_{bn}	The line to neutral voltage associated with phase b.
v_{carr}	The Triangular Carrier voltage.
v_{ca}	The line to line voltage associated with phase c and phase a.
v_{cn}	The line to neutral voltage associated with phase c.
v_{dc}	The DC-link voltage
v_{dq}	The voltage associated with the "dq" arbitrary reference frame.
v_d	The voltage associated with d arbitrary axis.

- v_{LL} The line-to-line voltage.
- v_{ph} The phase voltage.
- v_q The voltage variable associated with q arbitrary axis.
- v_{ref} The Voltage reference or modulating wave.
- W_c The co-energy of the system.
- W_m The energy stored in the permanent magnet.
- $W_{CL}(s)$ The closed loop transfer function of a system.
- $W_{OL}(s)$ The open loop transfer function of a system.
- Z The Impedance.

Chapter 1

INTRODUCTION

At the core of electric vehicles lies the motor drive system, a key technology that shapes their performance and reliability. Early electric vehicles primarily relied on DC motors because of their simplicity and mature technology. However, advancements in controllers, power electronics and AC speed regulation have paved the way for more advanced alternatives, including AC induction motors, permanent magnet motors, and switched reluctance motors.

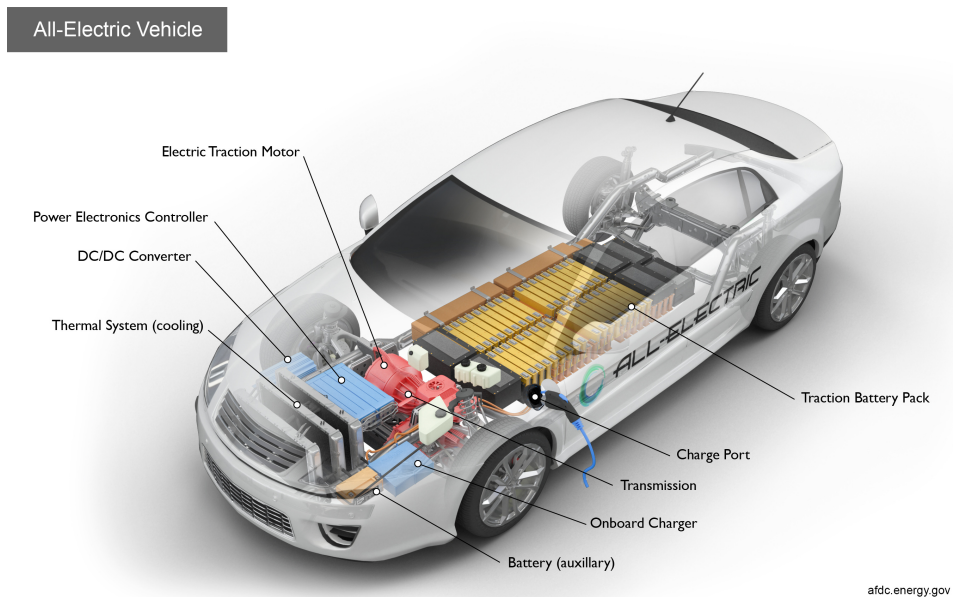


Figure 1.1: Electric Vehicle System

The development of Permanent Magnet Synchronous Motors (PMSM) was revolutionised in the 1980s with the development of third-generation permanent magnetic materials, which was a huge breakthrough. These materials changed the design and capabilities of PMSM, making them more competitive in the electric motor market. They are notable for their high remanence, coercive energy, and cost-effectiveness. Today, PMSMs are preferred for their uncomplicated layout, small size, low weight, excellent power factor, and consistent performance.[\[17\]](#)

PMSMs have found widespread use in both industrial and household settings, thanks to their impressive features such as high power density, efficiency, power factor, and precise control capabilities. This versatility has made them a top choice in various sectors. Furthermore, PMSMs are well known for their simple design, small size, lightweight build, and consistent performance. The Permanent Magnet



Figure 1.2: PMSM of an EV

Synchronous Motor (PMSM) operates on the principle of three-phase alternating current (AC) supply. This three-phase system involves three sets of windings or coils spaced 120 degrees apart around the motor's stator. Each winding set is energized by a separate phase of the AC power supply, creating a rotating magnetic field within the motor. This rotating magnetic field interacts with the permanent magnets embedded in the rotor, causing the rotor to turn synchronously with the rotating magnetic field. The synchronization occurs because the permanent magnets in the rotor are attracted to the rotating magnetic field produced by the stator windings.

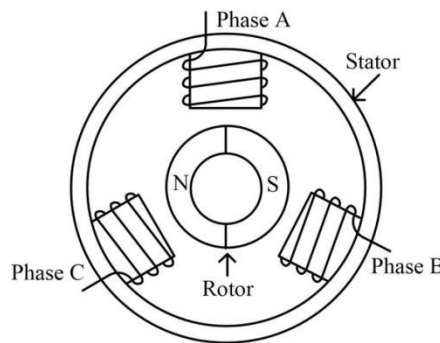


Figure 1.3: Basic Structure of PMSM

Employing advanced control techniques like field-oriented vector control and direct torque control, PMSMs deliver speed control and dynamic characteristics similar to separately excited DC machines. Additionally, their well-designed permanent magnetic circuit structure allows for superior field-weakening performance, enhancing their suitability for electric vehicle applications. Ultimately, PMSMs emerge as the optimal propulsion motor for electric vehicles and hybrid electric vehicles, promising a sustainable future for transportation.

Field-oriented control (FOC) for PMSM Also known as vector control, FOC provides better efficiency at higher speeds. It also guarantees optimized efficiency even during transient operation by perfectly maintaining the stator and rotor fluxes. FOC also gives better performance on dynamic load changes when compared to all other techniques. Similar to induction machines, PMSMs can be operated in field oriented control (FOC), allowing for a decoupling of the torque and flux producing stator current components. As a result, the d-current component of the stator current can be considered as the flux producing component, while the q-component is torque producing. In the base speed region, this d-component is usually set to zero to minimize stator losses and inverter current ratings. In the flux weakening region of PMSMs, a negative d-component is necessary to reduce the field in the machine.

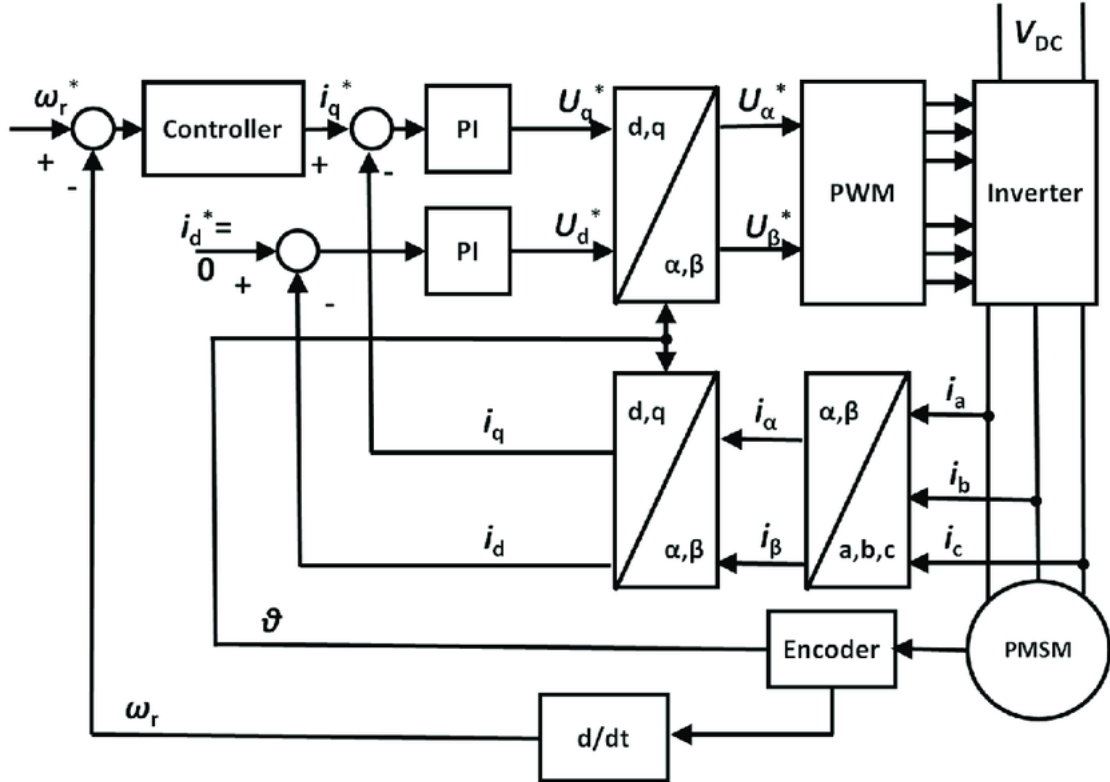


Figure 1.4: Basic FOC Diagram

1.1 Motivation

The rise of electric vehicles (EVs) has marked a significant shift towards sustainable transportation, driven by the imperative to mitigate environmental degradation and reduce dependence on fossil fuels. Within the realm of electric vehicle propulsion systems, permanent magnet synchronous motors (PMSMs) play a crucial role due to their high efficiency, power density, and precise control capabilities. Field-Oriented Control (FOC) emerges as a pivotal technique for optimizing the performance of PMSMs in EVs, offering enhanced efficiency, torque control, and dynamic response. As the automotive industry increasingly embraces electrification, the optimization of FOC for PMSMs presents a compelling avenue for advancing the efficiency, range, and overall performance of EVs. This thesis seeks to explore and analyze the implementation of FOC in PMSMs for EV applications, aiming to contribute to the advancement of sustainable transportation technologies.

1.2 Aims and Objectives

The objective of this research is to control the speed of PMSM using field-oriented control (FOC). The FOC algorithm needs two PI controllers to regulate both I_q and I_d and another one to regulate speed. The PMSM, Inverter, Space Vector Modulation, Current controllers, and Speed controllers are all modeled and simulated using MATLAB/SIMULINK software.

1.3 Summary

This research investigates the optimization of Field-Oriented Control (FOC) for Permanent Magnet Synchronous Motors (PMSMs) utilized in Electric Vehicles (EVs). Acknowledging the urgency of sustainable transportation solutions, the research emphasizes the significant role of PMSMs in EV propulsion systems due to their inherent efficiency and precise control capabilities. FOC is rising as a key technique for maximizing the performance of PMSMs in EVs, offering advantages such as enhanced efficiency, torque control, and dynamic response. Through thorough analysis and experimentation, the study aims to advance EV technology by improving the efficiency, range, and overall performance of PMSM-based propulsion systems through FOC.

Chapter 2

LITERATURE REVIEW

2.1 Permanent Magnet Synchronous Motor

2.1.1 History of Permanent Magnet Synchronous Motors (PMSMs)

Permanent Magnet Synchronous Motors (PMSMs) have evolved significantly since their first invention in the twentieth century. Initially, in the 1950s and 1960s, the development of high-energy permanent magnets such as Alnico was a key milestone. These magnets made it possible to create motors that were more efficient and performed better than ordinary induction motors. However, the promise of PMSMs was not completely realised due to restricted developments in power electronics and control approaches at the time.[\[16\]](#)

The 1970s and 1980s saw the development of rare-earth magnets, particularly neodymium-iron-boron (NdFeB) magnets, which provided even higher magnetic flux densities. This advancement significantly enhanced the torque and power density of PMSMs, making them more suitable for high-performance applications. Concurrently, developments in semiconductor technology facilitated the creation of more sophisticated and efficient power electronics, enabling precise control of PMSMs.

2.1.2 Rise of PMSMs in Electric Vehicles (EVs)

The automotive industry's pursuit of more efficient, reliable, and environmentally friendly propulsion systems led to the increased adoption of PMSMs in electric vehicles (EVs). The advantages of PMSMs, such as high power density, efficiency, and superior torque characteristics, align well with the requirements of EVs.[\[5\]](#)

The early 2000s marked a turning point for PMSMs in EVs, driven by the global emphasis on reducing greenhouse gas emissions and dependence on fossil fuels. Automakers began investing heavily in electric propulsion technologies, with PMSMs emerging as a preferred choice due to their superior performance metrics. Key milestones include the development of hybrid vehicles like the Toyota Prius, which utilized PMSM technology to achieve better fuel efficiency and lower emissions.

In the 2010s, the growth of the EV and hybrid EV market accelerated, with major manufacturers like Tesla, Porsche, Nissan, and BMW incorporating PMSMs in

their electric drivetrains. Tesla's Model 3, showcased the capabilities of PMSMs, delivering high performance and long-range capabilities that were previously unattainable with other motor types .

Research and development efforts continue to enhance PMSM technology, focusing on improving magnetic materials, reducing production costs, and developing advanced control strategies to further optimize motor performance. Innovations such as the integration of field-oriented control (FOC) techniques and sophisticated modulation methods have been pivotal in maximizing the efficiency and dynamic response of PMSMs in EV applications.[15]

2.2 Field Oriented Control (FOC)

Field-Oriented Control (FOC) is a control methodology used in motor drives to precisely control the torque and speed of Permanent Magnet Synchronous Motors (PMSMs). It achieves this by decomposing the stator current into two components: the torque-producing component (direct axis current) and the magnetizing component (quadrature axis current). By independently controlling these components, FOC ensures optimal motor performance across a wide range of operating conditions.[16] Field-Oriented Control (FOC) extends back to the late 1960s and early 1970s, when Werner Leonhard pioneered the concept. Leonhard's major work established the theoretical foundation for FOC by establishing the notion of decoupling torque and flux control in AC motor drives. FOC was initially created to improve the performance of DC motors, but it soon gained popularity as a strong control method for AC motors due to its ability to establish exact control of motor speed and torque.

[2] represents a significant milestone in the historical development of Field-Oriented Control (FOC). In this paper, [2] introduces the concept of field orientation and its application in closed-loop control systems for rotating-field machines. By proposing the "transvector" closed-loop control system, Blaschke lays the groundwork for modern FOC techniques, which enable precise control of torque and flux components in AC motor drives.

The advent of powerful digital signal processors (DSPs) and microcontrollers in the late 20th century enabled the practical implementation of FOC in real-world motor drive systems. Researchers and engineers developed sophisticated control algorithms and real-time processing capabilities, further enhancing the efficacy of FOC in controlling Permanent Magnet Synchronous Motors (PMSMs) and other AC motor types.[33] The adoption of digital control also facilitated the integration of advanced features such as sensorless control, adaptive control, and fault detection, further enhancing the performance and reliability of FOC systems. Real-time processing capabilities allowed for adaptive tuning of control parameters based on changing operating conditions, ensuring optimal performance across a wide range of scenarios.[16] and [3]. Moreover, advancements in power electronics, such as insulated gate bipolar transistors (IGBTs) and silicon carbide (SiC) devices, com-

plemented the digital control revolution by enabling faster switching speeds and higher power density. This, in turn, improved the responsiveness and efficiency of motor drive systems employing FOC.[28]

Field-Oriented Control (FOC) is implemented using two fundamental approaches: direct and indirect techniques. Direct FOC converts stator currents directly into a rotating reference frame, which simplifies the control method. In contrast, indirect FOC begins by determining the rotor flux position and speed before translating the stator currents into the rotor reference frame. A comprehensive comparison of these methods, including their advantages and limitations, can be found in reference.[16] Proportional-Integral (PI) and Proportional-Integral-Derivative (PID) controllers are widely employed in FOC systems to regulate motor currents and maintain optimum torque and speed levels. These controllers are simple and sturdy, and they operate well in a wide range of applications. [8] Model Predictive Control (MPC) is an advanced control strategy that has gained popularity in recent years for its ability to optimize system performance by considering future predictions of the system behavior. In FOC applications, MPC techniques are used to generate control actions based on a predictive model of the motor and load dynamics.[33] The first implementation of Model Predictive Control (MPC) in Field-Oriented Control (FOC) of motors can be attributed to [19]. Another advanced control strategy like sliding mode control (SMC) is discussed in [12].

2.3 Power Electronics and Inverter

The evolution of power electronics and inverters traces back to the early 20th century when researchers began exploring semiconductor devices and their potential applications in electrical systems. One of the foundational milestones in this journey was the development of the silicon-controlled rectifier (SCR) in the 1950s by General Electric. The SCR laid the groundwork for controlled rectification, enabling the efficient conversion of alternating current (AC) to direct current (DC) and vice versa.[28]

During the 1960s and 1970s, advancements in semiconductor technology led to the introduction of new power devices such as the power diode, power transistor, and insulated-gate bipolar transistor (IGBT). These devices revolutionized power electronics by offering higher efficiency, faster switching speeds, and improved reliability. Additionally, the emergence of pulse-width modulation (PWM) techniques during this period enabled precise control of voltage and current waveforms, paving the way for more efficient and flexible power conversion systems.[28],[33]

In the late 20th century, the focus shifted towards the development of inverters for renewable energy applications, particularly in solar and wind power systems. The demand for grid-connected inverters capable of converting DC power from solar panels or wind turbines into AC power compatible with the utility grid surged. This led to significant research and development efforts aimed at improving the efficiency, reliability, and grid integration capabilities of inverters.

The early 21st century witnessed the rapid growth of power electronics in vari-

ous sectors, including electric vehicles (EVs), industrial automation, and renewable energy. In the EV sector, inverters play a crucial role in converting DC power from the battery into AC power to drive the electric motor. The quest for higher power density, efficiency, and thermal management in EV inverters drove innovation in semiconductor materials, cooling technologies, and control algorithms.[3]

Looking ahead, the future of power electronics and inverters is poised for further advancements driven by emerging technologies in semiconductors (e.g., silicon carbide and gallium nitride), advanced packaging techniques, and machine learning algorithms for predictive maintenance and fault detection. These developments promise to unlock new opportunities for efficient, resilient, and sustainable energy conversion systems, shaping the landscape of power electronics for decades to come.[29],[13]

2.4 Modulation Techniques

Modulation techniques play a crucial role in the control of motor drives, especially in Field-Oriented Control (FOC) systems. These techniques are employed to generate the switching signals for the power electronics devices in the inverter, thereby controlling the output voltage waveform applied to the motor. In the literature, various modulation techniques have been studied and applied in motor drive systems to achieve optimal performance and efficiency.[16] ,[14].

Sinusoidal Pulse Width Modulation (SPWM) is one of the most widely used modulation techniques in FOC systems. It involves modulating the width of pulses in the inverter output waveform to approximate a sinusoidal voltage waveform. SPWM is known for its simplicity and ease of implementation, making it suitable for a wide range of motor drive applications [3],[28].

Space Vector Pulse Width Modulation (SVPWM) is an advanced modulation technique that offers superior performance compared to SPWM. SVPWM operates by generating voltage vectors in a rotating reference frame and synthesizing them to achieve the desired output voltage waveform. This technique allows for higher voltage utilization and improved harmonic performance, resulting in smoother motor operation and reduced losses [16].

Carrier-Based Pulse Width Modulation (CBPWM) strategies, such as the Carrier-Based Sinusoidal PWM (CS-PWM) and Carrier-Based Space Vector PWM (CSVPWM), are commonly used in FOC systems. These techniques involve comparing the reference voltage signal with a carrier waveform to generate the PWM signals for the inverter switches. CBPWM strategies offer simplicity and flexibility in implementation, making them suitable for real-time control applications [14].

Selective Harmonic Elimination (SHE) techniques aim to minimize harmonic distortion in the output voltage waveform by selectively eliminating specific harmonics. This is achieved by solving a set of nonlinear equations to determine the

optimal switching angles that cancel out targeted harmonics. SHE techniques are particularly useful in applications where low harmonic distortion is critical, such as in grid-connected systems and sensitive loads [22].

2.5 FOC Applications

Field-Oriented Control (FOC) has found widespread applications in various real-world scenarios, particularly in the control of Permanent Magnet Synchronous Motors (PMSMs). One prominent application is in electric vehicle propulsion systems, where FOC ensures precise control of motor torque and speed, leading to improved vehicle performance and efficiency [15]. Additionally, FOC plays a crucial role in renewable energy generation systems, such as wind turbines and hydroelectric generators. By accurately controlling the speed and torque of PMSMs, FOC enables efficient energy conversion and optimal power generation from renewable sources [10].

In industrial automation and robotics, FOC is utilized to achieve high-precision motion control used in servo drives in various manufacturing processes and robotic applications. By seamlessly regulating motor speed and torque, FOC enhances the overall efficiency and productivity of industrial systems, while also ensuring smooth and accurate operation [8]. Furthermore, FOC has made significant strides in aerospace and marine propulsion systems, where it enables precise control of motor performance in challenging operating environments. Whether in aircraft propulsion or marine propulsion systems, FOC ensures reliable and efficient motor operation, contributing to overall system performance and safety [33]. (FOC) has found widespread applications in various real-world scenarios, particularly in the control of Permanent Magnet Synchronous Motors (PMSMs), which is integral to electric vehicles (EVs) and hybrid electric vehicles (HEVs). In the automotive industry, FOC ensures precise control of motor torque and speed, leading to improved vehicle performance and efficiency [16],[5]. Electric vehicles rely on FOC to regulate the speed and torque of the motor, thereby providing smooth acceleration and deceleration, as well as efficient energy conversion during regenerative braking. Similarly, hybrid electric vehicles employ FOC to seamlessly transition between the internal combustion engine and electric motor, optimizing fuel efficiency and reducing emissions [8].

Chapter 3

PERMANENT MAGNET SYNCHRONOUS MOTOR

3.1 Permanent Magnet Synchronous Motor

In the 1950s, dc machines with PM field excitation were developed thanks to the availability of new-generation PM with a significant energy density. Compact DC machines were produced when PMs were introduced to replace electromagnetic poles with windings that needed an electric energy supply source. Similarly, in synchronous machines, the PM poles in the rotor replace the conventional electromagnetic field poles, cutting out the need for the brush assembly and slip rings.[\[16\]](#) This allows for accurate torque and speed control, making PMSMs suitable for various applications like electric vehicles, industrial automation, and renewable energy applications.

3.2 Structure of PMSM Stator

The stator of a Permanent Magnet Synchronous Motor (PMSM) is a crucial component that plays a significant role in the motor's operation. It typically consists of a laminated iron core, stator windings, and a stator housing. The laminated iron core provides mechanical support and serves as a path for magnetic flux. The stator windings, arranged in a three-phase configuration, are coils of insulated wire wound around the stator core as shown in 3.1. These windings produce a rotating magnetic field that interacts with the rotor's permanent magnets. The stator housing encloses and protects the stator components, ensuring the motor's integrity. The design and construction of the stator, including factors such as the number of stator slots, winding arrangement, and choice of materials, significantly impact the PMSM's efficiency, torque production, and overall performance.

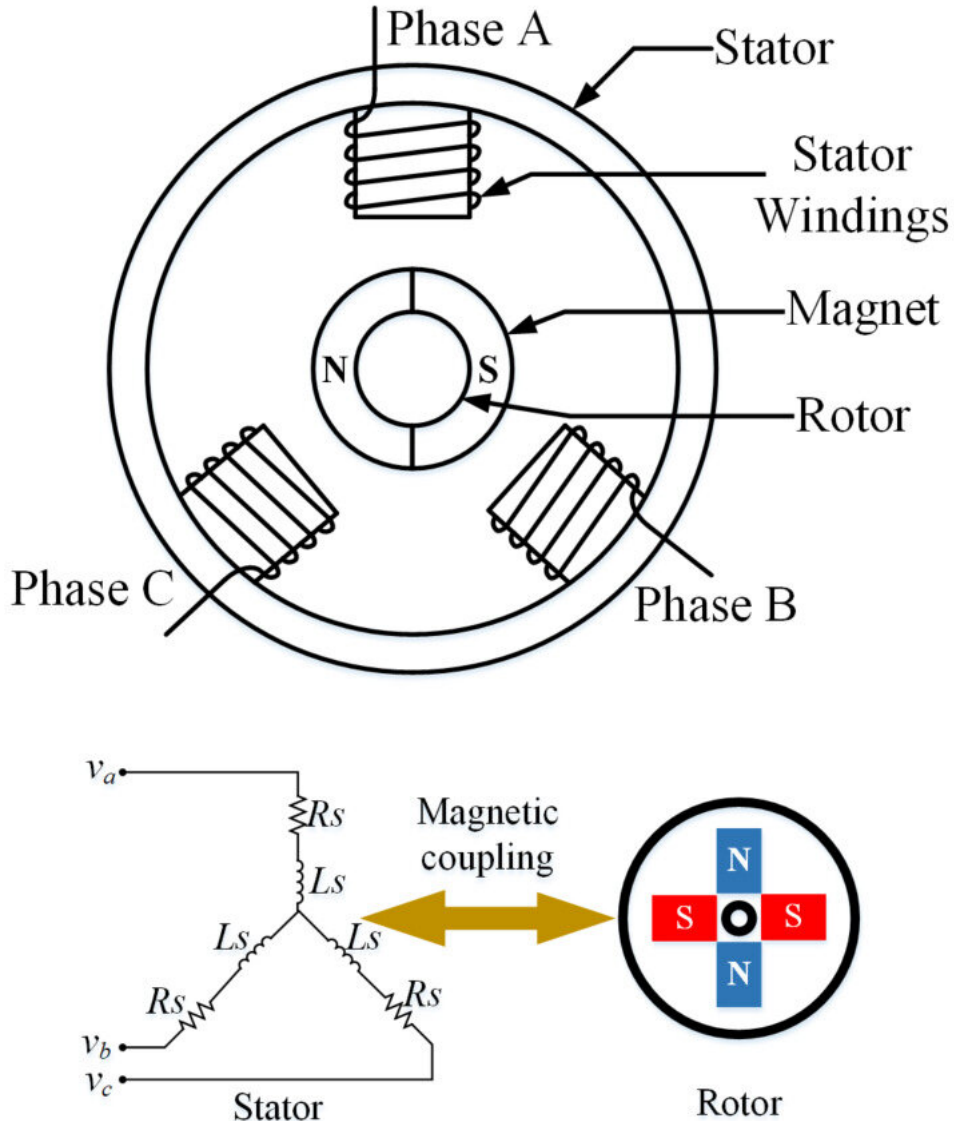


Figure 3.1: PMSM simplified structure

3.3 Structure of PMSM Rotor

The PM synchronous machine is simply created by utilizing PM poles instead of the wound-rotor synchronous machine field winding. The stator features a three-phase distributed armature winding, much like in a traditional synchronous machine. A synchronously rotating sinusoidal air-gap flux arises when three-phase sinusoidal currents are introduced into the armature winding. As a result, depending on the applied frequency, the PM rotor with the same number of poles as the revolving air-gap flux always revolves in synchronism.^[5]

The rotor is the rotating part of the motor and contains permanent magnets. These magnets are typically made of materials such as neodymium, samarium-cobalt, or ferrite (Ceramics).

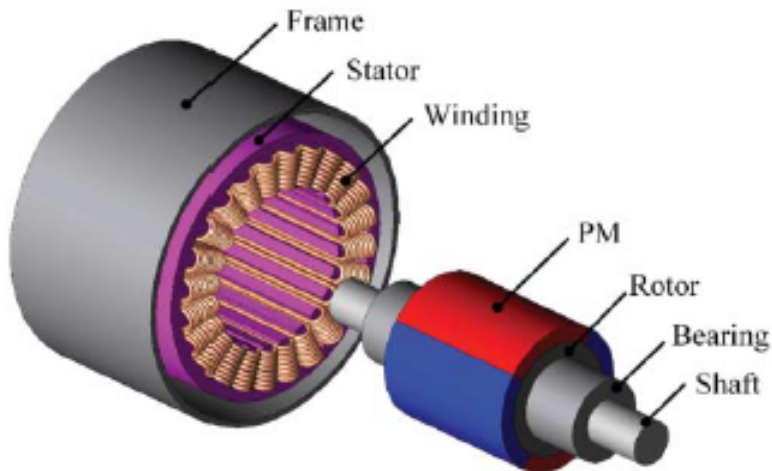


Figure 3.2: PMSM exploded diagram

There are several varieties of PMSMs due to the various arrangements of magnets on the rotor. This section describes a few common and study-style configurations and how they affect winding inductances, the air gap flux density, and reluctance torque—which can increase the synchronous torque or magnet produced torque.

3.3.1 Surface Mount PMSM (SM-PMSM)

Figure 3.3 demonstrates the magnets mounted on the rotor exterior surface. Since it confronts the air gap directly without the obstruction of any other medium, such as rotor laminations, this configuration offers the maximum air gap flux density. Lower structural integrity and mechanical robustness are disadvantages of such an arrangement as they are not snugly fitted into the rotor laminations to their entire thickness. In practical terms, PMs are buried inside the rotor laminations, which offer some mechanical strength. The magnets are then bonded to the rotor using Kavilor tape, further enhancing the mechanical strength of the rotor and magnet combination. Surface mount PMSMs are machines that have this particular configuration of magnets.[\[16\]](#)

High-speed applications—typically those above 3000 rpm—are not recommended for them, however machines with extremely tiny rotor diameters can nonetheless reach speeds of up to 50,000 rpm. This machine's structure shows that the reluctance variation between the direct and quadrature axes is relatively low. Consequently, the variance between the quadrature and direct axis inductances in this

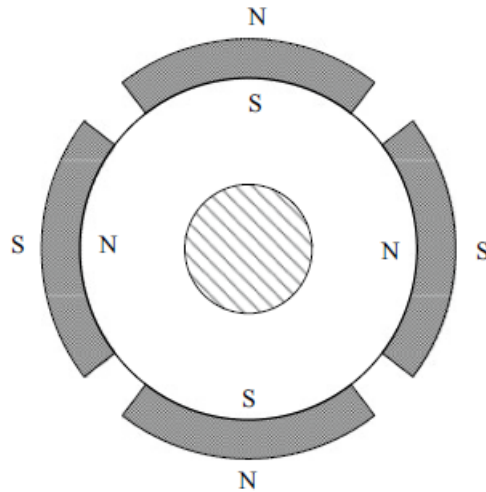


Figure 3.3: *SM-PMSM Structure*

machine is negligible (less than 10%). This specific fact affects the surface mount PMSM drives' characteristics, control, and operation.[16]

3.3.2 Surface-Inset PMSM (SIPM)

The magnets installed in the rotor's outer peripheral grooves, which give the rotor's cylindrical surface uniformity. Furthermore, this configuration is far more mechanically robust than surface mount machines because, unlike surface mount PMSM (SM-PMSM), the magnets in this arrangement are fully and mechanically embedded in the rotor, providing it with mechanical strength from the inside out. In the case of SPM, bracing magnets onto the rotor with tapes and leaving lateral air spaces between the magnets does not result in the highest mechanical strength.[16]

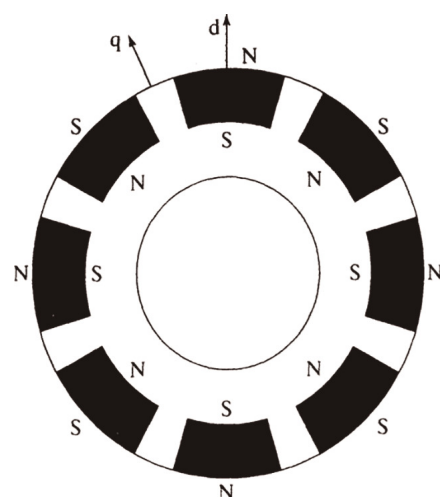


Figure 3.4: *SIPM Structure*

Whereas in the surface inset PMSM, it is mostly unwarranted and even if it is used, it can be bound uniformly as the rotor lamination and magnet surfaces make a uniform surface unlike that of the SPM. The ratio between the quadrature and direct axes inductances can be as high as 2–2.5 in this machine. The machine with this rotor configuration is known as inset PMSM.[16]

3.3.3 Interior PMSM (IPMSM)

Interior PMSMs are another sub-type of PMSMs where permanent magnets are embedded within the body of the rotor. This design offers unique advantages and considerations compared to surface mount PMSMs. By embedding magnets within the rotor body, interior PMSMs can achieve higher torque densities compared to surface mount designs, as the magnetic flux is concentrated closer to the rotor axis. Permanent magnets in the interior rotor are protected by pole pieces. The reluctance torque generated by the asymmetry of the rotor magnetic circuit structure can improve the overload capacity and the power density of the motor.

the PMs are radially magnetized and buried inside the rotor. Compared with the surface-inset one, this topology enables the PMs well protected from flying apart, thus further improving the mechanical integrity for high-speed operation. Also, because of its d-q saliency, an additional reluctance torque is generated. Differing from the surface-inset one, this interior-radial topology adopts linear PMs that are easier for insertion and are easily machinable.[5]

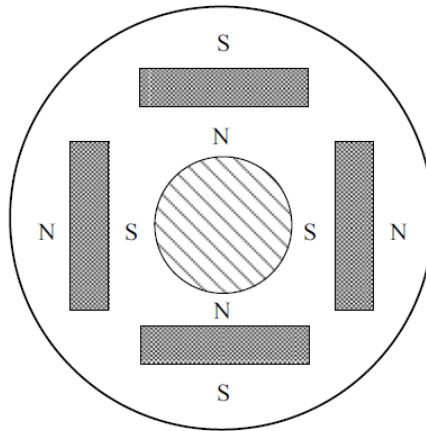


Figure 3.5: IPMSM Structure

IPMSM is widely applied across industries due to its efficiency, power density, and torque capabilities. It powers electric vehicles, hybrid electric vehicle, drives industrial automation processes, enhances energy efficiency in HVAC systems, contributes to renewable energy generation, and improves performance in home appliances, showcasing its versatility across various sectors.

3.4 Theory of Operation

The interaction between the stator's rotating magnetic field and the permanent magnets on the rotor is the basis for the operation of PMSM. As the stator windings are arranged in a three-phase configuration, typically spaced 120 degrees apart for balanced system. When supplied with power from a balanced three-phase source, the stator windings produce a rotating magnetic field with constant amplitude and angular frequency. This rotating magnetic field induces an electromagnetic force in the rotor, causing it to rotate. The magnetic poles of the permanent magnets interact with the rotating magnetic field produced by the stator, resulting in a torque that drives the rotor to rotate.

3.4.1 Rotating Magnetic Field of a three phase motor

Three phases are achieved by connecting identical coils coiled around the stator of a three phase induction motor. The phase windings are electrically separated by 120 degrees. Figure 3.6 depicts the phase winding arrangement of a two-pole, three-phase induction motor.[10]

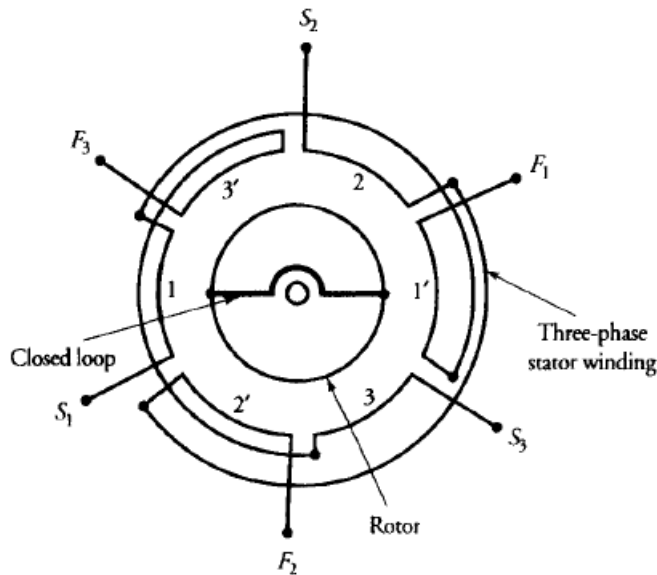


Figure 3.6: Winding arrangement of a three-phase two-pole induction motor.

When the windings are connected to a balanced three-phase source, we expect the currents in all windings to be equal in magnitude but displaced in phase by 120°. The design of each phase winding is such that the spatial distribution of the flux in the air-gap due to that phase winding alone is almost sinusoidal. If we consider the current in phase-1 as the reference, then the currents in the three phases.[10]

$$i_a = I_m \sin \omega t \quad (3.1)$$

$$i_b = I_m \sin \omega t - 120^\circ \quad (3.2)$$

$$i_c = I_m \sin \omega t + 120^\circ \quad (3.3)$$

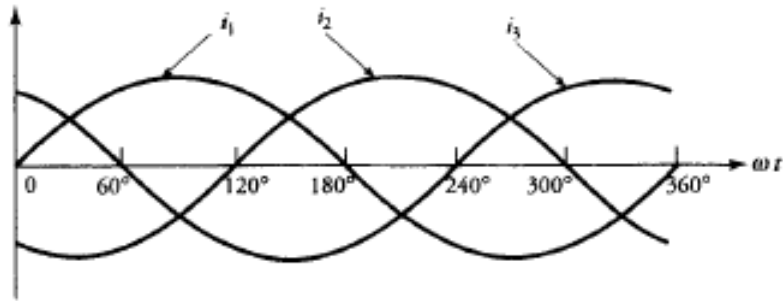


Figure 3.7: The current waveforms in the stator windings of a three-phase motor.

where I_m is the amplitude of each phase current, and $\omega = 2\pi f$ is the angular frequency of the source. Under linear conditions, the flux produced by each current also varies sinusoidally. Therefore, the current waveform can also be labeled the flux waveform.[10]

$$\Phi_a = \Phi_m \sin \omega t \quad (3.4)$$

$$\Phi_b = \Phi_m \sin \omega t - 120^\circ \quad (3.5)$$

$$\Phi_c = \Phi_m \sin \omega t + 120^\circ \quad (3.6)$$

the phase windings upon excitation produce a uniform magnetic field that rotates RMF along the periphery of the air-gap at the synchronous speed. If ϕ_m is the maximum value of the flux produced by the maximum current I_m , in each phase, the strength of the uniform revolving magnetic field is

$$\Phi_r = \frac{3}{2} \Phi_m \quad (3.7)$$

The interpretation of equation (3.7) is discussed thoroughly in chapter 3 in [10].

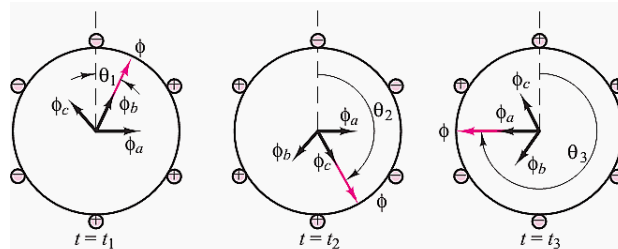


Figure 3.8: RMF direction at different positions

The resultant magnetic field produces one north magnetic pole and one south magnetic pole in the air gap, i.e., the number of magnetic poles is two. In this two-pole motor, the mmf makes one mechanical revolution per complete cycle of the current.

Figure (3.9) shows four-pole motor that has two sets of three-phase windings, the mmf (magneto-motive force) produces two north and south poles in the air gap. In this case, one cycle of the current corresponds to a half mechanical revolution of the mmf. Thus one revolution of the mmf needs two cycles of the current. The number of electrical cycles required to complete a mechanical rotation is equal to the number of pole pairs. Thus, in a P-pole motor, there is a relationship between the mechanical angle θ_m and the electrical angle θ_e .[14]

$$\theta_e = \frac{P}{2} \theta_m \quad (3.8)$$

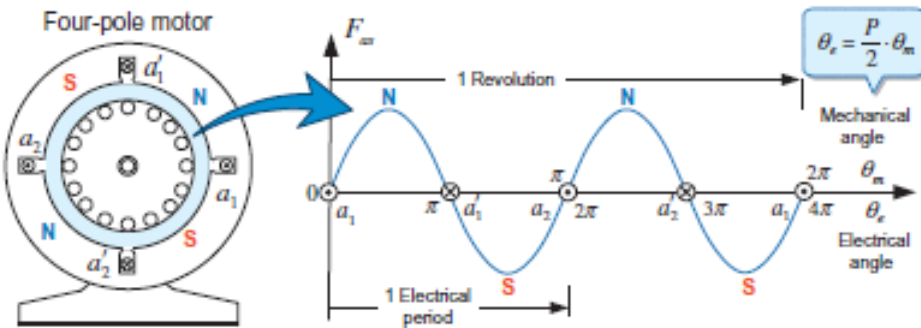


Figure 3.9: MMF Distribution by phase as current in the four-pole motor.

The above equation establishes a link between the mechanical angle of rotation and the angle of the induced emf. This is one of the most important relationships in the study of rotating machines. Differentiating equation (3.8)

$$\omega_e = \frac{P}{2} \omega_m \quad (3.9)$$

Note that $\omega = 2\pi f$ where f is frequency in (Hz)

$$f = \frac{P}{4\pi} \omega_m \quad (3.10)$$

The synchronous speed N_s in revolutions per minute (rpm) at which the flux revolves around the periphery of the air-gap. [10]

$$\omega_m = \frac{2\pi}{60} N_s \quad (3.11)$$

$$N_s = \frac{120}{p} f \quad (3.12)$$

For example, for a two-pole induction motor fed by currents of 60 Hz, the synchronous speed is 3600 r/min.

Consequently, in terms of the rotating magnetic field, what is observed in induction motors nonetheless remains applicable for PMSM. Both types of motors rely on the interaction between magnetic fields to produce motion. In an induction motor, the rotating magnetic field is created by the alternating currents in the stator windings, inducing a current in the rotor, which in turn generates its own magnetic field and causes the rotor to rotate. In a PMSM, the rotating magnetic field is produced by both the stator windings and the permanent magnets in the rotor. The interaction between the stator and rotor fields results in synchronous motion.

3.4.2 Starting of Synchronous Motor

The field winding is energized to produce alternate poles on its periphery. The rotating field created by the armature can be visualized as if two magnets, a north pole and a south pole, are rotating at a constant (synchronous) speed just above the poles of the rotor. The force of attraction between the rotor's north and south poles typically forces the rotor in the direction of the rotating field when they are partially above one another.

Owing to the heavy mass of the rotor, it takes time before it can start moving, but by then the revolving field has reversed its polarity. The rotor is now oriented to rotate in the opposite direction due to the force of repulsion between the two similar polarity poles. As the rotor tries to rotate in the opposite direction, the revolving field has reversed its polarity once again. Thus, each pole on the rotor is acted upon by a rapidly reversing force of equal magnitude in both directions. The average torque thus developed by the rotor is zero.[10]

Therefore, a synchronous motor is not self-starting. Hence, to start a synchronous motor, we must either provide some means for it to develop starting torque by itself or drive the rotor at nearly its synchronous speed by another prime mover and then synchronize it by exciting the field winding.[10]

3.4.2.1 Methods of Starting of Synchronous Motors

A small induction motor is used as a prime mover, coupled to synchronous motor. When it rotates the rotor of the synchronous motor near to the synchronous speed, the main switch and DC switch of the field winding of the synchronous motor are closed.[23] This is applicable for a field excited synchronous machine.

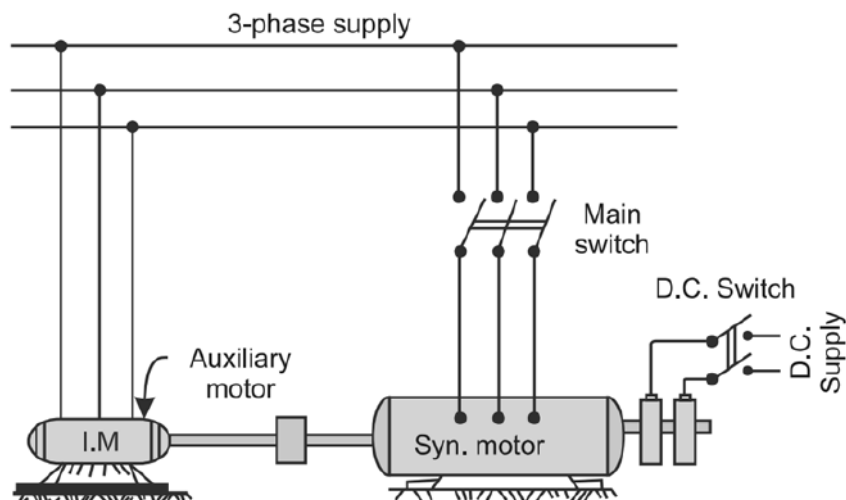


Figure 3.10: Starting of synchronous motor by auxiliary motor diagram

Another method is that the motor's pole faces include an extra winding that is referred to as the damper winding. A short-circuit winding, the damper winding, is also known as a squirrel-cage winding. Squirrel-cage windings for small machines involve placing the rotor laminations in a mould and then pushing molten conducting material—typically aluminum—through the slots. Melted conducting material simultaneously fills the holes in the mould on either side of the rotor. A conducting bar is formed by the conducting material that extends from one end of the slot to the other. The entire one-piece construction looks like a squirrel cage, hence the name. For large machines, the squirrel-cage winding may be formed by driving metal bars into the slots one at a time and then shorting them with annular conducting strips on both ends.[\[10\]](#) which makes PMSM motor as induction motor and start online as induction motor.

As for the starting method of PMSMs used in variable speed drives, we can start the motor slowly at a reduced frequency by using a PWM inverter. In this case, a high starting torque can be developed by using the information of the rotor initial position. [\[14\]](#)

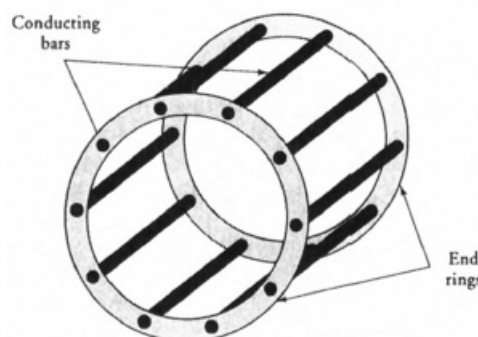


Figure 3.11: A squirrel-cage damper winding.

Chapter 4

MATHEMATICAL MODELING OF PMSM

The modeling of permanent magnet synchronous motors (PMSMs) is a pivotal aspect within the realm of electric motor design and control. As electrification continues to evolve across various industries, the demand for efficient, high-performance motor systems has intensified. PMSMs, characterized by their utilization of permanent magnets in the rotor, offer a compelling solution due to their superior efficiency, power density, and precise control capabilities. Understanding and accurately representing the behavior of PMSMs through mathematical models are fundamental steps in the design, and analysis of these advanced motor systems.

This chapter delves into the intricate procedure of modeling PMSMs, examining the key concepts, approaches, and aspects that are essential to creating thorough models that accurately depict these motors' dynamic behaviour. This chapter provides a thorough foundation for understanding the modelling aspects of PMSMs and their implications for motor design and control strategies through a thorough examination of modelling techniques, ranging from basic equivalent circuit models to advanced electromagnetic field simulations.

A key component of improving permanent magnet synchronous motors' (PMSMs') performance and efficiency is the development of precise dynamic models. In this context, the dynamic modelling of surface mount PMSMs in the abc stationary frame is the centrepiece of this chapter. After that, the model is transformed to two axis reference frames. The aim is to simplify the controller design procedure for the motor by employing the appropriate transformations, which will improve accuracy and effectiveness in motor control schemes. This chapter sets out for clarification of the intricacies of dynamic modeling with regard to surface mount PMSMs, emphasising the significant function of reference frame transformations in simplifying the controller design procedure and enabling these sophisticated motor systems to reach their maximum potential.

4.1 Mathematical Derivation of Electrical and Mechanical equations in "abc" stationary Frame

The equivalent circuit of a three-phase stationary abc reference frame for a permanent magnet synchronous motor (PMSM) provides a simplified representation of the motor's electrical behavior. In this circuit, the stator windings are typically represented as three independent phases labeled as a, b, and c. Each phase is associated with resistance, inductance, and back electromotive force (EMF) as shown in fig.4.1 which is a simple equivalent circuit of the actual phase winding in the motor.[10] The resistance represents the inherent electrical resistance of the winding, while the inductance accounts for the magnetic field generated by the stator current. The back EMF reflects the induced voltage due to the motor's rotation and is proportional to the rotor speed. Additionally, the equivalent circuit includes the magnetizing inductance, which represents the magnetizing effect of the permanent magnets on the rotor.

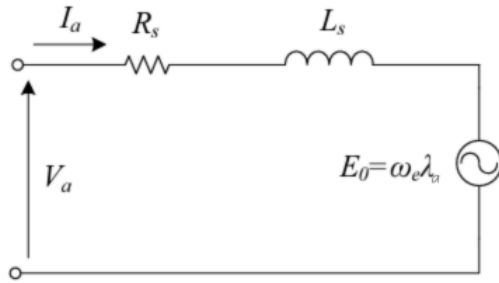


Figure 4.1: The per-phase equivalent circuit of synchronous motor

4.1.1 Electrical equations of PMSM

The voltage, v , of the stator winding, which is the external supplied voltage, can be defined as the sum of voltage drop across the winding resistance, r_i , and the induced voltage, or back emf, which is due to the time-varying flux linkage, $\frac{d}{dt}\lambda$. [6].

where v_{abc} is the 3×1 phase voltage matrix, i_{abc} is the 3×1 phase current matrix, λ_{abc} is the 3×1 phase stator flux linkage matrix, and R_s is 3×3 diagonal matrix describing the winding resistances:

$$v_{abc} = \begin{bmatrix} v_a \\ v_b \\ v_c \end{bmatrix}, i_{abc} = \begin{bmatrix} i_a \\ i_b \\ i_c \end{bmatrix}, \Lambda_{abc} = \begin{bmatrix} \lambda_a \\ \lambda_b \\ \lambda_c \end{bmatrix}, R_s = \begin{bmatrix} r_s & 0 & 0 \\ 0 & r_s & 0 \\ 0 & 0 & r_s \end{bmatrix} \quad (4.1)$$

$$v_a = r_a i_a + \frac{d}{dt} \lambda_a \quad (4.2)$$

$$v_b = r_b i_b + \frac{d}{dt} \lambda_b \quad (4.3)$$

$$v_c = r_c i_c + \frac{d}{dt} \lambda_c \quad (4.4)$$

where r_a , r_b and r_c are the stator winding resistances and they are equal $r_a = r_b = r_c = r_s$. Since the stator winding has the same number of turns and wound wire. i_a , i_b and i_c are the stator current. λ_a , λ_b and λ_c are the stator flux linkage. In matrix form, R_s is a diagonal matrix of the stator winding resistances, we have

$$v_{abc} = R_s i_{abc} + \frac{d}{dt} \Lambda_{abc} = \begin{bmatrix} r_s & 0 & 0 \\ 0 & r_s & 0 \\ 0 & 0 & r_s \end{bmatrix} \begin{bmatrix} i_a \\ i_b \\ i_c \end{bmatrix} + \begin{bmatrix} \lambda_a \\ \lambda_b \\ \lambda_c \end{bmatrix} \quad (4.5)$$

The flux linkage in the stator winding is defined as the product of both self and mutual inductance by the current, plus the flux which is established by the permanent magnet rotor.[6]

$$\lambda_a = L_{aa} i_a + M_{ab} i_b + M_{ac} i_c + \lambda_{ma} \quad (4.6)$$

$$\lambda_b = M_{ba} i_a + L_{bb} i_b + M_{bc} i_c + \lambda_{mb} \quad (4.7)$$

$$\lambda_c = M_{ca} i_a + M_{cb} i_b + L_{cc} i_c + \lambda_{mc} \quad (4.8)$$

where L_{ii} is self inductance of the stator winding, where $i \in a, b, c$. M_{ij} is the mutual inductance between the winding, where $j \in a, b, c$. λ_{mi} is the established flux on the stator winding by the permanent magnet.[1]

Therefore, we have the flux linkage in matrix form

$$\begin{bmatrix} \lambda_a \\ \lambda_b \\ \lambda_c \end{bmatrix} = \begin{bmatrix} L_{aa} & M_{ab} & M_{ac} \\ M_{ba} & L_{bb} & M_{bc} \\ M_{ca} & M_{cb} & L_{cc} \end{bmatrix} \begin{bmatrix} i_a \\ i_b \\ i_c \end{bmatrix} + \begin{bmatrix} \lambda_{ma} \\ \lambda_{mb} \\ \lambda_{mc} \end{bmatrix} \quad (4.9)$$

$$\Lambda_{abc} = L_s i_{abc} + \lambda_{mabc} \quad (4.10)$$

Where λ_{mabc} is the established flux on the stator winding by the permanent magnet, are periodic functions of θ_e . The stator windings are displaced by 120 electrical degrees. Denoting the magnitude of the flux linkages established by the permanent magnet as λ_m .

$$\lambda_{mabc} = \lambda_m \begin{bmatrix} \cos(\theta_e) \\ \cos(\theta_e - \frac{2\pi}{3}) \\ \cos(\theta_e + \frac{2\pi}{3}) \end{bmatrix} \quad (4.11)$$

where L_s is the 3×3 stator inductance matrix and is described by[6] as:

$$L_s = \begin{bmatrix} L_{aa} & M_{ab} & M_{ac} \\ M_{ba} & L_{bb} & M_{bc} \\ M_{ca} & M_{cb} & L_{cc} \end{bmatrix} \quad (4.12)$$

the stator inductances consist of the self inductances of the stator windings and the mutual-inductances between the stator windings. Furthermore, the stator self-inductances L_{aa} , L_{bb} and L_{cc} consist of the leakage inductance and the magnetizing inductance.

Unlike an induction motor, an IPMSM's self-inductance may vary dependent on the rotor's angular position since the rotor's position influences the effective air gap. as shown in fig.4.2 [14].

$$L_{aa} = L_{ls} + L_A - L_B \cos(2\theta_e) \quad (4.13)$$

$$L_{bb} = L_{ls} + L_A - L_B \cos(2(\theta_e - \frac{2\pi}{3})) \quad (4.14)$$

$$L_{cc} = L_{ls} + L_A - L_B \cos(2(\theta_e + \frac{2\pi}{3})) \quad (4.15)$$

Where L_{ls} represents the leakage inductance, L_A represents the average value of the magnetizing inductance, and L_B represents the variation in value of the magnetizing inductance.

where L_A can be expressed as [6]

$$L_A = (\frac{N_T}{P})^2 \frac{\mu_0 A}{l_g} \quad (4.16)$$

Where N_T is the total number of turns in a phase winding, μ_0 is the permeability of air, l_g is the axial length of one solenoid coil in the phase winding and A is the cross-sectional area of solenoid coil expressed as

$$A = \frac{\pi D_g^2}{4} \quad (4.17)$$

Where D_g is the inner diameter of the stator winding. Substitution of Eqn.(4.17) in Eqn. (4.16) yields the detailed expression for L_A :

$$L_A = (\frac{N_T}{P})^2 \frac{\pi \mu_0 D_g^2}{l_g} \quad (4.18)$$

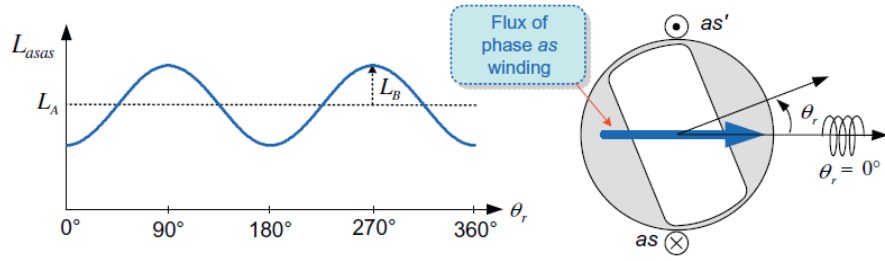


Figure 4.2: Self-inductance of phase as winding with respect to rotor positions.

Note that L_{aa} is shown as L_{asas} , phase a shown as phase as and θ_e is shown as θ_r in fig. 4.2.

The mutual-inductances between the stator windings also vary sinusoidally with respect to the angle θ_e as shown in fig. 4.3.

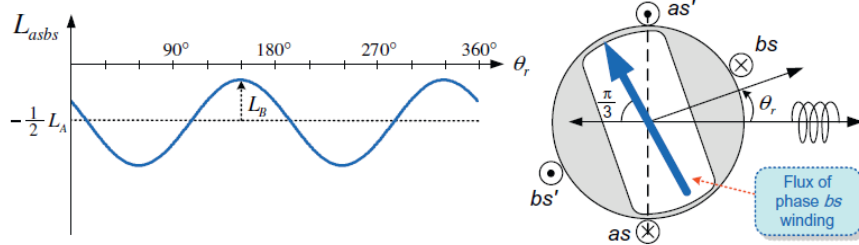


Figure 4.3: mutual-inductance between the phase as and bs stator windings.

Note that L_{ab} is shown as L_{asbs} , phase a shown as phase as, phase b shown as phase bs and θ_e is shown as θ_r in fig. 4.3.

$$L_{ab} = L_{ba} = -\frac{1}{2}L_A - L_B \cos(2(\theta_r - \frac{\pi}{3})) \quad (4.19)$$

$$L_{ac} = L_{ca} = -\frac{1}{2}L_A - L_B \cos(2(\theta_r + \frac{\pi}{3})) \quad (4.20)$$

$$L_{bc} = L_{cb} = -\frac{1}{2}L_A - L_B \cos(2\theta_r) \quad (4.21)$$

With these inductances, the stator inductance is given by

$$L_s = \begin{bmatrix} L_{ls} + L_A - L_B \cos(2\theta_r) & -\frac{1}{2}L_A - L_B \cos(2(\theta_r - \frac{\pi}{3})) & -\frac{1}{2}L_A - L_B \cos(2(\theta_r + \frac{\pi}{3})) \\ -\frac{1}{2}L_A - L_B \cos(2(\theta_r - \frac{\pi}{3})) & L_{ls} + L_A - L_B \cos(2(\theta_r - \frac{2\pi}{3})) & -\frac{1}{2}L_A - L_B \cos(2\theta_r) \\ -\frac{1}{2}L_A - L_B \cos(2(\theta_r + \frac{\pi}{3})) & -\frac{1}{2}L_A - L_B \cos(2\theta_r) & L_{ls} + L_A - L_B \cos(2(\theta_r + \frac{2\pi}{3})) \end{bmatrix} \quad (4.22)$$

All the inductances in the flux linkages of an IPMSM are time-varying, except for at a standstill of the motor. Therefore, the time-varying coefficients will appear in the voltage equations of an IPMSM. In the case of an SM-PMSM, we can easily obtain the flux linkages by letting $L_B = 0$.[14]

For SM-PMSM, the stator inductance is given by

$$L_s = \begin{bmatrix} L_{ls} + L_A & -\frac{1}{2}L_A & -\frac{1}{2}L_A \\ -\frac{1}{2}L_A & L_{ls} + L_A & -\frac{1}{2}L_A \\ -\frac{1}{2}L_A & -\frac{1}{2}L_A & L_{ls} + L_A \end{bmatrix} \quad (4.23)$$

Therefore, the voltage equation could be written as

$$v_{abc} = R_s i_{abc} + \frac{d}{dt} L_s i_{abc} + \frac{d}{dt} \lambda_{mabc} \quad (4.24)$$

4.1.2 Mechanical Equations of PMSM

To finish the motor's description, incorporate the mechanical equation into the PMSM model. Using Newton's second law of motion. [1]

$$J \frac{d\omega_m}{dt} = T_e - B\omega_m - T_L \quad (4.25)$$

$$\frac{d\theta_m}{dt} = \omega_m \quad (4.26)$$

where T_e is the developed electromagnetic torque, T_L is load torque, B is the viscous friction (or damping) coefficient and can be neglected for control purpose, and J is the inertia of the rotor. The relationship between the electrical and mechanical angular speeds is

$$\omega_e = \frac{P}{2} \omega_m \quad (4.27)$$

Therefore, the partial derivative of the magnetic stored co-energy with respect to the angular displacement is what is referred to as electromagnetic torque. The co-energy is expressed as [18] ,[1]:

$$W_c = \frac{1}{2} i_{abc}^T L_s i_{abc} + i_{abc}^T \lambda_{mabc} + W_{pm} \quad (4.28)$$

where W_{pm} is the energy stored in the permanent magnet, which is independent of angular displacement. therefore the torque is

$$T_e = \frac{\partial W_c}{\partial \theta_m} = \frac{P}{2} \frac{\partial W_c}{\partial \theta_e} \quad (4.29)$$

Therefore, due to independence with θ_e , the derivative of both the inductance matrix L_s and W_{pm} are zero. The electromagnetic torque can be obtained as follows:

$$T_e = \frac{P}{2} \lambda_m [i_a \ i_b \ i_c] \begin{bmatrix} -\sin \theta_e \\ \frac{1}{2} \sin \theta_e + \frac{\sqrt{3}}{2} \cos \theta_e \\ \frac{1}{2} \sin \theta_e - \frac{\sqrt{3}}{2} \cos \theta_e \end{bmatrix} \quad (4.30)$$

4.2 Reference Frame Theory

Reference frame theory, also known as coordinate transformation theory, plays a pivotal role in the analysis, modeling, and control of electrical machines, particularly in the domain of power electronics and motor drives. This theory provides a mathematical framework for simplifying the analysis of dynamic systems by transforming variables from one coordinate system to another. In the context of electrical machines, reference frame theory facilitates the transition between stationary and rotating frames of reference, enabling a more intuitive understanding of machine behavior and simplifying control algorithm design.

In this section, this transformation is set forth and, since many of its properties can be studied without the complexities of the machine equations, it is applied to the equations that describe resistive, inductive, and capacitive circuit elements. Using this approach, many of the basic concepts and interpretations of this general transformation are readily and concisely established. Extending the material presented in this chapter to the analysis of ac machines is straightforward, involving a minimum of trigonometric manipulations.

The two primary reference frames used in the analysis of electrical machines are the stationary reference frame (often denoted as abc or $\alpha\beta0$) and the rotating reference frame (denoted as dq or synchronous reference frame). In the stationary reference frame, the coordinates are fixed in space and aligned with the phases of the machine, making it suitable for analyzing steady-state conditions. On the other hand, the rotating reference frame rotates at the same angular velocity as the machine's rotor, simplifying the analysis of rotating machines by making many of the machine's dynamics time-invariant or stationary.

Key transformations used in reference frame theory include the Clarke and Park transformations. The Clarke transformation converts three-phase quantities from the abc frame to two-phase quantities in the stationary dq frame, while the Park transformation rotates these quantities to the rotating dq frame, aligning the d-axis with the rotor flux linkage.

4.2.1 Clarke's Transformation

The Clarke transformation is an essential mathematical tool for the analysis and control of three-phase systems, particularly when it comes to electric machines

like permanent magnet synchronous motors (PMSMs). Three-phase data from the stationary ABC reference frame is transformed into the more feasible orthogonal, two-dimensional $\alpha\beta0$ reference frame. By separating the direct and quadrature components of the three-phase variables, the Clarke transformation improves the capability to effectively control the motor thus enhancing its performance. This facilitates the system's analysis and control.[25]

Clarke's transformation can written as:

$$\mathbf{f}_{\alpha\beta0} = \mathbf{C}\mathbf{f}_{abc}$$

$$(\mathbf{f}_{\alpha\beta0})^T = [f_\alpha \ f_\beta \ f_0]$$

$$\mathbf{C} = \frac{2}{3} \begin{bmatrix} 1 & -\frac{1}{2} & -\frac{1}{2} \\ 0 & -\frac{\sqrt{3}}{2} & \frac{\sqrt{3}}{2} \\ \frac{1}{2} & \frac{1}{2} & \frac{1}{2} \end{bmatrix}$$

where

$$f_\alpha = f_a \quad (4.31)$$

$$f_\beta = \frac{1}{\sqrt{3}}f_a + \frac{2}{\sqrt{3}}f_b \quad (4.32)$$

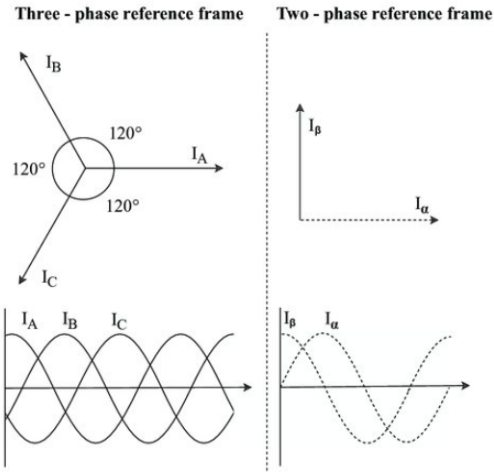


Figure 4.4: Clarke Transformation

The inverse of Clarke's transformation is given by

$$f_{abc} = \mathbf{C}^{-1}\mathbf{f}_{\alpha\beta0} \quad (4.33)$$

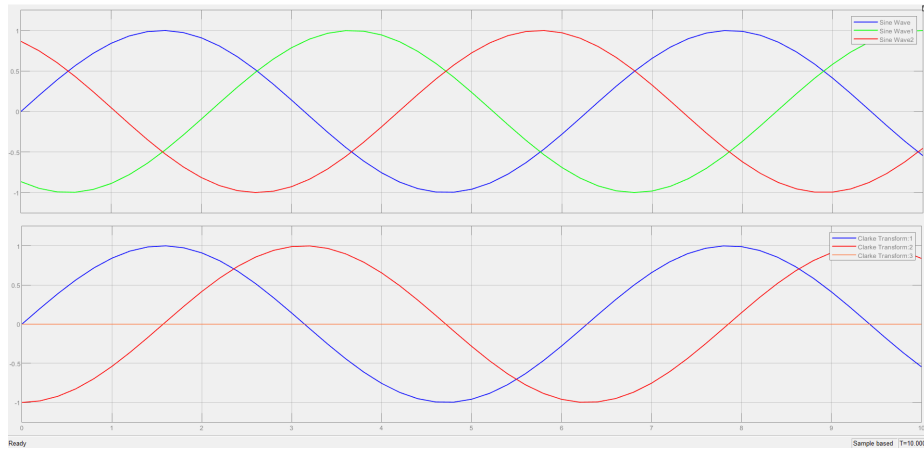


Figure 4.5: Clarke's Transformation demonstration in SIMULINK

4.2.2 Rotational Park's Transformation

Rotational Park's transformation, a fundamental concept in the field of electrical engineering and power electronics, plays a crucial role in the analysis and control of rotating electrical machines. Named after the American engineer Robert H. Park,[27] this transformation enables the transition from the stationary reference frame to the rotating reference frame, facilitating a more intuitive understanding and simplified analysis of dynamic systems, particularly in the context of synchronous machines and motor control.

Rotational Park's transformation is an essential component of reference frame theory, which forms the basis for advanced control strategies such as field-oriented control (FOC) and direct torque control (DTC). By transforming variables from the stationary reference frame ($\alpha\beta\theta$ or abc) to the rotating reference frame (dq or synchronous reference frame), Park's transformation aligns the d -axis with the rotor flux linkage, simplifying the analysis of rotating machines and enabling more effective control algorithms.

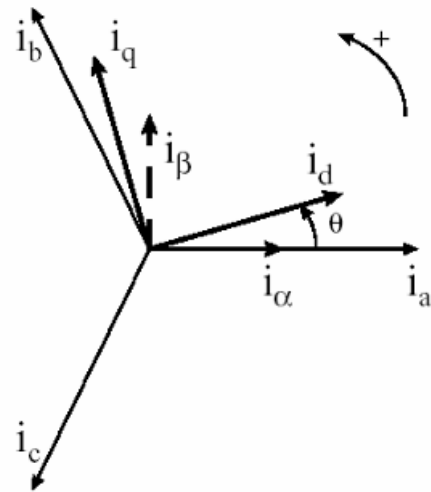
The transformation involves rotating the two-phase quantities from the stationary $\alpha\beta$ frame to the rotating dq frame by an angle equal to the rotor angle. This alignment of the reference frame with the rotor flux linkage decouples the dynamics of the machine, making many of the system's variables time-invariant or stationary, thereby simplifying control algorithm design.

Rotational Park's transformation is mathematically expressed as a matrix operation involving trigonometric functions, and it forms an integral part of the control algorithms implemented in modern motor drives and power electronic systems essentially (FOC) of both Induction motor and PMSM.

We can find the " $dq0$ " coordinate frame by transfer from $\alpha\beta0$ frame for three phase AC machine by simply using the Rotational Park's transformation matrix.[1]

$$f_{dq} = \mathbf{Q} f_{\alpha\beta} \quad (4.34)$$

$$f_{\alpha\beta} = \mathbf{Q}^{-1} f_{dq} \quad (4.35)$$

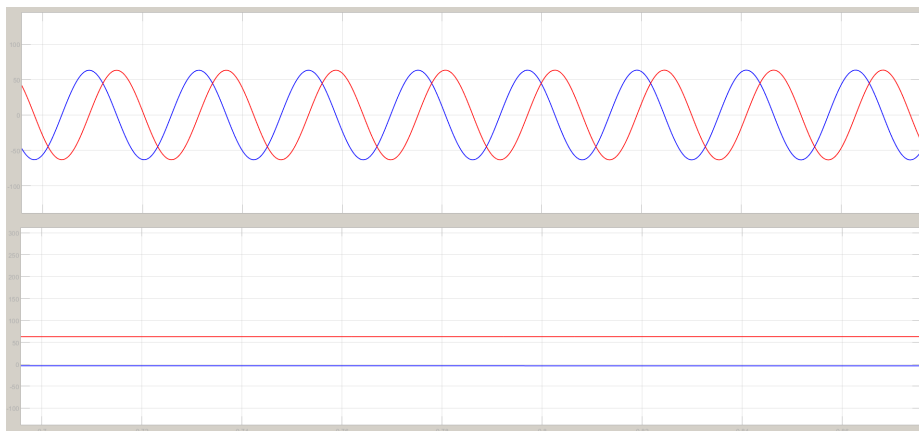
**Figure 4.6:** Park's Transformation

where

$$\mathbf{Q} = \begin{bmatrix} \cos \gamma & \sin \gamma \\ -\sin \gamma & \cos \gamma \end{bmatrix} \quad (4.36)$$

$$\mathbf{Q}^{-1} = \begin{bmatrix} \cos \gamma & -\sin \gamma \\ \sin \gamma & \cos \gamma \end{bmatrix} \quad (4.37)$$

Thereby, γ is arbitrary angle of "dq" coordinate frame.

**Figure 4.7:** Rotational Park's Transformation from $\alpha\beta$ frame to dq frame in SIMULINK

4.3 Mathematical Derivation of Electrical equations in "dq" coordinate Frame

Clarke's transformation and the rotational Park transformation are fundamental concepts in the analysis and control of electrical machines, particularly in power electronics and motor drives. Clarke's transformation converts three-phase quantities in the abc frame to two-phase quantities in the stationary dq frame, simplifying subsequent transformations. The resulting $\alpha\beta$ plane represents balanced and zero-sequence components. The rotational Park transformation aligns the stationary dq frame with the rotor flux linkage by rotating it by an angle equal to the rotor angle. This alignment facilitates more effective control algorithms and offers clearer insights into dynamic systems' behavior, enabling efficient motor control strategies. Together, these transformations provide a seamless transition between stationary and rotating reference frames, crucial for motor control techniques such as FOC.

Clarke's transformation involves mapping the three-phase variables onto a two-dimensional space, typically referred to as the $\alpha\beta$ plane, where the α -axis represents the magnitude of the balanced components, and the β -axis represents the zero-sequence component.

Following Clarke's transformation, the next step is the rotational Park transformation, which aligns the two-phase quantities from the stationary dq frame to the rotating dq frame by an angle equal to the rotor angle.

Applying these two transformations sequentially will map the "abc" coordinate frame, which is the stationary frame, to "dq" coordinate frame, which is the rotational frame, as shown in fig.4.8.

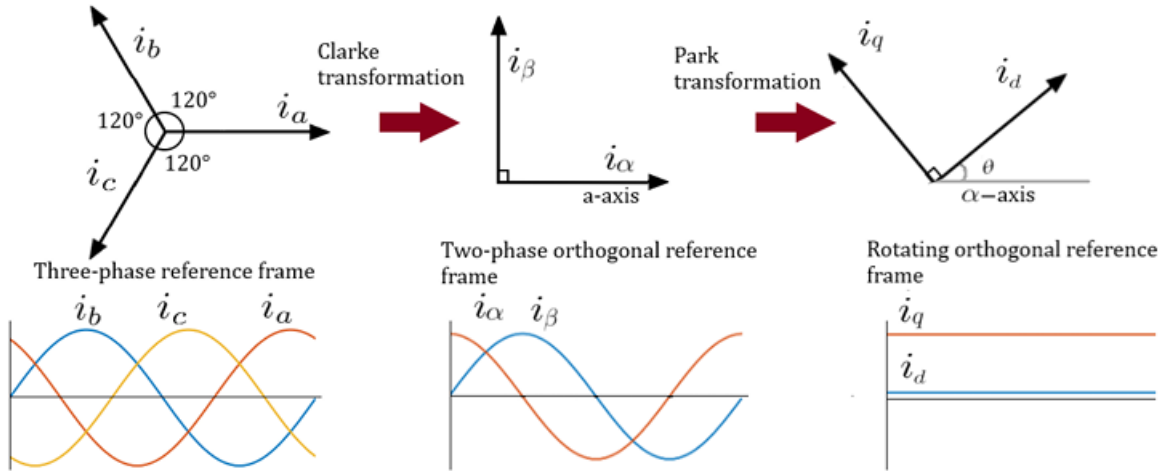


Figure 4.8: The three reference frames

4.3.1 "αβ0" Coordinate Frame Model of Permanent Magnet Synchronous Motor

The mapping in PMSM model reduces the number of equations from three to two and the number of stator variables in the equations by ignoring the zero component and utilizing Clarke's transformation to transform the equations from "abc" stationary reference frame to "αβ0" stationary reference frame.[1] thus the equations will be

$$v_{\alpha\beta 0} = \mathbf{C} v_{abc} \quad (4.38)$$

$$v_{\alpha\beta 0} = \mathbf{C} [R_s i_{abc} + \frac{d}{dt} \Lambda_{abc}] \quad (4.39)$$

where

$$i_{abc} = \mathbf{C}^{-1} i_{\alpha\beta 0} \quad (4.40)$$

$$\Lambda_{abc} = \mathbf{C}^{-1} \Lambda_{\alpha\beta 0} \quad (4.41)$$

Thus,

$$v_{\alpha\beta 0} = \mathbf{C} R_s \mathbf{C}^{-1} i_{abc} + \mathbf{C} \frac{d}{dt} \mathbf{C}^{-1} \Lambda_{abc} \quad (4.42)$$

The first part of the voltage equation could be written as

$$\mathbf{C} R_s \mathbf{C}^{-1} i_{\alpha\beta 0} = \frac{2}{3} \begin{bmatrix} 1 & -\frac{1}{2} & -\frac{1}{2} \\ 0 & \frac{\sqrt{3}}{2} & -\frac{\sqrt{3}}{2} \\ \frac{1}{2} & \frac{1}{2} & \frac{1}{2} \end{bmatrix} \begin{bmatrix} r_s & 0 & 0 \\ 0 & r_s & 0 \\ 0 & 0 & r_s \end{bmatrix} \begin{bmatrix} 1 & 0 & 1 \\ -\frac{1}{2} & \frac{\sqrt{3}}{2} & 1 \\ -\frac{1}{2} & \frac{\sqrt{3}}{2} & 1 \end{bmatrix} i_{\alpha\beta 0} \quad (4.43)$$

$$\mathbf{C} R_s \mathbf{C}^{-1} i_{\alpha\beta 0} = R_s I i_{\alpha\beta 0} \quad (4.44)$$

where I is an identity matrix.

The first part of the voltage equation could be written as

$$\mathbf{C} \frac{d}{dt} \mathbf{C}^{-1} \Lambda_{abc} = \mathbf{C} (\Lambda_{abc} \frac{d}{dt} \mathbf{C}^{-1} + \mathbf{C}^{-1} \frac{d}{dt} \Lambda_{abc}) \quad (4.45)$$

$$\mathbf{C} \frac{d}{dt} \mathbf{C}^{-1} \Lambda_{abc} = \frac{d}{dt} \Lambda_{abc} \quad (4.46)$$

Thus, the voltage equation in "αβ0" is

$$v_{\alpha\beta 0} = R_s i_{\alpha\beta 0} + \frac{d}{dt} \Lambda_{\alpha\beta 0} \quad (4.47)$$

Flux linkage in the "αβ0" coordinate frame could be expressed as

$$\Lambda_{\alpha\beta 0} = \mathbf{C}\Lambda_{abc} \quad (4.48)$$

$$\Lambda_{\alpha\beta 0} = \mathbf{C}L_s \mathbf{C}^{-1} i_{\alpha\beta 0} + \mathbf{C}\lambda_{mabc} \quad (4.49)$$

The equation's first component might be expressed in Eqn. (4.50).

$$\mathbf{C}L_s \mathbf{C}^{-1} i_{\alpha\beta 0} = \frac{2}{3} \begin{bmatrix} 1 & -\frac{1}{2} & -\frac{1}{2} \\ 0 & \frac{\sqrt{3}}{2} & -\frac{\sqrt{3}}{2} \\ \frac{1}{2} & \frac{1}{2} & \frac{1}{2} \end{bmatrix} \begin{bmatrix} L_{ls} + L_A & -\frac{1}{2}L_A & -\frac{1}{2}L_A \\ -\frac{1}{2}L_A & L_{ls} + L_A & -\frac{1}{2}L_A \\ -\frac{1}{2}L_A & -\frac{1}{2}L_A & L_{ls} + L_A \end{bmatrix} \begin{bmatrix} 1 & 0 & 1 \\ -\frac{1}{2} & \frac{\sqrt{3}}{2} & 1 \\ -\frac{1}{2} & \frac{\sqrt{3}}{2} & 1 \end{bmatrix} i_{\alpha\beta 0} \quad (4.50)$$

The Eqn. (4.50) is simplified to [25]

$$\mathbf{C}L_s \mathbf{C}^{-1} i_{\alpha\beta 0} = \begin{bmatrix} L_{ls} + \frac{3}{2}L_A & 0 & 0 \\ 0 & L_{ls} + \frac{3}{2}L_A & 0 \\ 0 & 0 & L_{ls} \end{bmatrix} i_{\alpha\beta 0} \quad (4.51)$$

The second component of Eqn. (4.49) could be written as

$$\mathbf{C}\lambda_{mabc} = \frac{3}{2}\lambda_m \begin{bmatrix} 1 & -\frac{1}{2} & -\frac{1}{2} \\ 0 & \frac{\sqrt{3}}{2} & -\frac{\sqrt{3}}{2} \\ \frac{1}{2} & \frac{1}{2} & \frac{1}{2} \end{bmatrix} \begin{bmatrix} \cos(\theta_e) \\ \cos(\theta_e - \frac{2\pi}{3}) \\ \cos(\theta_e + \frac{2\pi}{3}) \end{bmatrix} \quad (4.52)$$

Which is reduced to

$$\mathbf{C}\lambda_{mabc} = \lambda_m \begin{bmatrix} \cos(\theta_e) \\ \sin(\theta_e) \\ 0 \end{bmatrix} \quad (4.53)$$

Thus, the flux-linkage equations could be written as

$$\Lambda_{\alpha\beta 0} = \begin{bmatrix} L_{ls} + \frac{3}{2}L_A & 0 & 0 \\ 0 & L_{ls} + \frac{3}{2}L_A & 0 \\ 0 & 0 & L_{ls} \end{bmatrix} i_{\alpha\beta 0} + \lambda_m \begin{bmatrix} \cos(\theta_e) \\ \sin(\theta_e) \\ 0 \end{bmatrix} \quad (4.54)$$

Consequently, the flux-linkage derivative in the $\alpha\beta0$ stationary frame is [1]:

$$\frac{d}{dt}\Lambda_{\alpha\beta0} = L_{\alpha\beta0}\frac{d}{dt}i_{\alpha\beta0} + \frac{d}{dt}\lambda_{m\alpha\beta0} \quad (4.55)$$

Which expands to

$$\frac{d}{dt} \begin{bmatrix} \lambda_\alpha \\ \lambda_\beta \\ \lambda_0 \end{bmatrix} = \begin{bmatrix} L_{ls} + \frac{3}{2}L_A & 0 & 0 \\ 0 & L_{ls} + \frac{3}{2}L_A & 0 \\ 0 & 0 & L_{ls} \end{bmatrix} \frac{d}{dt} \begin{bmatrix} i_\alpha \\ i_\beta \\ i_0 \end{bmatrix} + \omega_e \lambda_m \begin{bmatrix} -\sin(\theta_e) \\ \cos(\theta_e) \\ 0 \end{bmatrix} \quad (4.56)$$

Consequently, $L_{s\alpha\beta0}$ and $\lambda_{s\alpha\beta0}$ are the matrix of constant inductance and the flux that the rotor magnetic field establishes in the stator in the stationary coordinate frame. Thus, the voltage Eqn. (4.42) could be written and expanded as

$$\begin{bmatrix} v_\alpha \\ v_\beta \\ v_0 \end{bmatrix} = \begin{bmatrix} r_s & 0 & 0 \\ 0 & r_s & 0 \\ 0 & 0 & r_s \end{bmatrix} \begin{bmatrix} i_\alpha \\ i_\beta \\ i_0 \end{bmatrix} + \begin{bmatrix} L_{ls} + \frac{3}{2}L_A & 0 & 0 \\ 0 & L_{ls} + \frac{3}{2}L_A & 0 \\ 0 & 0 & L_{ls} \end{bmatrix} \frac{d}{dt} \begin{bmatrix} i_\alpha \\ i_\beta \\ i_0 \end{bmatrix} + \omega_e \lambda_m \begin{bmatrix} -\sin(\theta_e) \\ \cos(\theta_e) \\ 0 \end{bmatrix} \quad (4.57)$$

Applying Clarke's transformation to the electromagnetic torque Eqn.(4.30) from "abc" stationary reference frame to " $\alpha\beta0$ " stationary reference frame. Thus, the electromagnetic torque equation in " $\alpha\beta0$ " coordinate frame becomes

$$T_e = \frac{P}{2}[\mathbf{C}^{-1}i_{\alpha\beta0}]^T \frac{d}{d\theta_e} \lambda_{mabc} \quad (4.58)$$

Which expands to

$$T_e = \frac{P}{2} \begin{bmatrix} 1 & -\frac{1}{2} & -\frac{1}{2} \\ 0 & \frac{\sqrt{3}}{2} & -\frac{\sqrt{3}}{2} \\ \frac{1}{2} & \frac{1}{2} & \frac{1}{2} \end{bmatrix}^T \begin{bmatrix} i_\alpha \\ i_\beta \\ i_0 \end{bmatrix} \begin{bmatrix} -\sin(\theta_e) \\ \cos(\theta_e) \\ 0 \end{bmatrix} \quad (4.59)$$

Simplifying Eqn. (4.59) to

$$T_e = \frac{3P}{4} \lambda_m (-i_\alpha \sin(\theta_e) + i_\beta \cos(\theta_e)) \quad (4.60)$$

By elimination of the zero component in Eqns. (4.54) and (4.57), the flux linkage and stator voltage, which can still be obtained based on the rotor angle.

$$\begin{bmatrix} \lambda_\alpha \\ \lambda_\beta \end{bmatrix} = \begin{bmatrix} L_{ls} + \frac{3}{2}L_A & 0 \\ 0 & L_{ls} + \frac{3}{2}L_A \end{bmatrix} \begin{bmatrix} i_\alpha \\ i_\beta \end{bmatrix} + \lambda_m \begin{bmatrix} \cos(\theta_e) \\ \sin(\theta_e) \end{bmatrix} \quad (4.61)$$

$$\begin{bmatrix} v_\alpha \\ v_\beta \end{bmatrix} = \begin{bmatrix} r_s & 0 \\ 0 & r_s \end{bmatrix} \begin{bmatrix} i_\alpha \\ i_\beta \end{bmatrix} + \begin{bmatrix} L_{ls} + \frac{3}{2}L_A & 0 \\ 0 & L_{ls} + \frac{3}{2}L_A \end{bmatrix} \frac{d}{dt} \begin{bmatrix} i_\alpha \\ i_\beta \end{bmatrix} + \omega_e \lambda_m \begin{bmatrix} -\sin(\theta_e) \\ \cos(\theta_e) \end{bmatrix} \quad (4.62)$$

4.3.2 "dq" Coordinate Frame Model of Permanent Magnet Synchronous Motor

A key component of PMSM analysis and control, the "dq" coordinate frame model is a key technology that advances improvements in a number of industries, including renewable energy, automotive and aerospace. This model provides an incredibly clear and accurate framework for understanding the dynamic behaviour of PMSMs. It is developed from the notion of rotating reference frames. The "dq" model reduces the complexity of PMSM dynamics by separating the three-phase stator and rotor variables into two orthogonal components, d and q, which are oriented in relation to the axes that produce torque and magnetic flux, respectively. Because of this simplification, complex control systems like field-oriented control (FOC) are able to be implemented, which maximise motor performance in terms of torque production, efficiency, and speed regulation. The theoretical foundations of the "dq" coordinate frame model, practical implications, and advanced uses in PMSM modeling are examined. This subsection demonstrates how this idea transformed electric propulsion systems and advanced the next stage of technical advancements.

By applying Rotational Park's transformation to the stationary PMSM model to the equations Eqns. (4.62) and (4.61) we obtained in the preceding subsection for the voltage and flux linkage, we get the "dq" Coordinate Frame Model of Permanent Magnet Synchronous Motor which is an essential part in the controlling of PMSM to maximize motor performance.

Recall that γ is an arbitrary angle of "dq" coordinate frame and the angular speed of this frame is $\frac{d}{dt}\gamma = \omega_0$. [1]

The flux linkage in "dq" arbitrary rotating coordinate frame could be written as

$$\Lambda_{dq} = \mathbf{Q}L_s\mathbf{Q}^{-1}i_{dq} + \mathbf{Q}\lambda_{m\alpha\beta} \quad (4.63)$$

Since L_s is a constant matrix. Therefore,

$$\mathbf{Q}L_s\mathbf{Q}^{-1} = L_s\mathbf{Q}\mathbf{Q}^{-1} = L_s$$

The established flux due to the permanent magnet becomes

$$\mathbf{Q}\lambda_{m\alpha\beta} = \begin{bmatrix} \cos\gamma & \sin\gamma \\ -\sin\gamma & \cos\gamma \end{bmatrix} \lambda_m \begin{bmatrix} \cos(\theta_e) \\ \sin(\theta_e) \end{bmatrix} \quad (4.64)$$

This is simplified to

$$\mathbf{Q} \lambda_{m\alpha\beta} = \lambda_m \begin{bmatrix} \cos(\gamma - \theta_e) \\ \sin(\gamma - \theta_e) \end{bmatrix} \quad (4.65)$$

Therefore, the flux linkage equation in the "dq" arbitrary rotating coordinate frame could be written as

$$\begin{bmatrix} \lambda_d \\ \lambda_q \end{bmatrix} = \begin{bmatrix} L_d & 0 \\ 0 & L_q \end{bmatrix} \begin{bmatrix} i_d \\ i_q \end{bmatrix} + \lambda_m \begin{bmatrix} \cos(\gamma - \theta_e) \\ \sin(\gamma - \theta_e) \end{bmatrix} \quad (4.66)$$

Here, the inductances on the d-axis and q-axis is expressed as

$$L_d = L_{ls} + \frac{3}{2}L_{Ad} \quad (4.67)$$

$$L_q = L_{ls} + \frac{3}{2}L_{Aq} \quad (4.68)$$

in case of the SM-PMSM $L_d = L_q$ whereas in IPMSM $L_d < L_q$

The stator voltage in the "dq" arbitrary rotating coordinate frame could be written as

$$v_{dq} = \mathbf{Q}R_s\mathbf{Q}^{-1} + \mathbf{Q}\frac{d}{dt}(\mathbf{Q}^{-1}\Lambda_{dq}) \quad (4.69)$$

Where the first component of the equation could be expressed and simplified to

$$\mathbf{Q}R_s\mathbf{Q}^{-1} = R_s\mathbf{Q}\mathbf{Q}^{-1} = R_s \quad (4.70)$$

The second component could be written as

$$\mathbf{Q}\frac{d}{dt}(\mathbf{Q}^{-1}\Lambda_{dq}) = \mathbf{Q}\frac{d}{dt}(\mathbf{Q}^{-1})\Lambda_{dq} + \mathbf{Q}\mathbf{Q}^{-1}\frac{d}{dt}(\Lambda_{dq}) \quad (4.71)$$

where

$$\mathbf{Q}\frac{d}{dt}(\mathbf{Q}^{-1})\Lambda_{dq} = \omega_0 \begin{bmatrix} 0 & -1 \\ 1 & 0 \end{bmatrix} \begin{bmatrix} \lambda_d \\ \lambda_q \end{bmatrix} \quad (4.72)$$

$$\mathbf{Q}\mathbf{Q}^{-1}\frac{d}{dt}(\Lambda_{dq}) = \frac{d}{dt}(\Lambda_{dq}) \quad (4.73)$$

$$\mathbf{Q}\frac{d}{dt}(\mathbf{Q}^{-1}\Lambda_{dq}) = \omega_0 \begin{bmatrix} -\lambda_q \\ \lambda_d \end{bmatrix} + \frac{d}{dt}(\Lambda_{dq}) \quad (4.74)$$

Thus, the voltage equation in the "dq" arbitrary rotating coordinate frame could be written as

$$v_{dq} = R_s i_{dq} + \omega_0 \begin{bmatrix} -\lambda_q \\ \lambda_d \end{bmatrix} + \frac{d}{dt}(\Lambda_{dq}) \quad (4.75)$$

The electromagnetic torque Eqn.(4.60) could be written in "dq" arbitrary rotating coordinate frame as

$$T_e = \frac{3P}{4} \lambda_m [\mathbf{Q}^{-1} i_{dq}]^T \begin{bmatrix} -\sin(\theta_e) \\ \cos(\theta_e) \end{bmatrix} \quad (4.76)$$

$$T_e = \frac{3P}{4} \lambda_m \begin{bmatrix} i_d & i_q \end{bmatrix} \begin{bmatrix} \sin(\gamma - \theta_e) \\ \cos(\gamma + \theta_e) \end{bmatrix} \quad (4.77)$$

Thus, in this case, where the rotor and the arbitrarily rotating frame rotate synchronously at the same angle, $\theta_e = \gamma$ and $\omega_e = \omega_0$. Thus, the flux linkage, the voltage, and the electromagnetic torque become:

$$\begin{bmatrix} \lambda_d \\ \lambda_q \end{bmatrix} = \begin{bmatrix} L_d & 0 \\ 0 & L_q \end{bmatrix} \begin{bmatrix} i_d \\ i_q \end{bmatrix} + \begin{bmatrix} \lambda_m \\ 0 \end{bmatrix} \quad (4.78)$$

$$\begin{bmatrix} v_d \\ v_q \end{bmatrix} = \begin{bmatrix} r_s & 0 \\ 0 & r_s \end{bmatrix} \begin{bmatrix} i_d \\ i_q \end{bmatrix} + \begin{bmatrix} L_d & 0 \\ 0 & L_q \end{bmatrix} \frac{d}{dt} \begin{bmatrix} i_d \\ i_q \end{bmatrix} + \omega_e \begin{bmatrix} -\lambda_q \\ \lambda_d \end{bmatrix} \quad (4.79)$$

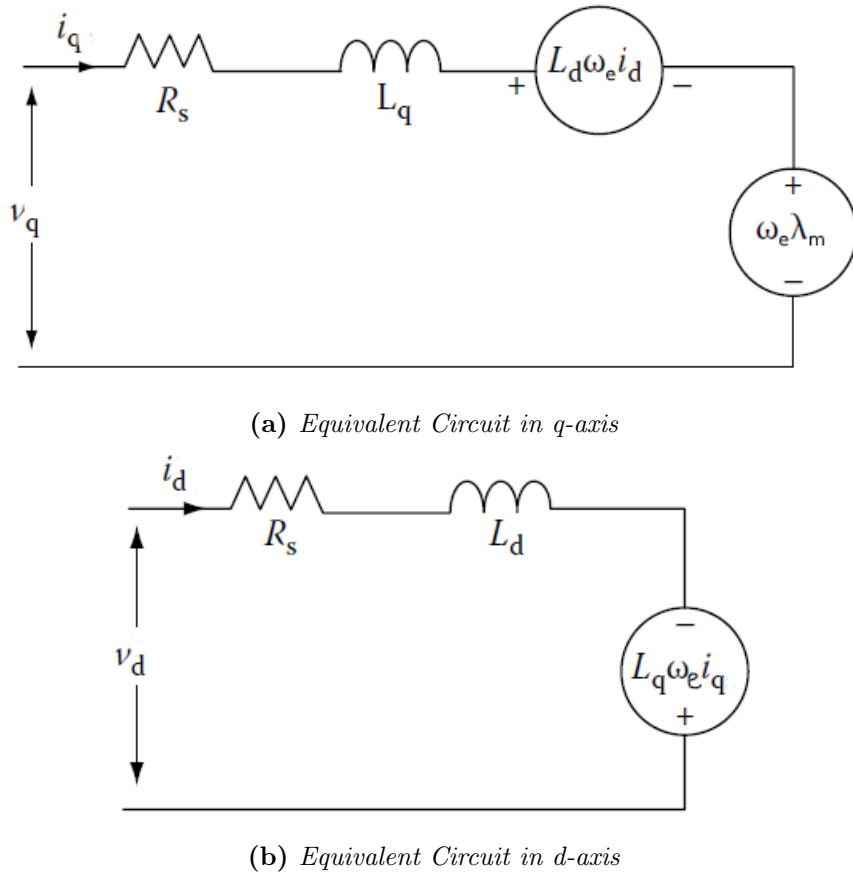
$$T_e = \frac{3}{2} \frac{P}{2} [\lambda_m i_q + (L_d - L_q) i_q i_d] \quad (4.80)$$

Consequently, the dynamic model of PMSM in "dq" arbitrary rotating coordinate frame could be written as

$$\begin{bmatrix} v_d \\ v_q \end{bmatrix} = \begin{bmatrix} r_s & 0 \\ 0 & r_s \end{bmatrix} \begin{bmatrix} i_d \\ i_q \end{bmatrix} + \begin{bmatrix} L_d & 0 \\ 0 & L_q \end{bmatrix} \frac{d}{dt} \begin{bmatrix} i_d \\ i_q \end{bmatrix} + \omega_e \begin{bmatrix} L_q & 0 \\ 0 & L_d \end{bmatrix} \begin{bmatrix} -i_q \\ i_d \end{bmatrix} + \omega_e \begin{bmatrix} 0 \\ \lambda_m \end{bmatrix} \quad (4.81)$$

Recall that $\omega_e = \frac{P}{2} \omega_m$ The mechanical equation could be written as

$$\frac{d\omega_m}{dt} = \frac{1}{J} (T_e - T_L - B\omega_m) \quad (4.82)$$

**Figure 4.9:** *Equivalent Circuits in dq-frame*

In the steady-state model of a PMSM, the motor dynamic equations are simplified, and parameters such as inductances, resistances, and back electromotive force (EMF) constants are assumed to be constant. Additionally, it is assumed that the rotor flux remains constant during steady-state operation.

The steady state model is just like the dynamic model but without the term of $L_d \frac{d}{dt} i_d$ and $L_q \frac{d}{dt} i_q$ because at steady state the inductor acts as short circuit so The Steady state model of PMSM in "dq" arbitrary rotating coordinate frame could be written as [16]

$$\begin{bmatrix} v_d \\ v_q \end{bmatrix} = \begin{bmatrix} r_s & 0 \\ 0 & r_s \end{bmatrix} \begin{bmatrix} i_d \\ i_q \end{bmatrix} + \omega_e \begin{bmatrix} L_q & 0 \\ 0 & L_d \end{bmatrix} \begin{bmatrix} -i_q \\ i_d \end{bmatrix} + \omega_e \begin{bmatrix} 0 \\ \lambda_m \end{bmatrix} \quad (4.83)$$

Chapter 5

FIELD-ORIENTED CONTROL AND INVERTERS

In motor drive systems, the main control object is the motor's output torque. This is due to the fact that the torque of the driving motor may be controlled to regulate the position or speed of loads. There are two methods of the torque control of alternating current (AC) motors: average torque control and instantaneous torque control. For general-purpose applications that do not require precise speed or torque control, such as fans, blowers, and pump drives, average torque control is a cost-effective variable-speed control approach. The major purpose of control in these applications is to maintain the average speed of the motor/load, which is frequently accomplished by regulating the motor's average torque. A typical example of the average torque control technique (also called the scalar control method) is the constant V/f control in the induction motor drives. However, this method can control the motor torque only in steady state conditions and therefore cannot be used to control the dynamic behavior of the motor.[\[14\]](#)

In contrast, high-performance applications like robots, lifts, CNC machines, and automation line drives necessitate rapid torque control. For these applications, precise speed/torque control along with fast, dynamic reaction is essential. To achieve these goals, the motor's instantaneous torque must be controlled. For direct current (DC) motors, instantaneous torque control can be easily achieved through control of the armature current. AC motors require a complex technique referred to as vector control. The field-oriented control approach is a common vector control method. Direct torque control is an additional strategy to regulate instantaneous torque. Although less sophisticated than vector control, this technique is less often used.

Field-Oriented Control (FOC) is a complex control approach used in numerous types of industrial applications, significantly electric motor drives, to achieve superior performance. At its foundation, the FOC decouples the control of the motor's magnetic flux and torque components, facilitating independent regulation and optimization of both. FOC simplifies the control effort by aligning the stator current and rotor flux in a rotating reference frame, leading to higher efficiency, greater dynamic response, and reduced torque ripples. due to its capacity to provide precise

and efficient motor control over a wide range of operating conditions, this technique of control has been implemented in numerous applications in electric cars, renewable energy systems, robotics, and other fields. Despite its computational complexity, developments in digital signal processing and microcontroller technology have made FOC more practical for real-time application, highlighting its significance in vector control of AC motors.

FOC had been developed in the 1980s for the purpose of oscillating flux and torque responses in inverter-fed induction and synchronous motor drives, having initially appeared in AC drive research in the late 1960s. Inverter failure due to strong current transients was a significant obstacle to the market launch of inverter-fed AC drives. Compared to these AC drives, the separately excited DC motor drives performed well, with excellent dynamic control of flux and torque. The performance of DC motor drives depends on their capacity to independently regulate flux and torque. Flux is regulated by the field current, also known as the flux-producing current. Keeping a constant field current and flux, the torque is controlled exclusively by the armature current, which may be considered the torque-producing current. Controlling the field and armature current magnitudes as they are DC variables, the flux and electromagnetic torque are controlled precisely in a separately excited DC motor drive. The key to it, then lies in finding an equivalent flux-producing current and torque-producing current (i.e., the armature current) in AC machines leading to the control of the flux and torque channels in them. The key to that, for ac drives, came in two forms: (1) the machine modeling in space phasor form, which reduced a three-phase machine into a machine with one winding each on stator and rotor, thereby making it equivalent to separately excited DC machine this can be achieved through the reference frame transformation, which explained in the preceding chapter. and (2) the ability of the inverter to produce a current phasor with absolute control of its magnitude, frequency, and phase. Both these features are exploited to make the PMSM drive system a high-performance drive system with independent control of its mutual flux and electromagnetic torque.[16]

5.1 Derivation of FOC

The FOC separates the torque and flux channels in the machine through stator excitation inputs. Vector control for PMSM works similarly to that of induction motor drives. Many variations of the vector control but similar to that of an induction machine are possible. This section discusses how the vector control of the three-phase PMSM is derived from the dynamic model.[16] Considering the currents as inputs, the three-phase currents are

$$i_a = I_m \sin(\omega_e t + \delta) \quad (5.1)$$

$$i_b = I_m \sin(\omega_e t + \delta - \frac{2\pi}{3}) \quad (5.2)$$

$$i_c = I_m \sin(\omega_e t + \delta + \frac{2\pi}{3}) \quad (5.3)$$

where ω_e is the electrical rotor speed and δ is the angle between the rotor field and stator current phasor, known as the torque angle.

The rotor field travels at a speed of ω_e electrical rad/s, which is equal to the rotor speed in electrical rad/s. The q- and d-axes stator currents in the rotor reference frames are obtained after applying Clarke's and Park's transformations in Chapter 4 on PMSM modeling.[16]

$$\begin{bmatrix} i_q \\ i_d \end{bmatrix} = \frac{2}{3} \begin{bmatrix} \cos(\omega_e t) & \cos(\omega_e t - \frac{2\pi}{3}) & \cos(\omega_e t + \frac{2\pi}{3}) \\ \sin(\omega_e t) & \sin(\omega_e t - \frac{2\pi}{3}) & \sin(\omega_e t + \frac{2\pi}{3}) \end{bmatrix} \begin{bmatrix} i_a \\ i_b \\ i_c \end{bmatrix} \quad (5.4)$$

Substituting Equations 5.1 through 5.3 into Equation 5.4, the stator currents in the rotor reference frames are obtained as

$$\begin{bmatrix} i_q \\ i_d \end{bmatrix} = i_s \begin{bmatrix} \sin(\delta) \\ \cos(\delta) \end{bmatrix} \quad (5.5)$$

where i_s is the resultant current vector of i_q and i_d in the dq reference frame, also referred to as the stator current phasor.

The fact that the q- and d-axes currents are constants in rotor reference frames is to be noted, as the torque angle δ is a constant for a given load torque. Thus, the phasor diagram of the machine could be drawn as shown in Fig.5.1. The rotor flux and its linkages are on the d-axis of the machine, which is right on the rotor and rotates at the angular velocity of ω_e electrical rad/s measured from the stator reference frame by its instantaneous position of θ_e radian, which can be obtained from the product of angular velocity and time, assuming that the initial position of the rotor is zero.[16] The stator current phasor, which is the result of quadrature and direct axes currents in the rotor reference frame, is supplied at an angular frequency of rotor electrical speed, i.e., ω_e electrical rad/s with a phase of δ radian from the rotor flux linkage phasor. The differential velocity between the current phasor and the rotor is zero. But it has a phase difference of δ radian, which is a constant for a given torque and programmed into the stator currents. The resolution of the stator current phasor on the rotating direct and quadrature axes gives i_d and i_q , respectively, and correspond to the current components given by Equation 5.5. Note that they are constants for a given stator current phasor and torque angle.

The stator current component along the rotor flux axis, i.e., along the rotating d-axis, can only produce a flux and hence can be appropriately named as the flux-producing component of the stator current and denoted as i_f . This current only

partially contributes to the d-axis flux, and the remaining part of the rotor flux is contributed by the permanent magnets of the machine.[16] The component in quadrature with the rotor flux can produce a torque in interaction with the rotor flux and hence may be appropriately named the torque producing current, i_T , very similar to the armature current of the separately excited DC machine. They may then be represented in terms of the stator currents on the q- and d-axes as

$$i_q = i_T \quad (5.6)$$

$$i_d = i_f \quad (5.7)$$

In order to complete the phasor diagram, the voltage phasor can be assumed to be leading the stator current phasor by an angle ϕ , whose cosine is the power factor of the machine and which may be recalled from the fundamentals. Its components along the d- and q-axes are v_{ds}^r and v_{qs}^r , respectively, and they are shown in Fig.5.1.

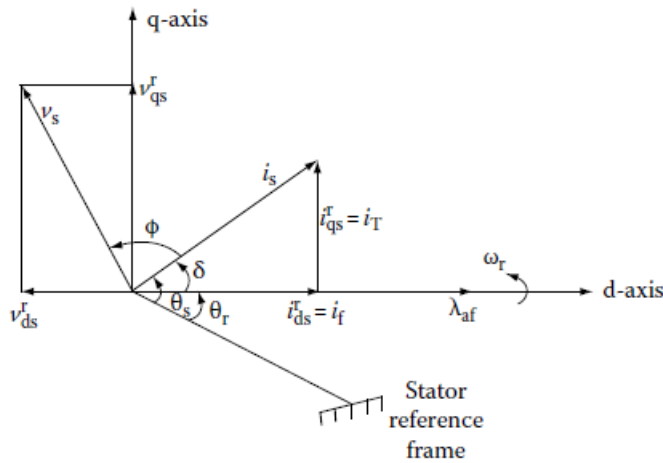


Figure 5.1: Phasor Diagram of PMSM. [16]

Note that i_d and i_q are shown as i_{ds}^r and i_{qs}^r , v_d and v_q are shown as v_{ds}^r and v_{qs}^r , while θ_e and ω_e are shown as θ_r and ω_r finally, λ_m is shown as λ_{af} in Fig.5.1

5.1.1 Electromagnetic Torque

Recalling the torque equation from chapter 4, which was given by

$$T_e = \frac{3}{2} \frac{P}{2} [\lambda_m i_q + (L_d - L_q) i_q i_d] \quad (5.8)$$

Assuming that the stator flux current component is zero by making the torque angle equals 90° , i.e., $i_d = 0$. Thus, getting the torque equation as [16]

$$T_e = \frac{3}{2} \frac{P}{2} \lambda_m i_q = K_1 \lambda_m i_q \quad (5.9)$$

where

$$K_1 = \frac{3}{2} \frac{P}{2} \quad (5.10)$$

Note that the torque-producing component of the stator current phasor is equal to the stator current phasor magnitude itself, as the torque angle becomes equal to 90° . Under this circumstance, the PMSM becomes exactly analogous to a separately excited DC machine, as seen from the torque expression, where the torque is produced by the interaction of the rotor flux and stator current, whereas in the DC machine, it is produced by the interaction of the stator flux and rotor (well-known as armature) current.[16]

Substituting for the quadrature and direct axis stator currents in the rotor reference frames from Equation 5.5 in the torque expression, the torque is expressed in terms of the stator current magnitude and the torque angle as

$$T_e = \frac{3}{2} \frac{P}{2} [\lambda_m i_s \sin(\delta) + \frac{1}{2} (L_d - L_q) i_s^2 \sin(2\delta)] \quad (5.11)$$

The first component of the equation on the right-hand side corresponds to the synchronous torque caused by the interaction of the PM field and the stator current, while the second term stands for the torque produced by a reluctance fluctuation, also known as the reluctance torque. Fig 5.2 depicts the torque of the PMSM. The equation shows that electromagnetic torque is determined by stator current magnitude and torque angle, while machine inductances and rotor flux linkages remain constant.

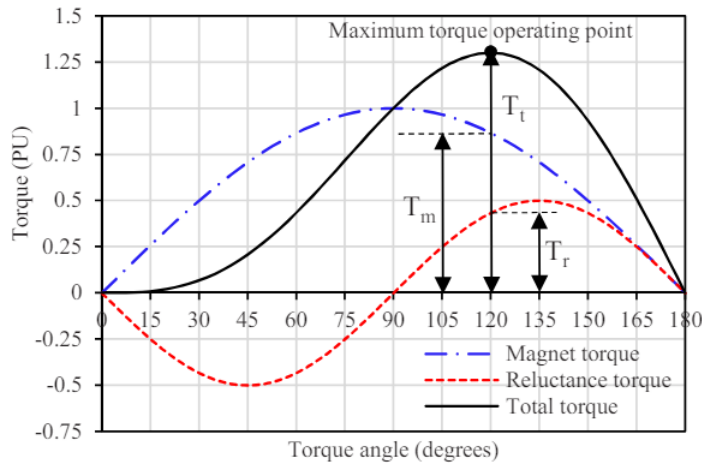


Figure 5.2: Torque graph of PMSM. [11]

Where T_m is the torque due to the interaction of the PM field and the stator current, T_r is the reluctance torque, and T_t is referred to as the total torque ($T_t = T_e$).

5.1.2 Mutual Flux Linkages

Mutual flux linkages in the air gap are established by rotor and stator flux linkages. Control requires weakening the flux in the air gap, similar to how it is done in a separately excited DC motor. Rotor flux linkages are focused along the d-axis (e.g., north pole of a two-pole PM rotor), with zero quadrature axis component. However, stator flux linkages have two non-zero components: one along the direct axis and another along the quadrature axis which are $L_d i_d$ and $L_q i_q$, respectively, where L_d and L_q are the direct and quadrature axes inductances, respectively. The flux combine with the rotor flux linkages in both direct and quadrature directions to give the result air gap or mutual flux linkages.[\[16\]](#) The result of the mutual direct and quadrature flux linkages is obtained by their phasor sum, the magnitude of which is given as

$$\lambda_{mr} = \sqrt{(\lambda_d)^2 + (\lambda_q)^2} \quad (5.12)$$

where,

$$\lambda_d = \lambda_m + L_d i_d \quad (5.13)$$

$$\lambda_q = L_q i_q \quad (5.14)$$

The phase of the mutual flux linkages is given by the arc-tan of the ratio between the quadrature-to-direct-axis mutual flux linkages.

5.1.3 Key Results

This section's primary findings serve as the foundation for controlling the PMSM drive and its implementation. The summary serves as an aid for relatively simple reference.[\[16\]](#)

1. Control of phase δ (e.g. torque angle), and the magnitude of the current phasor, i_s , achieved through the inverter through torque and its control.
2. Control of the angular frequency of the phasor current determines the rotor speed, ω_e electrical rad/s.
3. The PMSM drive resembles to the separately excited DC motor drive. To do this, find the equivalent of the DC machine's field and armature currents in the PMSMs, i_f and i_T , respectively. They are components of the stator current phasor and referred to as flux- and torque-producing components of stator current.
4. Independent control of the electromagnetic torque and the mutual flux is exercised through the torque- and flux-producing stator current components, similar to that of the separately excited DC motor drive with its independent control of its armature and field currents.

5.2 Control Strategies

FOC is based on the rotor flux orientation. To regulate the torque of a PMSM, control the stator current vector. Using vector control, PMSM can be controlled similarly to a DC motor, resulting in adequate performance. The FOC approach is frequently employed in high-performance motor drives.

To control the electromagnetic torque, the allocation of the excitation current component i_d and the torque current component i_q should be considered according to the electromagnetic torque as shown in equation 5.8. Currently, the $i_d = 0$ control and the maximum torque per ampere (MTPA) control are the most popular vector control strategies.[\[9\]](#)

5.2.1 $i_d = 0$ Control Strategy

$i_d = 0$ vector control strategy involves regulating the excitation current i_d to zero. Consequently, the electromagnetic torque is related to the torque current i_q . As shown in Fig.5.3, the permanent flux linkage λ_m is on the d-axis and rotates with the rotor electrical position θ_e to achieve the rotor flux orientation. The excitation current is zero, and the torque current is equal to the amplitude of the stator current vector. The stator voltage vector is u , and the stator current vector is i .

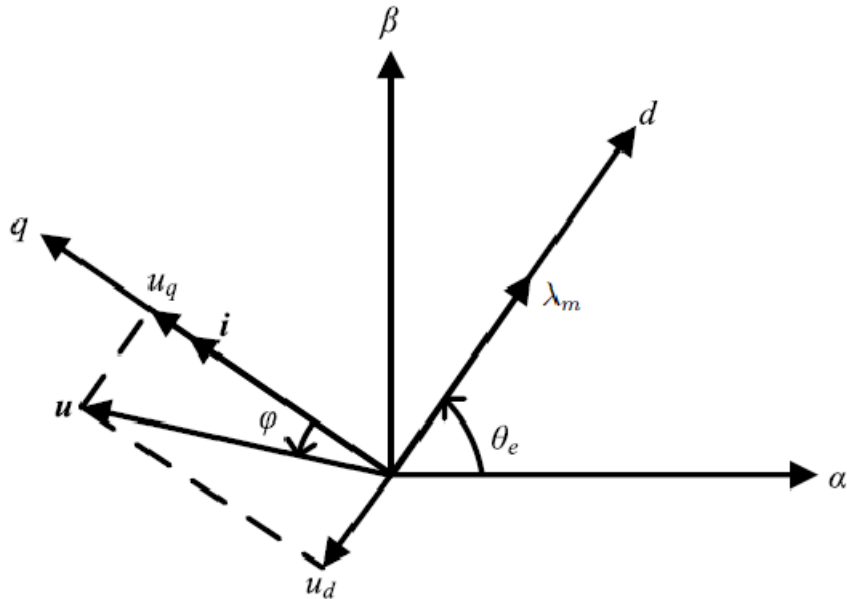


Figure 5.3: Space vector diagram of $i_d = 0$ control. [\[9\]](#)

In this control mode, the torque generation is realized by controlling i_q . Therefore, the control system is simple to implement, and high-performance torque control can be achieved. This control mode is ideal for SM-PMSM drives since it minimises stator current while maintaining the same output torque. However, for the interior PMSM, the sacrifice of the reluctance torque component will reduce the efficiency of the motor. With the increase of the load, the stator current increases gradually,

and the cross-axis flux increases accordingly, which increases the angle between the stator voltage vector and the stator current vector, resulting in the decrease of the power factor.[9]

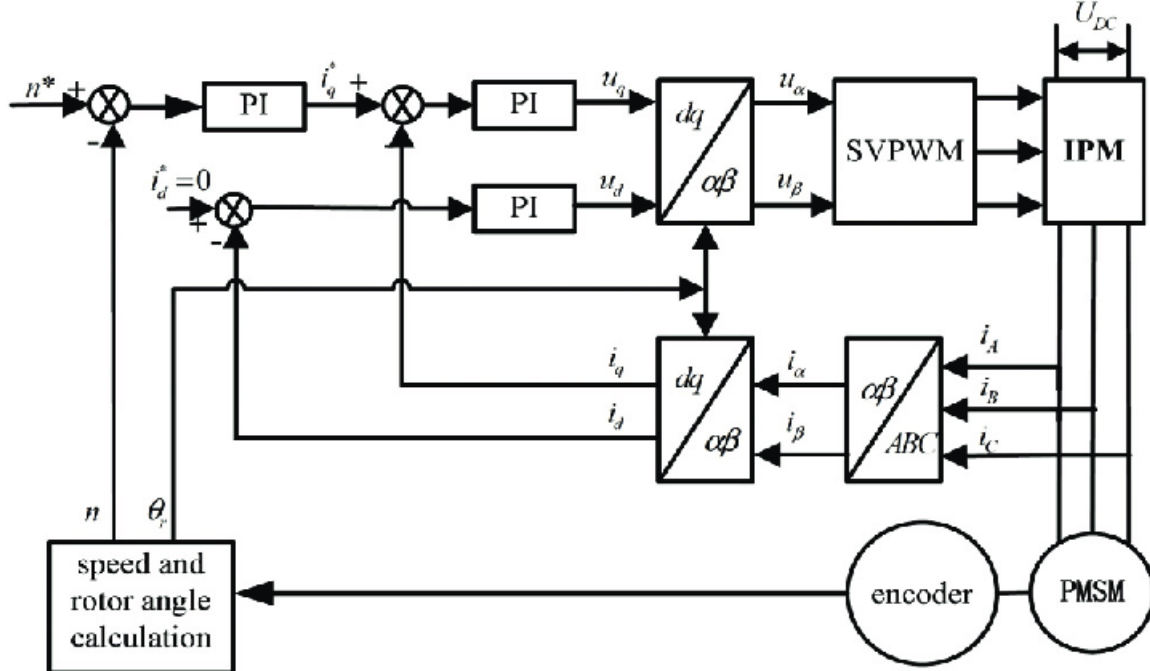


Figure 5.4: FOC Block diagram of $i_d = 0$ control. [20]

5.2.2 Maximum Torque Per Ampere Control (MTPA)

MTPA is a vector control method to minimize the stator current under the same output torque for interior PMSM. The MTPA point is the point closest to the origin among the points on the constant torque curve in the current plane. And, the MTPA point is also the point with the minimum magnitude in the constant torque curve as shown in Fig.5.5.

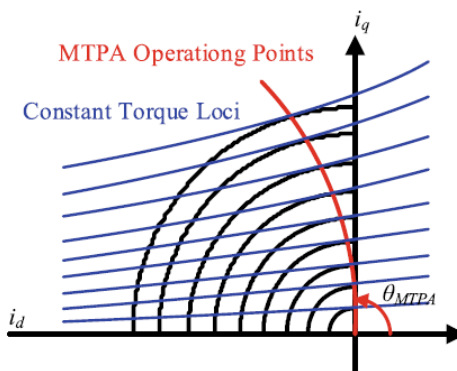


Figure 5.5: MTPA operating points and the constant torque loci in the current plane. [9]

In Fig.5.6, the constant torque locus is shown in the current plane at the synchronous reference frame. As can be seen, no matter whether $\frac{\partial T_e}{\partial \delta} > 0$ or $\frac{\partial T_e}{\partial \delta} < 0$, the magnitude of the vector is larger than the middle vector. In order to achieve MTPA vector control, the stator current should satisfy the following constraint [9],

$$\frac{\partial T_e}{\partial \delta} = \frac{3P}{4} i_s [\lambda_m \cos(\delta) + (L_d - L_q) i_s \cos(2\delta)] = 0 \quad (5.15)$$

which is the partial differentiation of equation 5.11 with respect to the torque angle δ .

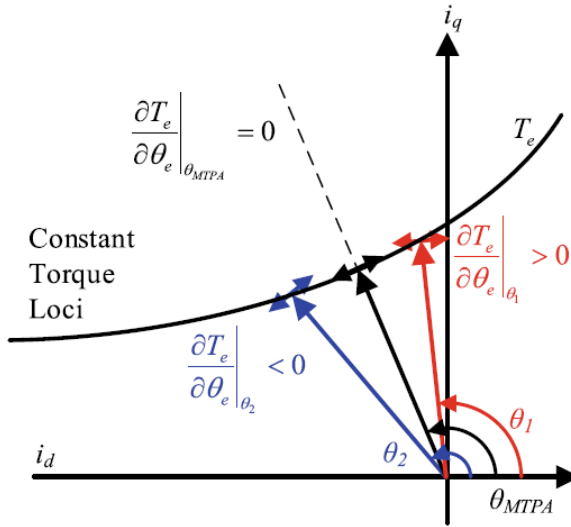


Figure 5.6: Locus of the constant torque in the current vector plane [9]

The current angle of the MTPA point δ_{MTPA} can be derived from equation 5.15 as follows

$$\delta_{MTPA} = \cos^{-1} \left(\frac{-\lambda_m + \sqrt{\lambda_m^2 + 8(L_d - L_q)^2 i_s^2}}{4(L_d - L_q) i_s} \right) \quad (5.16)$$

From equation 5.5 , the exciting current and the torque current components in MTPA control mode can be obtained as

$$i_{d|MTPA}^* = i_s \cos \delta_{MTPA} \quad (5.17)$$

$$i_{q|MTPA}^* = i_s \sin \delta_{MTPA} \quad (5.18)$$

where $i_{d|MTPA}^*$ is the d-axis current reference in MTPA control mode, $i_{q|MTPA}^*$ is the q-axis current reference in MTPA control mode. Thus, the optimal exciting current and torque current components can be obtained for a desired torque by using the MTPA control strategy.[9]

The FOC block diagram with MTPA is shown in Fig.5.7

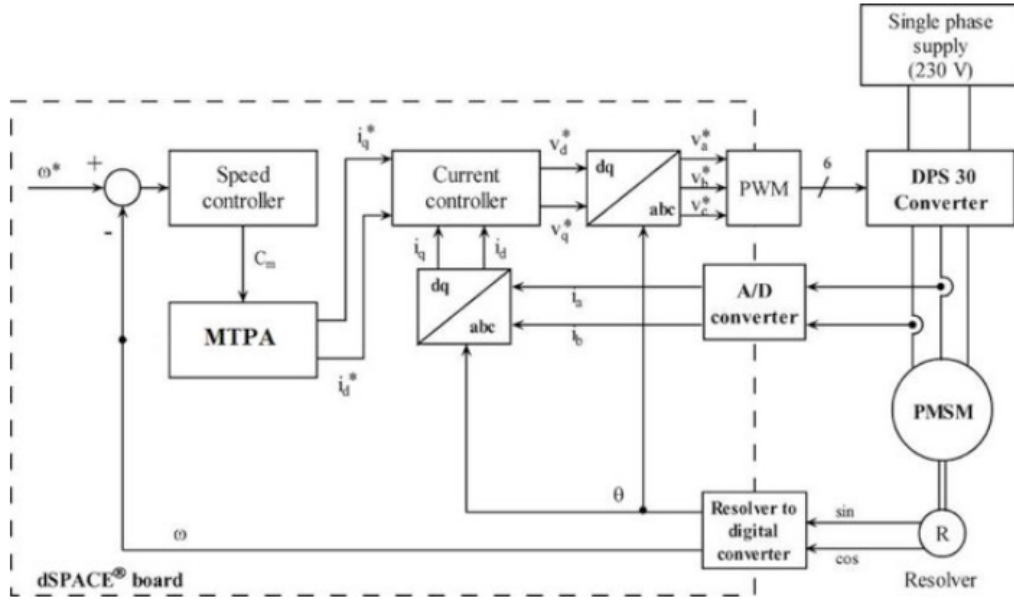


Figure 5.7: FOC Block diagram of MTPA control strategy [4]

5.2.3 Flux-Weakening Control

5.2.3.1 Principle of the Flux-Weakening Control

PMSM drives restrict the amplitudes of the stator current and voltage vector to the rated current of the IGBT and the DC-link voltage. The maximum voltage and current are designated as U_{smax} and I_{smax} , respectively.[9] Generally, the amplitude of the stator current and the voltage vector should meet the following constraints:

$$|i| \leq I_{smax} \quad (5.19)$$

$$|u| \leq U_{smax} \quad (5.20)$$

where $|i|$ and $|u|$ are the amplitude of the stator current vector and stator voltage vector, respectively.

As can be seen from equation 4.81, if PMSM operates in steady state, the differential terms in the voltage equation are equal to zero. Meanwhile, when the motor operates beyond the base speed, the voltage drop on the stator resistance can be neglected.[9] Ultimately, the motor voltage equations can be represented as

$$v_d = -\omega_e L_q i_q \quad (5.21)$$

$$v_q = \omega_e L_d i_d + \omega_e \lambda_m \quad (5.22)$$

Thus, the voltage boundary can be obtained in equation 5.23

$$(L_d i_d + \lambda_m)^2 + (L_q i_q)^2 \leq \left(\frac{U_{smax}}{\omega_e} \right)^2 \quad (5.23)$$

$$i_d^2 + i_q^2 \leq I_{smax}^2 \quad (5.24)$$

From equation 5.23 that the voltage boundary of the interior PMSM is an elliptical cluster with the point $(\frac{\lambda_m}{L_d}, 0)$ as the center and the length and the radius are reduced proportionally with the increase of the operation speed. The current boundary is shown as equation 5.24, which is a circle centered on the origin. The radius of the current limit circle is I_{smax} , Fig.5.8 depicts this clearly.

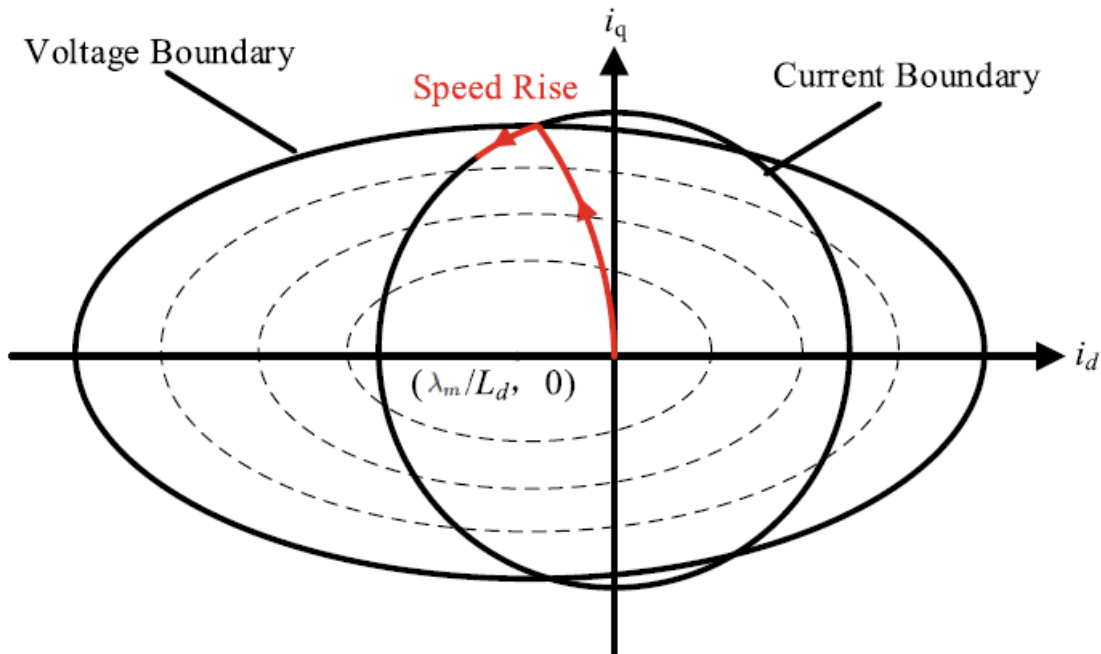


Figure 5.8: Schematic diagram of voltage and current boundary [9]

As the speed increases, the voltage limit ellipse gets smaller towards the centre. In the flux-weakening operation, the current trajectory can only move to the left in the d-axis when it intersects the voltage and current boundaries, as shown by the arrow-line.[9]

5.2.3.2 Flux-Weakening Control Scheme

The voltage closed-loop flux-weakening method is the most commonly used flux-weakening scheme. The amplitude of the stator voltage vector $|u^*|$ is compared with the limit voltage U_{smax} . When $|u^*| < U_{smax}$, the PI regulator is positively saturated, and therefore, $\Delta i_d = 0$. Otherwise, when $U_{smax} \leq |u^*|$, the PI regulator will work to produce a negative Δi_d to reduce the reference of the d-axis current. this can be shown in Fig.5.9.

The voltage closed-loop flux-weakening method integrated with the vector control strategy is shown in Fig.5.9. The vector control scheme consists of the current loop and the speed loop. The d-q-axes current references are allocated by MTPA

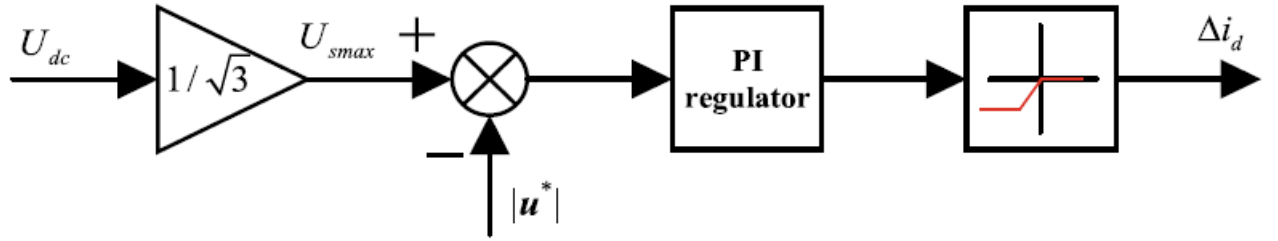


Figure 5.9: Block diagram of the voltage closed-loop flux-weakening scheme[9]

control strategy to maximize the electromagnetic torque when the motor operates below the base speed. The voltage references v_d^* and v_q^* are used to calculate the amplitude of the stator voltage vector. When $|u^*| > U_{smax}$, the negative Δid is added to the d-axis current reference directly.

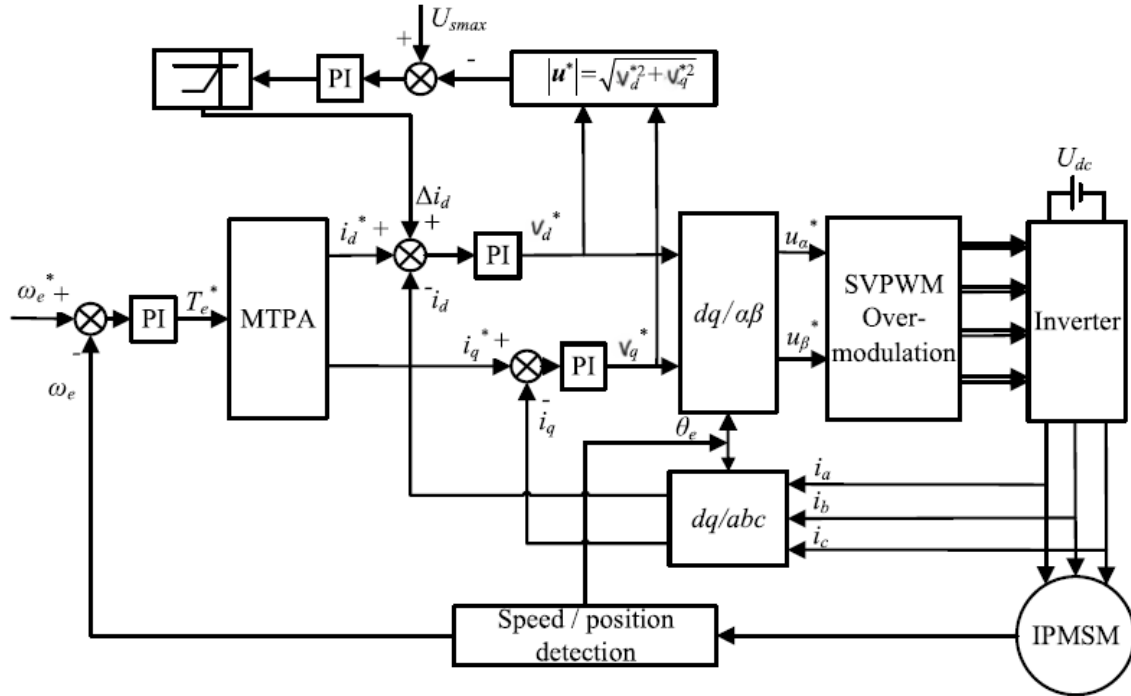


Figure 5.10: Block diagram of the voltage closed-loop flux-weakening control and MTPA control[9]

Numerous flux-weakening control algorithms have been developed throughout the years, including single current regulation and voltage angle adjustment. While each technique has unique features, they should adhere to the same design principles as outlined above.

5.3 PI Controllers

The proportional controller, commonly referred to as the PI controller, is a crucial element of the industrial automation and control system. It is a closed-loop feedback control method that attempts to adjust the process variable by manipulating it depending on the difference between the set-point and the process variable. It finds a balance between responding swiftly to errors and long-term error elimination. Tuning the controller allows adjustment to meet the desired value.

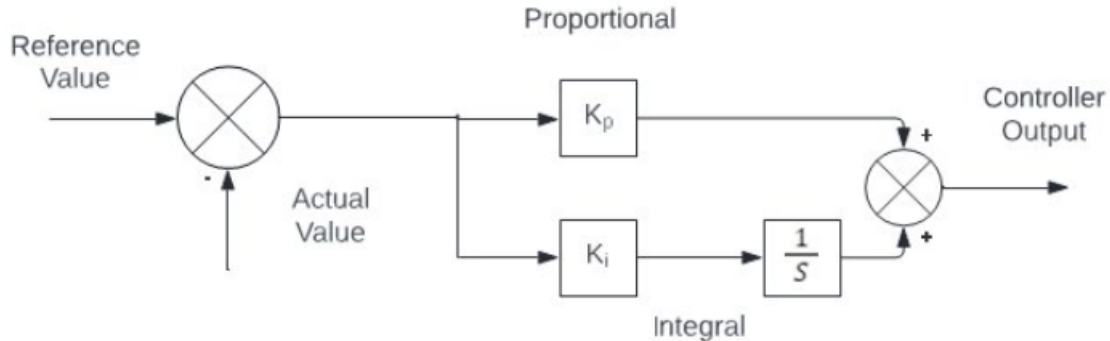


Figure 5.11: Block diagram of the PI controller[31]

where, K_p is the proportional gain and K_i is the integral gain.

PI controller is a combination of Proportional controller action and Integral controller action which is designed to regulate a process variable based on its set-point and manipulated variable. Also, it can be identified as a combination of proportional and integral controllers. The transfer function of the PI controller can be expressed as

$$G_C(s) = K_p \frac{1 + T_i s}{T_i s} \quad (5.25)$$

Where, $G_C(s)$ is the transfer function of the PI controller, K_p is the proportional gain and T_i is the integral time constant. $T_i = \frac{K_p}{K_i}$

As shown Fig.5.4, the PI controller is a fundamental and critical component in the (FOC) approach for controlling the speed and torque of PMSM. It plays a pivotal role in regulating both speed and current. Thus ensuring precise control over motor performance. In the FOC scheme, there typically exists one PI controller dedicated to regulating motor speed, ensuring that it tracks the desired reference speed accurately. Additionally, for controlling the motor currents along the d-axis (i_d) and q-axis (i_q), there are usually two separate PI controllers. These controllers ensure that the motor currents align with the reference values, thereby controlling the torque production effectively.

Furthermore, in advanced control strategies such as flux weakening, an additional PI controller may be employed as shown in Fig.5.10. Flux weakening allows

the motor to operate beyond its rated speed by reducing the flux weakening current component, thereby enabling higher speeds while maintaining stable operation. Consequently, if flux weakening is employed, an extra PI controller is necessary to regulate the flux weakening current component, ensuring smooth transition and optimal performance across the extended speed range. Thus, the PI controller stands as a cornerstone in the FOC strategy, facilitating precise control over PMSM speed, torque, and, when applicable, flux weakening.

5.3.1 The Current Controller

The task of the current controller is to set the component of the motor voltages v_d and v_q in such a way that the desired current component i_d^* and i_q^* are set. In order to achieve the maximum Torque per ampere (MTPA), the desired d-current component is set to zero in case of SM-PMSM in the case of MTPA of IPMSM the i_d^* and i_q^* values are calculated through equations 5.17 and 5.18.

The voltage references v_d^* and v_q^* that are produced from the two current regulators which then are transformed to into the $\alpha\beta$ frame then fed to the space vector pulse width modulation unit (SVPWM) or then transformed again to the abc frame then fed to the sinusoidal pulse width modulation unit (SPWM) to generate pulsing signals to the power switches of the inverter. as shown in chapter 4 equation 4.81 the voltage equations have dependency on each other which makes the system a coupled system with two actuating variables i_d and i_q . in order to compensate this coupling effect a dynamic cross-axis decoupling control using feed-forward control by considering that the desired voltages consist of an initial voltages level and a change in voltage Δv as follows[30]:

$$v_d^* = v_d^f + \Delta v_d^* \quad (5.26)$$

$$v_q^* = v_q^f + \Delta v_q^* \quad (5.27)$$

where the initial voltage level v_d^f and v_q^f are considered as follows:

$$v_d^f = -\omega_e L_q i_q \quad (5.28)$$

$$v_q^f = \omega_e L_d i_d + \omega_e \lambda_m \quad (5.29)$$

The change in voltage is relative to the output of the current controller considering the current controller transfer function as $G_{ci}(s)$ while the controller input is the error value between the desired and the actual current values. The delta voltage is illustrated as:

$$\Delta v_d^* = G_{ci}(s)(i_d^* - i_d) \quad (5.30)$$

$$\Delta v_q^* = G_{ci}(s)(i_q^* - i_q) \quad (5.31)$$

By substituting equations 5.31 and 5.30 in 5.28 and 5.29

$$v_d^* = -\omega_e L_q i_q + [G_{ci}(s)(i_d^* - i_d)] \quad (5.32)$$

$$v_q^* = \omega_e L_d i_d + \omega_e \lambda_m + [G_{ci}(s)(i_q^* - i_q)] \quad (5.33)$$

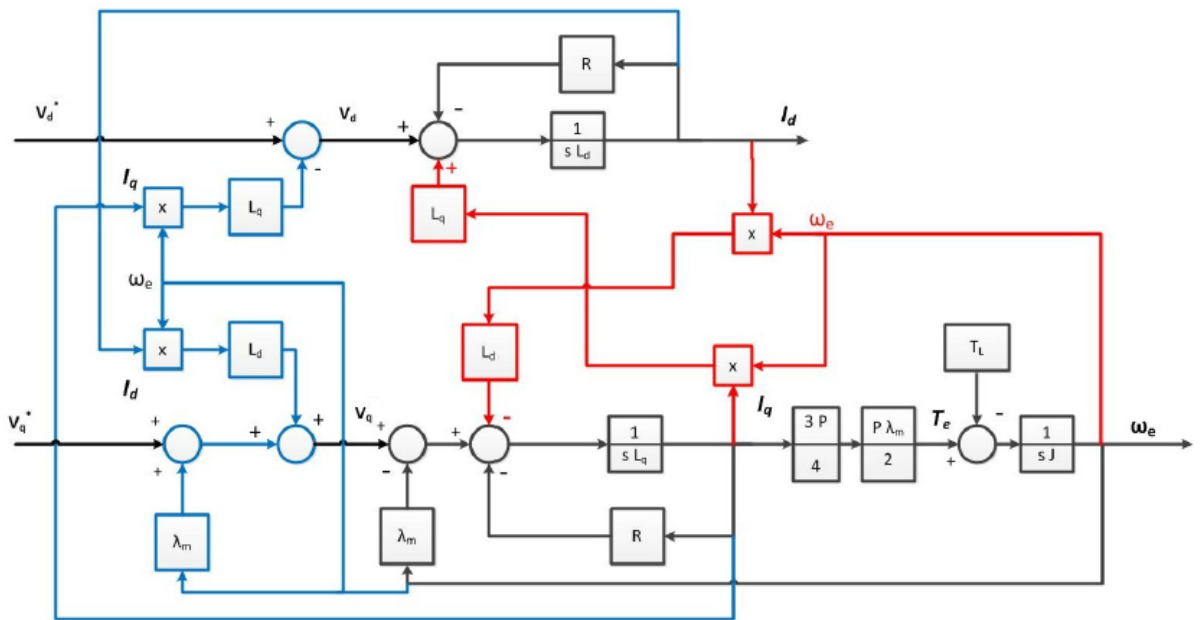


Figure 5.12: Dynamic Cross-Axis Decoupling Control[1]

5.3.2 The Speed Controller

The speed controller's duty is to produce the torque needed for this current controller loop. The maximum current of the motor and power electronics limits the proportional current to achieve the necessary torque i_q^* before applying it to the current controller. This ensures that the current remains within the motor's range. The desired torque is relevant to the difference in value between the desired and actual speed ω_r^* and ω_r respectively, while the generating torque current component i_q^* is related to the desired torque through the equation considering the desired value of the d current component is set to zero to achieve the maximum torque per current amp (MTPA) for the SM-PMSM which is $i_d = 0$ control strategy.[30] As for the IPMSM the MTPA of the IPMSM, the values i_d^* and i_q^* are calculated through equations 5.17 and 5.18.

$$i_q^* = \frac{4}{3P\lambda_m} T_e^* \quad (5.34)$$

To compute the net desired electromagnetic torque T_e^* , the speed controller transfer function $G_{cs}(s)$ is multiplied by the error speed value.

$$T_e^* = (\omega_r^* - \omega_r) G_{cs}(s) \quad (5.35)$$

5.3.3 Controllers Design

The system has two loops: an inner loop with the current controller, plant, and delay time constant, and an outside loop with the speed controller and delay time constant. A speed controller controls the current component that produces the necessary torque to reach the desired speed. The proportional current to this desired torque i_d^* is limited by the maximum current of the motor before being applied to the current controller. This ensures that the current remains within the motor's range. The delay time constants refer to the system delays caused by sensors, switching circuits, and control implementation.[30] The magnitude optimum is an optimum approach that helps identify the optimal controller settings for a specific configuration. The Symmetrical Optimum criterion is more known because of its successful application in the control of electric motor drives.

The method used to tune the controllers is discussed thoroughly in [32] and [26].

5.3.3.1 Design of the Current Controller

The current controller is designed using the magnitude-optimum technique. The plant transfer function is based on an RL-element without considering the effect of the EMF. The back EMF is not considered due as it has been feed-forward compensated through the dynamic cross-axis decoupling as shown above. Thus, the plant transfer function could be expressed as

$$G_s(s) = \frac{I(s)}{V(s)} \quad (5.36)$$

where

$$G_s(s) = \frac{1}{R_s + sL_q} = \frac{1}{R_s} \cdot \frac{1}{1 + sT_{cs}} \quad (5.37)$$

where T_{cs} is the stator time constant shown. R_s is the stator resistance, and L_q is the q-axis inductance. The same goes for the d-axis.

Considering $T_{\sigma I}$ as the total delay time constants of the inner control loop, the plant transfer function can then be expressed as:

$$G_s(s) = \frac{1}{(R_s + sL_q)(1 + sT_{\sigma I})} \quad (5.38)$$

Let $K_s = \frac{1}{R_s}$. Thus, the transfer function could be expressed as

$$G_s(s) = \frac{K_s}{(1 + sT_s)(1 + sT_{\sigma I})} \quad (5.39)$$

Introducing K_p as the proportional gain and T_i as the integral time constant of the PI current controller.

$$G_C(s) = K_p \frac{1 + T_i s}{T_i s} \quad (5.40)$$

Therefore, the open loop transfer function $W_{OL}(s)$, which is The product of the plant and the current controller transfer functions could be represented as

$$W_{OL}(s) = K_p \frac{1 + T_i s}{T_i s} \cdot \frac{K_s}{(1 + sT_s)(1 + sT_{\sigma I})} \quad (5.41)$$

The magnitude optimal technique has the following design rule: the zero T_i of the controller needs to be determined in such a way that pole zero cancellation between dominant time constant of the object T_{cs} . $T_i = T_{cs}$. Therefore, the open-loop transfer function could be expressed as

$$W_{OL}(s) = K_p \frac{1}{T_i s} \cdot \frac{K_s}{(1 + sT_{\sigma I})} \quad (5.42)$$

Considering the normalized gain K_n [30] to be expressed as

$$K_n = \frac{T_{\sigma I}}{T_s} \cdot K_p \cdot K_s \quad (5.43)$$

Substituting it in equation 5.42.

$$W_{OL}(s) = K_n \frac{1}{sT_e} \cdot \frac{1}{(1 + sT_{\sigma I})} \quad (5.44)$$

$$W_{OL}(j\omega) = K_n \frac{1}{j\omega T_e} \cdot e^{-j\omega T_e} \quad (5.45)$$

The normalized frequency could be represented as

$$\Omega = \omega \cdot T_{\sigma I} \quad (5.46)$$

The open-loop transfer function expressed as a function of the normalized frequency

$$W_{OL}(j\Omega) = K_n \cdot \frac{e^{-j\Omega}}{j\Omega} \quad (5.47)$$

The closed-loop transfer function could be expressed as

$$W_{CL}(s) = \frac{W_{OL}(s)}{1 + W_{OL}(s)} = \frac{1}{1 + s \frac{T_{\sigma I}}{K_n} + s^2 \frac{T_{\sigma I}^2}{K_n}} \quad (5.48)$$

$$W_{CL}(\Omega) = \frac{K_n e^{-j\Omega}}{j\Omega + K_n e^{-j\Omega}} = \frac{K_n}{j\Omega e^{j\Omega} + K_n} = \frac{K_n}{K_n - \Omega \sin(\Omega) + j\Omega \cos(\Omega)} \quad (5.49)$$

phase margin ϕ_R , This phase implies the system is on the verge of instability and is calculated through the open-loop transfer function $W_{OL}(\Omega)$ has to be solved for the cross-over normalized frequency of unity magnitude.[30]

$$\|W_{OL}(\Omega)\|^2 = 1 \quad (5.50)$$

This equation yields the cross-over normalized frequency

$$\Omega = K_n \quad (5.51)$$

$$W_{OL}(K_n) = e^{j(-\frac{\pi}{2} - k_n)} \quad (5.52)$$

The phase margin is defined as

$$\phi_R = \pi + \angle W_{OL}(K_n) = \pi + (-\frac{\pi}{2} - k_n) = \frac{\pi}{2} - k_n \quad (5.53)$$

Choosing the normalized gain $K_n = \frac{1}{2}$ as the magnitude optimum design rule [30] will result in a phase margin of $\phi_R = 61^\circ$. The bandwidth of the current controller is the 3 dB-point at which the magnitude is a factor of $\frac{1}{\sqrt{2}}$ of the maximum amplitude, where it is shown as

$$\|W_{CL}(\Omega)\|^2 = \frac{1}{2} \quad (5.54)$$

This equation results that normalized bandwidth is expressed as

$$K_n = \omega_{B\phi} \sin(\omega_{B\phi}) \quad (5.55)$$

With $K_n = \frac{1}{2}$, the resulting normalized bandwidth will be $\omega_{B\phi} = 0.74$. The relationship between the normalized bandwidth and the system inner loop time delay $T_{\sigma I}$ can be expressed as[30]:

$$f_{B\phi} = \frac{\omega_{B\phi}}{2\pi T_{\sigma I}} \quad (5.56)$$

From equation 5.56, It demonstrates that there is an inverse relationship between the bandwidth frequency and the current controller time delay.[30] since the system is of the second order, so by comparing the coefficients with a standard second order system shown in equation 5.56.

$$G(s) = \frac{1}{1 + \frac{2\zeta s}{\omega_n} + \frac{s^2}{\omega_n^2}} \quad (5.57)$$

$$\omega_n = \frac{\sqrt{K_n}}{T_{\sigma I}} \quad (5.58)$$

$$\zeta = \frac{1}{2\sqrt{K_n}} = \frac{1}{\sqrt{2}} \quad (5.59)$$

Therefore,

$$\frac{T_{\sigma I}}{K_n} = \frac{2\zeta}{\omega_n} \quad (5.60)$$

$$K_n = \frac{1}{2} = \frac{T_{\sigma I}\omega_n}{\frac{2}{\sqrt{2}}} \quad (5.61)$$

$$\omega_n = \frac{\sqrt{2}}{2T_{\sigma I}} \quad (5.62)$$

The bode plot diagram for the system closed inner loop transfer function is shown in Fig.5.13

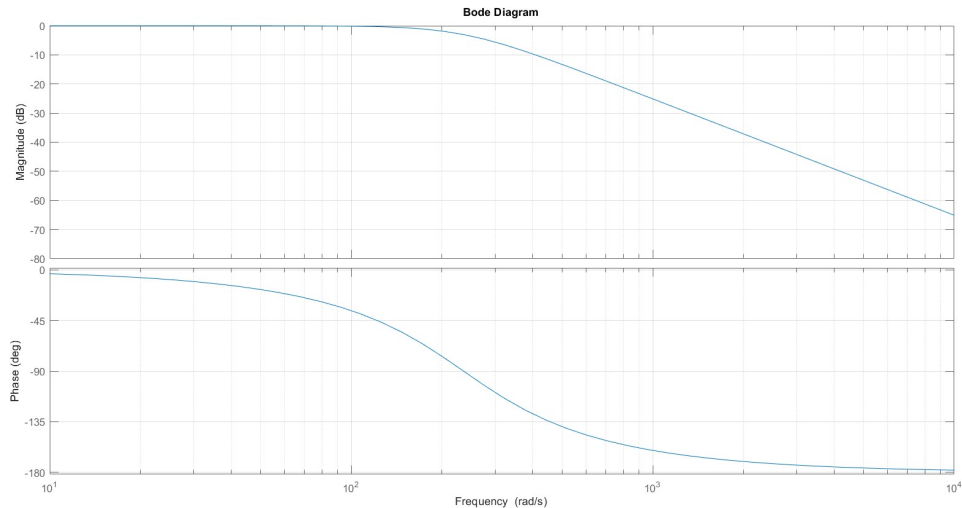


Figure 5.13: Bode plot of closed current controller loop

Substitute in equation 5.43

$$\frac{T_{\sigma I}\omega_n}{2\zeta} = \frac{T_{\sigma I}}{T_{cs}} \cdot K_p \cdot K_s \quad (5.63)$$

$$\frac{\sqrt{2}\omega_n}{2} = \frac{K_p \cdot K_s}{T_{cs}} \quad (5.64)$$

$$K_p = \frac{\sqrt{2} \cdot \omega_n \cdot T_{cs}}{2K_s} \quad (5.65)$$

Substituting equation 5.62 in 5.65

$$K_p = \frac{T_{cs}}{2K_s \cdot T_{\sigma I}} = \frac{T_{cs} \cdot R_s}{2 \cdot T_{\sigma I}} \quad (5.66)$$

The step response for the system closed inner loop transfer function is shown in Fig.5.14

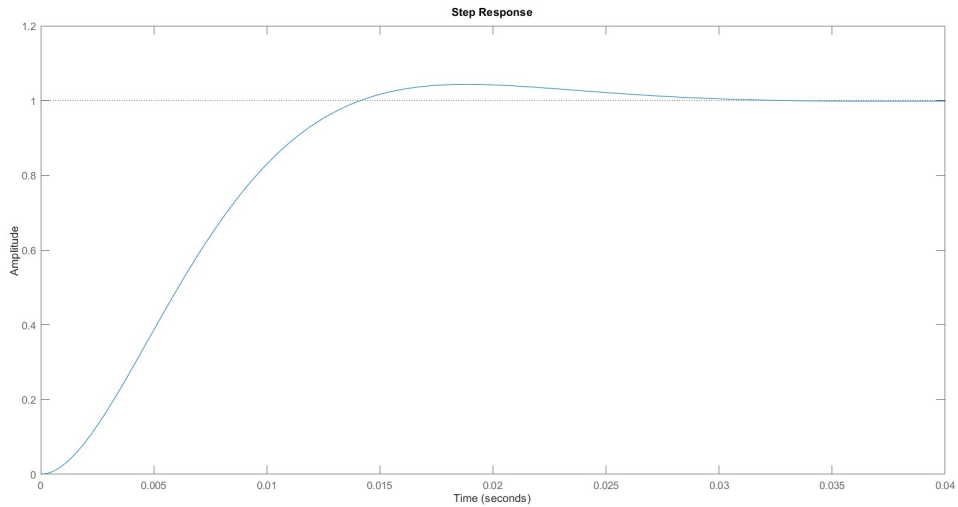


Figure 5.14: Step response of the closed loop function

5.3.3.2 Design of the Speed Controller

A PI-type controller is also employed for speed controller. The symmetrical optimum method is used to design the speed controller. The control parameters are calculated with respect to the results obtained in the current controller. Considering $T_{\sigma s}$ as the total delay time constants of the speed controller and the K_p as the speed controller gain.[\[30\]](#) The outer open loop transfer function is illustrated as follows:

$$W_{OL}(s) = K_p \left(1 + \frac{1}{sT_i} \right) \cdot \frac{1}{sJ} \cdot \frac{1}{1 + sT_{\sigma s}} = \frac{K_p (1 + sT_i)}{s^2 \cdot J \cdot T_i \cdot (1 + sT_{\sigma s})} \quad (5.67)$$

The outer closed loop transfer function can then be expressed as:

$$W_{CL}(s) = \frac{W_{OL}(s)}{1 + W_{OL}(s)} \quad (5.68)$$

Let the square root of a be the ratio between the speed controller reset time and the speed controller delay time constant.[30] Considering the symmetrical optimum design rule method, the cross over frequency should be

$$T_i = a^2 \cdot T_{\sigma s} \quad (5.69)$$

$$\omega_c = \frac{1}{aT_{\sigma s}} = \frac{a}{T_i} \quad (5.70)$$

$$a = \frac{\frac{1}{T_{\sigma s}}}{\omega_c} \quad (5.71)$$

The loop gain at the cross over frequency shall be unity magnitude[30]

$$||W_{CL}(\omega_c)|| = 1 \quad (5.72)$$

Thus, the speed controller proportional gain could be expressed as

$$K_p = \frac{J}{aT_{\sigma s}} \quad (5.73)$$

Choosing $a = 4$ as the symmetrical optimum design rule.[30] Therefore, the speed controller proportional gain could be written as

$$K_p = \frac{J}{4T_{\sigma s}} \quad (5.74)$$

The bode plot diagram for the closed inner loop transfer function of the system is shown in Fig.5.15

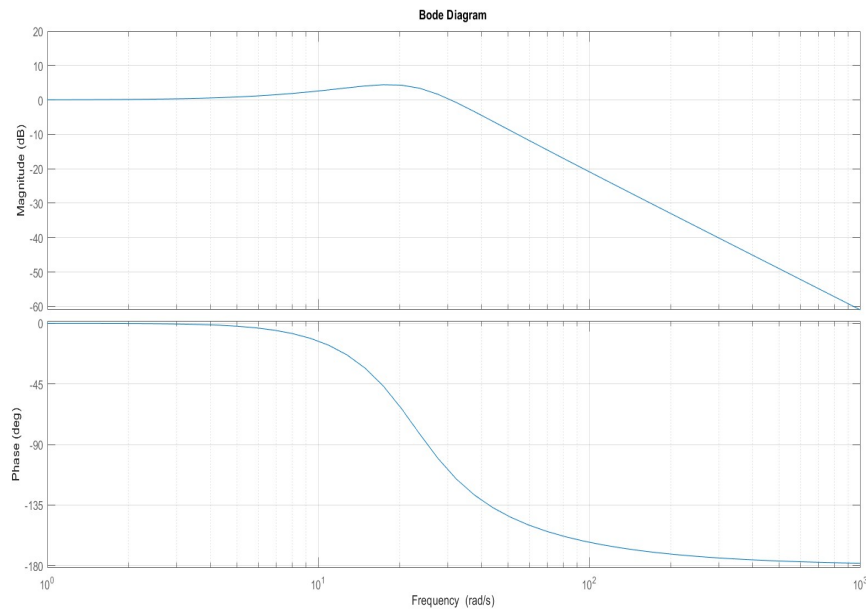


Figure 5.15: Bode plot of closed Speed controller loop

5.4 Inverters and Modulation Techniques

Inverters and modulation techniques are fundamental elements in power electronics, crucial to converting DC to AC power efficiently and accurately. They find extensive applications in diverse sectors such as renewable energy integration, motor drives, uninterruptible power supplies, and industrial processes. By enabling the integration of renewable energy sources such as solar photovoltaics (PV) and wind turbines into the grid and providing precise control over AC motor drives for variable speed applications, inverters play a central role in modern power systems. Modulation techniques, such as pulse-width modulation (PWM), govern the switching of power semiconductor devices within the inverter to regulate output voltage and frequency. These techniques, including carrier-based PWM, space vector modulation (SVM), and selective harmonic elimination (SHE), offer flexibility in achieving desired output waveforms while minimizing harmonic distortion and improving efficiency.[28] Understanding and implementing modulation techniques are crucial for optimizing inverter performance, improving system efficiency, and mitigating electromagnetic interference (EMI).

5.4.1 Inverters

Inverters are essential components of modern power systems, enabling the efficient and precise conversion of direct current (DC) to alternating current (AC). Their relevance extends to a variety of fields, including renewable energy integration, electric cars, uninterruptible power supply, and industrial applications. As the world moves towards cleaner and more sustainable energy sources, inverters play an important role in supporting the integration of renewable energy sources such as solar photovoltaic (PV) and wind turbines into the grid.

The development of inverter technology has been distinguished by significant improvements in efficiency, reliability, and usefulness. From traditional thyristor-based inverters to current high-frequency pulse width modulation (PWM) inverters, the landscape has changed significantly as a result of technological developments in semiconductor devices, control algorithms, and power electronics design.[15]

5.4.1.1 Insulated Gate Bipolar Transistor (IGBT)

Insulated Gate Bipolar Transistors (IGBTs) are widely used in motor drive applications. IGBTs combine MOSFETs' high input impedance with bipolar transistors' low on-state voltage drop, leading to an ideal combination of switching speed and conduction losses. Therefore, they are suitable for medium- to high-power applications such as motor drives, where efficiency and controllability are essential. In addition, other semiconductor devices like MOSFETs (Metal-Oxide-Semiconductor Field-Effect Transistors) and SCRs (Silicon-Controlled Rectifiers) find applications in specific inverter topologies and markets. MOSFETs, known for their fast switching speed and low conduction losses, are favored in high-frequency switching applications. The choice of semiconductor device depends on factors such as power

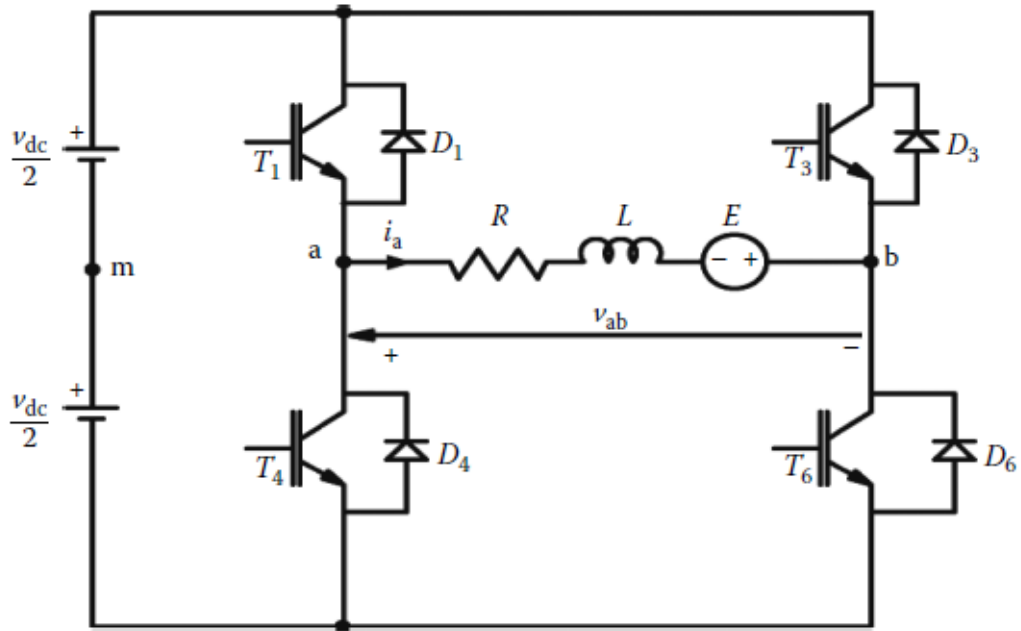


Figure 5.16: Full-wave single-phase inverter [16]

rating, switching frequency, cost considerations, and specific application requirements. In motor drive systems, IGBT-based inverters dominate the landscape due to their robustness, efficiency, and suitability for variable-speed control applications.

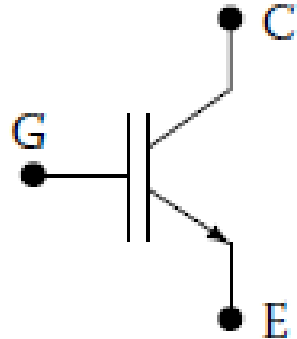


Figure 5.17: IGBT symbol [16]

The current available ratings of these devices are 1.2 kA at 3.3 kV and 0.6 kA at 6.6 kV, with an on-state voltage drop of 5 V. Higher currents are available at reduced voltages with much fewer on-state conduction voltage drops. Commercial improvement of maximum current (1 kA) and voltage (15 kV) ratings is expected in the near future. The switching frequency is usually around 20 kHz for many of the devices and its utilization at high power is at low frequency because of switching losses and electromagnetic interference (EMI) concerns.[16]

5.4.1.2 Three Phase Inverters

Single-phase inverters cover low-range power applications and three-phase inverters cover medium- to high-power applications. The main purpose of these topologies is to provide a three-phase voltage source where the amplitude, phase, and frequency of the voltages should always be controllable. Three-phase inverters are power electronics devices that convert direct current (DC) into three-phase alternating current (AC). It generally consists of six power semiconductor switches connected in a bridge arrangement. The inverter uses pulse-width modulation (PWM) techniques for generating three sinusoidal output voltages with variable amplitude and frequency.

In operation, the inverter changes the DC input voltage to the output phases in a controlled manner, constructing the waveform of the desired AC output and making it capable of controlling the speed and torque of the motor. Three-phase inverters are essential for operating AC motors because they give efficient and precise control over motor operation, resulting in smooth performance, reduced noise, and increased energy efficiency.

Three-phase inverters play an important role in increasing productivity and operating efficiency in industrial and electric vehicles, since the power source of EVs is a battery and a DC source. Thus, to power up and control the PMSM, which is a three-phase AC motor, three-phase inverters are essential.

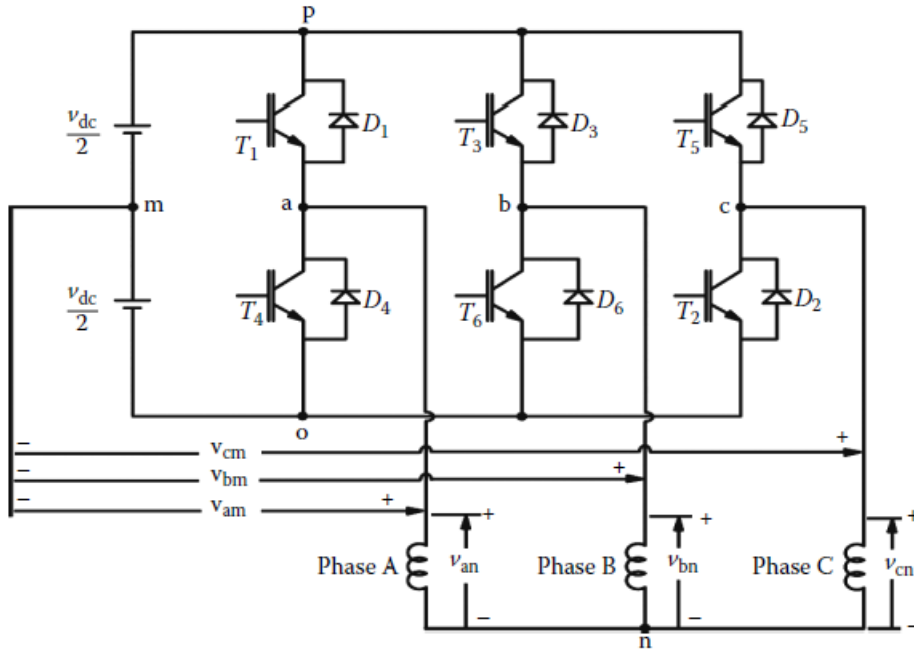


Figure 5.18: Three phase inverter [16]

5.4.1.2.1 Three phase inverter 120° conduction mode.

The 120-degree conduction mode is a fundamental operating mode of three-phase inverters, required for producing balanced three-phase AC voltages. In this mode,

each inverter leg conducts for 120 degrees of the electrical cycle, successively switching the DC input across phases. This sequence generates a sinusoidal output waveform with a phase shift of 120 degrees between consecutive phases, as required for balanced three-phase operation.

The switching sequence is controlled via pulse-width modulation (PWM) techniques, which vary the duration of each switching interval to regulate the amplitude and frequency of the output voltage.

The output line voltages can be determined as follows [1]:

$$v_{ab} = v_{ab} - v_{bn} \quad (5.75)$$

$$v_{bc} = v_{bn} - v_{cn} \quad (5.76)$$

$$v_{ca} = v_{cb} - v_{an} \quad (5.77)$$

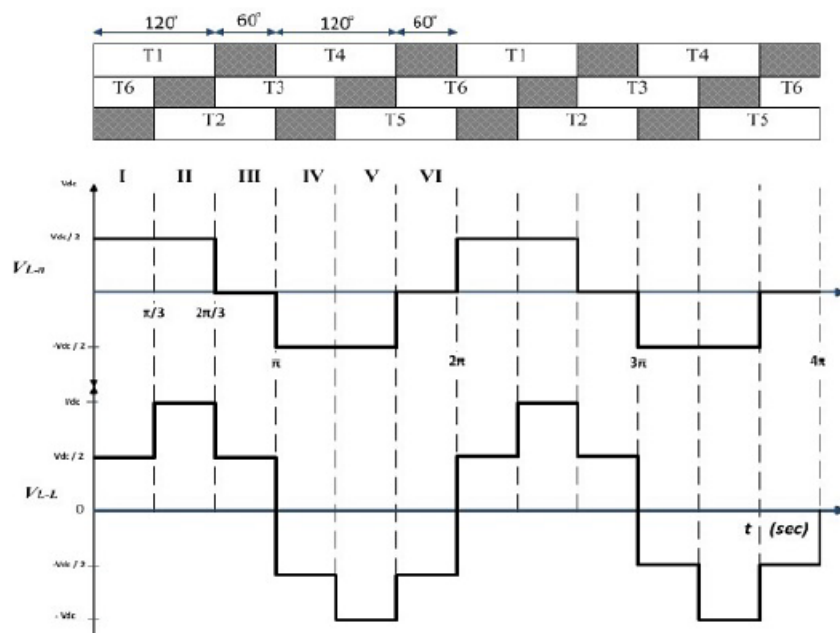


Figure 5.19: 120° conduction mode Line to Neutral Voltage and Line to Line voltage [1]

Therefore, the root mean square line and phase voltage are ($V_{LL} = 0.707V_{dc}$), and phase voltage ($V_{ph} = 0.408V_{dc}$).

Subsequently, the line-to-line voltage has a six-step waveform every cycle, whereas the phase voltage is a quasi square wave. The 120-degree phase shift applies to both the line and phase voltages.[1]

Simulations of both Phase voltages and line-to-line voltages of three phase inverter with $V_{dc} = 200V$ are shown in Fig. 5.20 and Fig. 5.21, respectively.

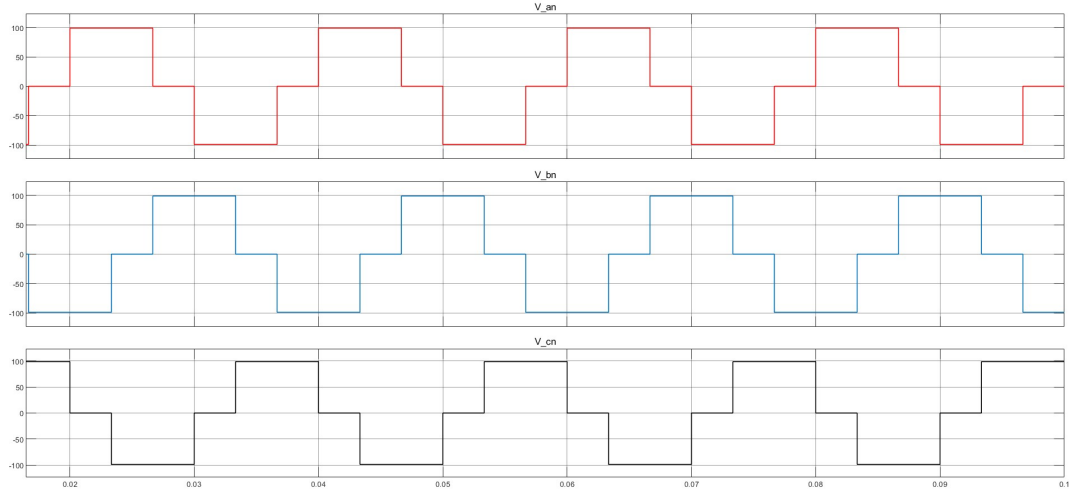


Figure 5.20: 120° conduction mode Line to Neutral Voltage

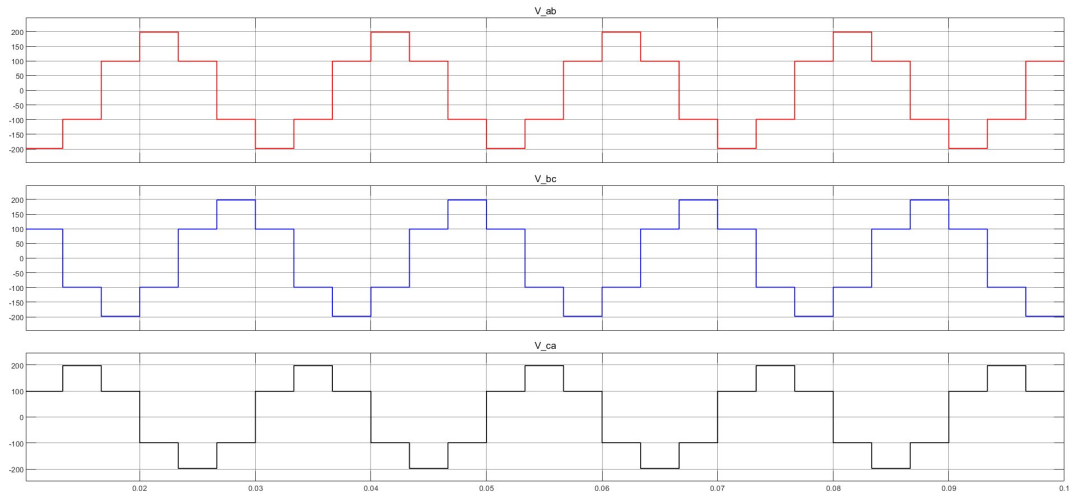


Figure 5.21: 120° conduction mode line to line Voltage

5.4.1.2.2 Three phase inverter 180° conduction mode.

The 180° conduction mode is the fundamental operating mode of three-phase inverters that is commonly used to generate balanced three-phase AC voltages. In this mode, each inverter leg conducts for 180° of the electrical cycle, with adjacent phases having conduction times that overlap. This produces a sinusoidal output waveform with a phase shift of 120° between consecutive phases, which satisfies the requirements for balanced three-phase operation. In this mode, each IGBT conducts for 180° of a cycle. In one branch, such as branch T1 and T4, T1 conducts for 180° , T4 for the next 180° , again T1 for 180° , and so on. The second and third branches work in the same manner.

The same voltage equations applied for the 120° conduction mode also apply here. For example, in an interval T1, T6, and T2 are conducting as shown in Fig.5.23. Assume current i flowing from the DC source and impedance Z in each phase. Thus, the equation could be written as

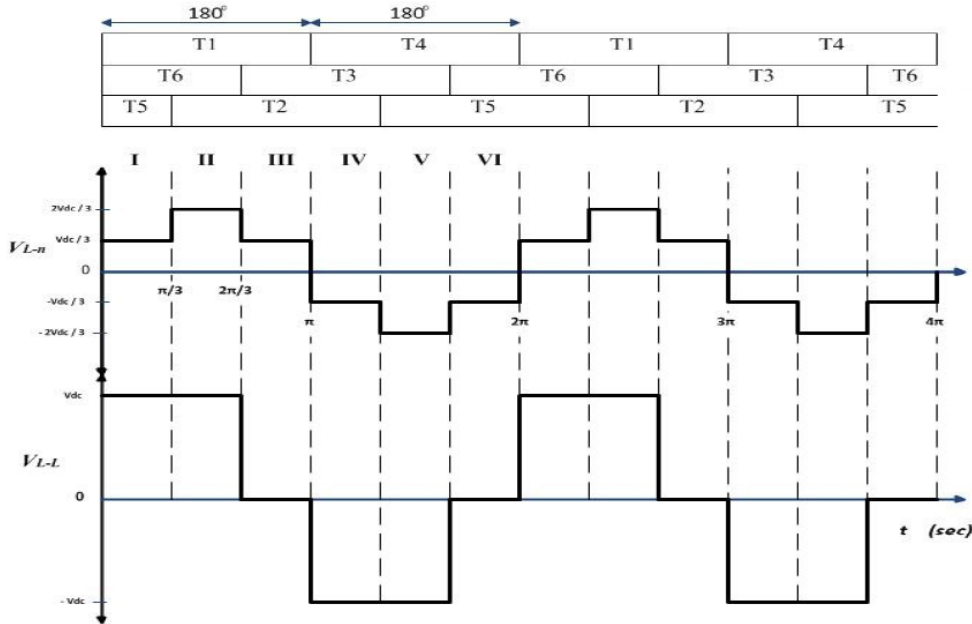


Figure 5.22: 180° conduction mode Line to Neutral Voltage and Line to Line voltage [1]

$$i = \frac{V_{dc}}{Z + \frac{1}{2}Z} = \frac{2}{3} \frac{V_{dc}}{Z} \quad (5.78)$$

Therefore,

$$V_{an} = iZ = \frac{2}{3} \frac{V_{dc}}{Z} Z = \frac{2}{3} V_{dc} \quad (5.79)$$

$$V_{bn} = V_{cn} = i \frac{Z}{2} = \frac{2}{3} \frac{V_{dc}}{Z} \frac{Z}{2} = \frac{1}{3} V_{dc} \quad (5.80)$$

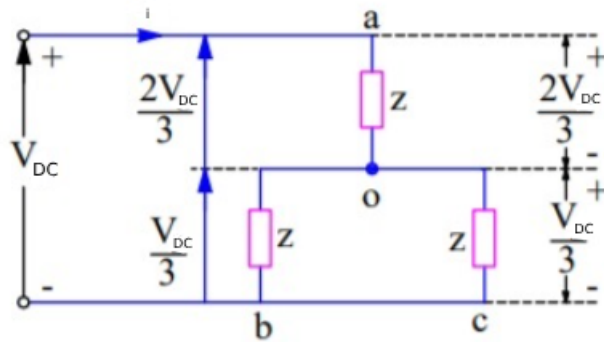


Figure 5.23: 180° conduction mode where T_1 , T_6 and T_2 are ON and the rest are OFF

Simulations of both Phase voltages and line to line voltages of three phase inverter with $V_{dc} = 200V$ is shown in Fig.5.24 and Fig.5.25 respectively.

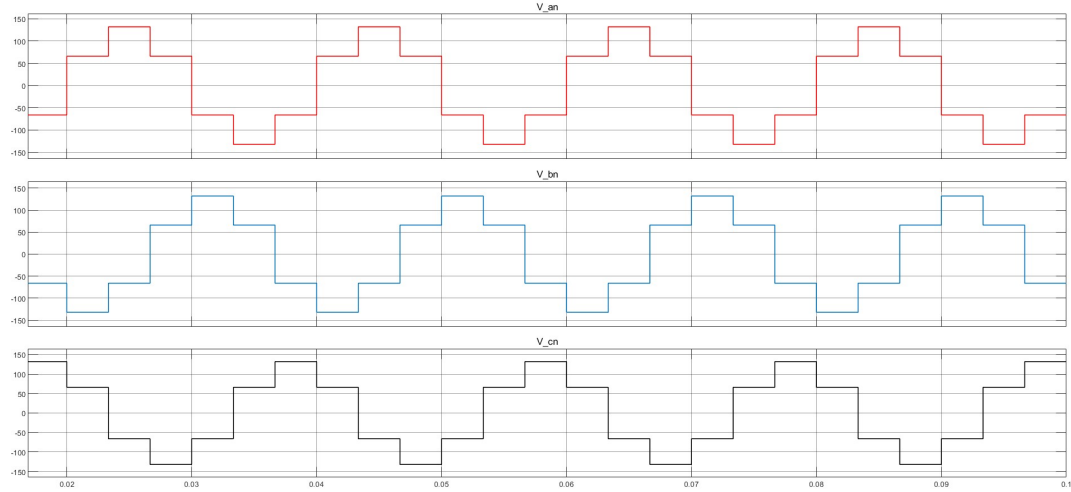


Figure 5.24: 180° conduction mode Line to Neutral Voltage

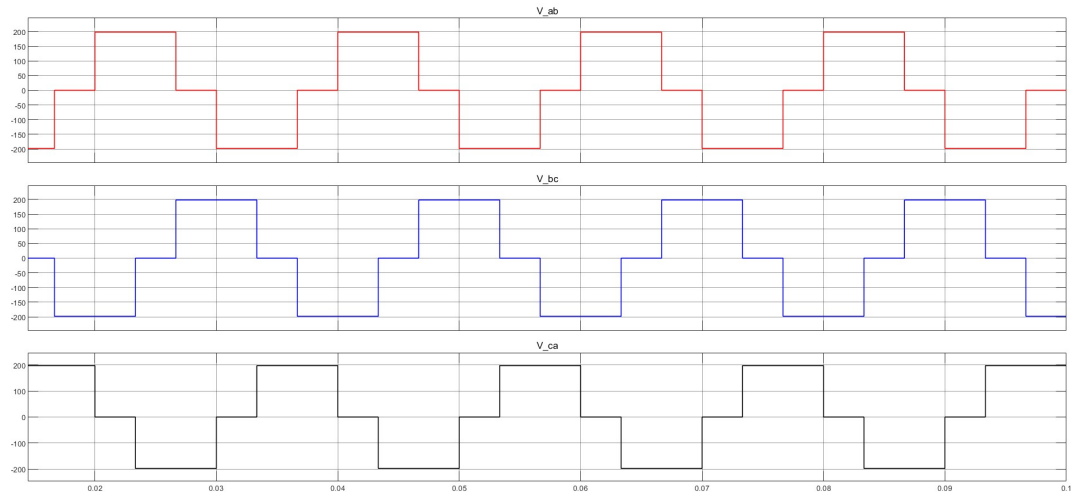


Figure 5.25: 180° conduction mode line to line Voltage

5.4.2 Modulation Techniques

In variable-speed AC drives with voltage-fed inverters, controlling the inverter's voltage and frequency output is essential for controlling the motor's torque and speed. Pulse-width modulation methods aim to achieve control of the voltage output of an inverter over the maximum possible range and with minimum distortion. Pulse-width modulation facilitates voltage and frequency control within the inverter. As a result, a variable-voltage DC-link is not necessary. A PWM inverter is often powered by an uncontrolled diode bridge rectifier with a small filter at the output, but in the case of EVs, the inverter is powered directly from the battery. Various PWM techniques have been developed to regulate inverters in variable-speed drives. All of these techniques use variations in the basic square-wave pole voltage to create a periodic waveform with the required fundamental frequency and amplitude. All PWM schemes, in general, aim to maximize the fundamental harmonics and selectively eliminate a few lower harmonics.

5.4.2.1 SQUARE-WAVE PWM

This modulation technique compares a symmetrical triangular carrier wave to a square-wave reference (modulating wave). Half-bridge inverter switches are triggered by the intersection of two waves. By matching the carrier wave's frequency with a multiple of three times the frequency of the reference signals, the carrier wave would effectively complete three cycles in the time it takes for one cycle of each reference signal. The resulting pole voltage waveforms will be identical with 120° phase relationships. The line-to-line voltage waveform depends on the phase relationship between the carrier and the modulating waves.

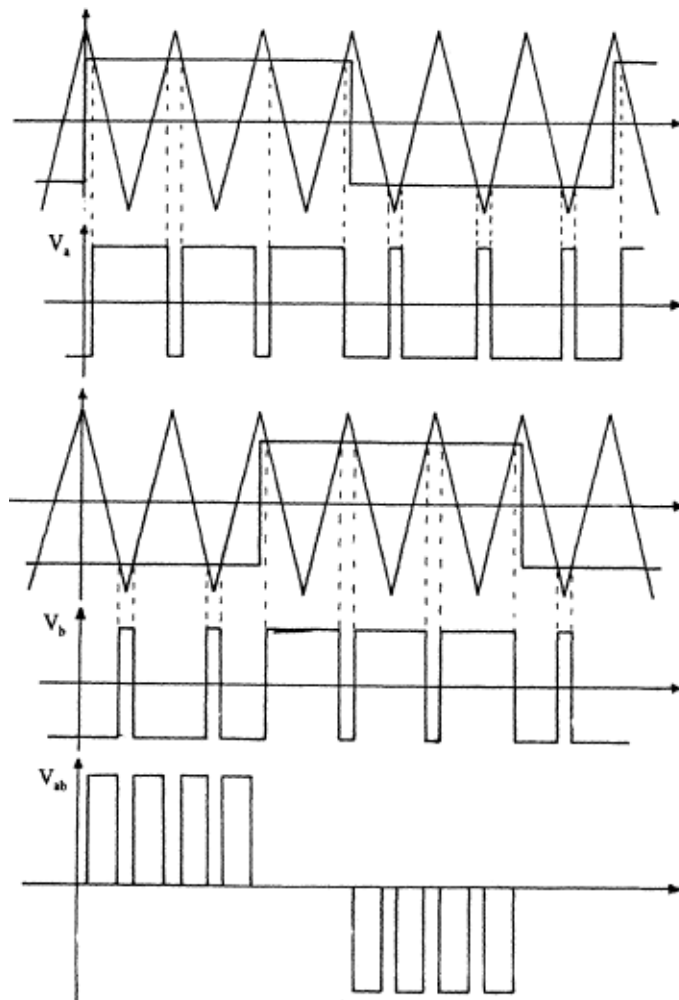


Figure 5.26: Square Wave Modulation.[\[7\]](#)

The ratio of the reference signal amplitude A_r and frequency f_r to the carrier signal amplitude A_c and frequency f_c is controlled to control the width of the pulse and hence control the magnitude of the output voltage. This ratio is known as the Modulation Index, MI. [\[28\]](#) and [\[24\]](#)

$$MI = \frac{A_r}{A_c} \quad (5.81)$$

5.4.2.2 SINUSOIDAL PWM (SPWM)

Sinusoidal PWM is a typical PWM technique similar to the square wave PWM with a single change where the reference signal is not square signal but a sinusoidal one. In this PWM technique, the sinusoidal AC voltage reference v_{ref} is compared with the high-frequency triangular carrier wave v_{cr} in real time to determine switching states for each pole in the inverter. After comparing, the switching states for each pole can be determined based on the following rule:

- Voltage reference $v_{ref} >$ Triangular Carrier v_{cr} : upper switch is turned on (pole voltage = $\frac{V_{dc}}{2}$)
- Voltage reference $v_{ref} <$ Triangular Carrier v_{cr} : lower switch is turned on (pole voltage = $-\frac{V_{dc}}{2}$)

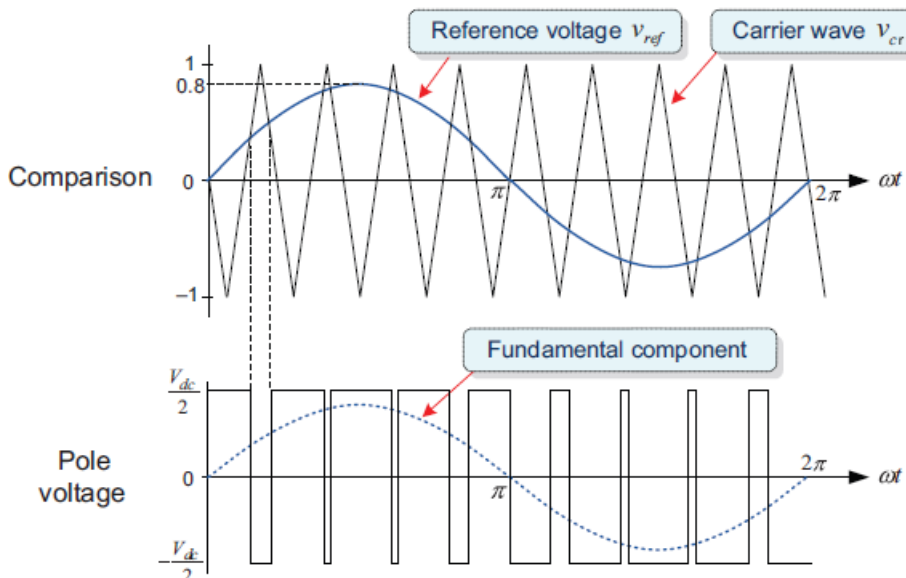


Figure 5.27: Sinusoidal PWM technique.[14]

The peak-to-peak value of the triangle carrier wave is represented as the DC link voltage (V_{dc}). To achieve linear modulation in this PWM approach, the voltage reference (v_{ref}) amplitude must be less than the peak of the triangular carrier (v_{cr}). i.e., $v_{ref} \leq \frac{V_{dc}}{2}$. Since this PWM technique utilizes a high frequency carrier wave for voltage modulation, this kind of PWM technique is called a carrier-based PWM technique.

However, when the reference exceeds the peak of the triangular carrier (i.e., $MI > 1$), the inverter cannot produce an output voltage linearly proportional to the reference voltage. The range of $MI > 1$ is called the overmodulation region, where the linearity of the modulation is lost.[14]

The maximum linear output voltage, $\frac{V_{dc}}{2}$, that could be achieved by the SPWM technique corresponds to 78.5% of the maximum output voltage, $\frac{2V_{dc}}{\pi}$, by the six-step inverter. Therefore, when using the PWM technique, the attainable maximum

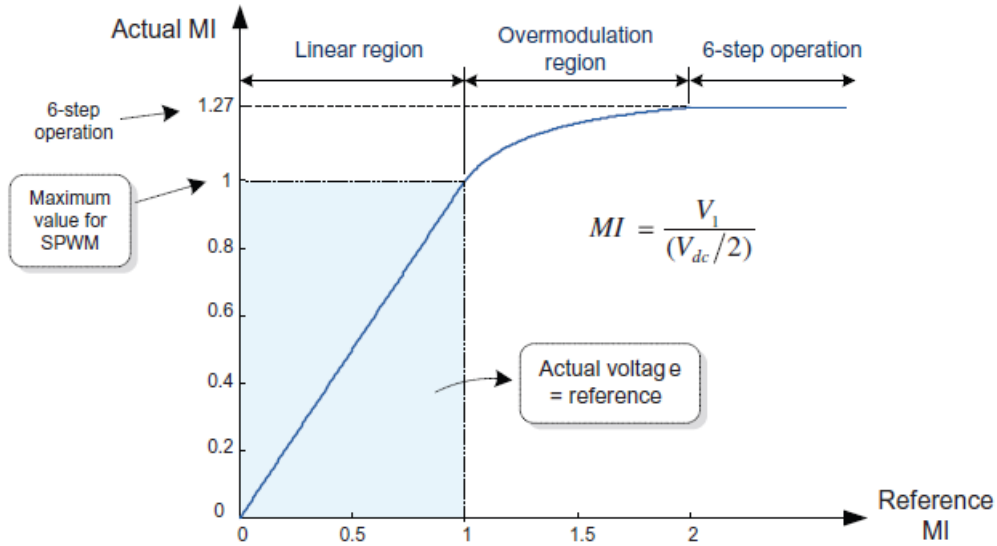


Figure 5.28: Voltage modulation range for SPWM.[14]

limit of the linear modulation range is inevitably less than the maximum output voltage of an inverter.

The SPWM technique has the extra advantage of maintaining a consistent switching frequency. Constant switching frequency simplifies thermal design for switching devices by allowing for easy calculation of their losses. Furthermore, having well-defined harmonic characteristics makes it easier to construct a low-pass filter to eliminate them.

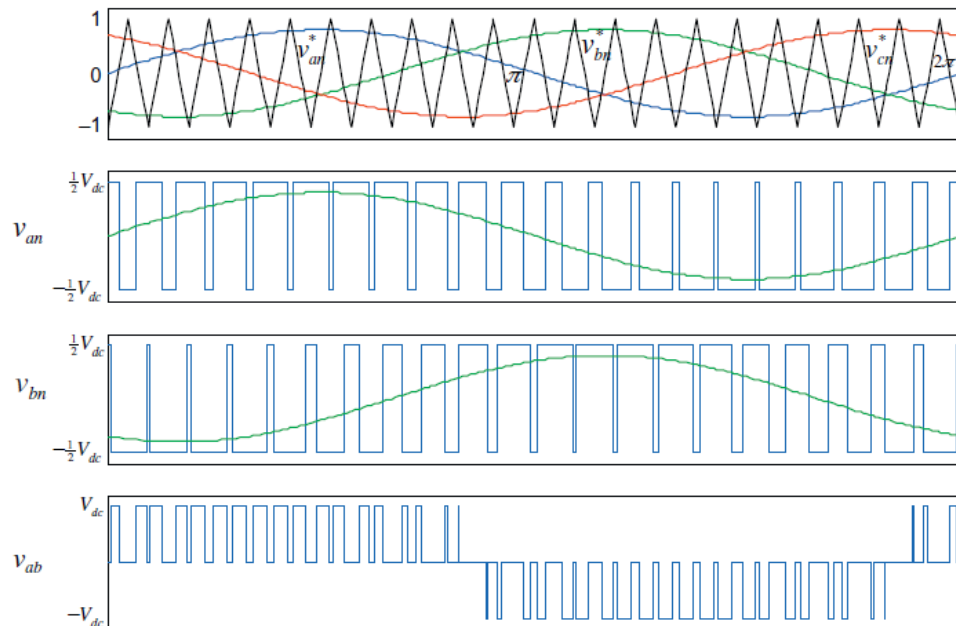


Figure 5.29: SPWM technique for a three-phase inverter.[14]

5.4.2.3 THIRD HARMONIC INJECTION PWM (THIPWM)

The SPWM technique excels compared to programmed PWM in terms of dynamic performance due to its ability to modulate voltage at every sample interval and fixed switching frequency. However, this approach has limitations.

The voltage linearity range is only 78.5% of the six-step operation, resulting in poor waveform quality in the high modulation range. Newer PWM approaches have been developed to deal with these issues. To improve voltage linearity, the modulating signal has been modified to become non-sinusoidal. Third-harmonic injection PWM can increase the fundamental component of output voltages by 15.5% compared to traditional SPWM techniques.

The SPWM approach performs accurately when the sinusoidal voltage reference (v^*) is below the peak of the triangular carrier. This restricts the range of linear modulation in the SPWM approach. When the peak of the voltage reference (v^*) exceeds the peak of the triangular carrier (i.e., $MI > 1$), a pulse drops, which indicates no intersection between the voltage reference and the triangular carrier. Consequently, the linear relationship between the voltage reference and the output voltage cannot be maintained.[14] This can be seen in Fig.5.30.

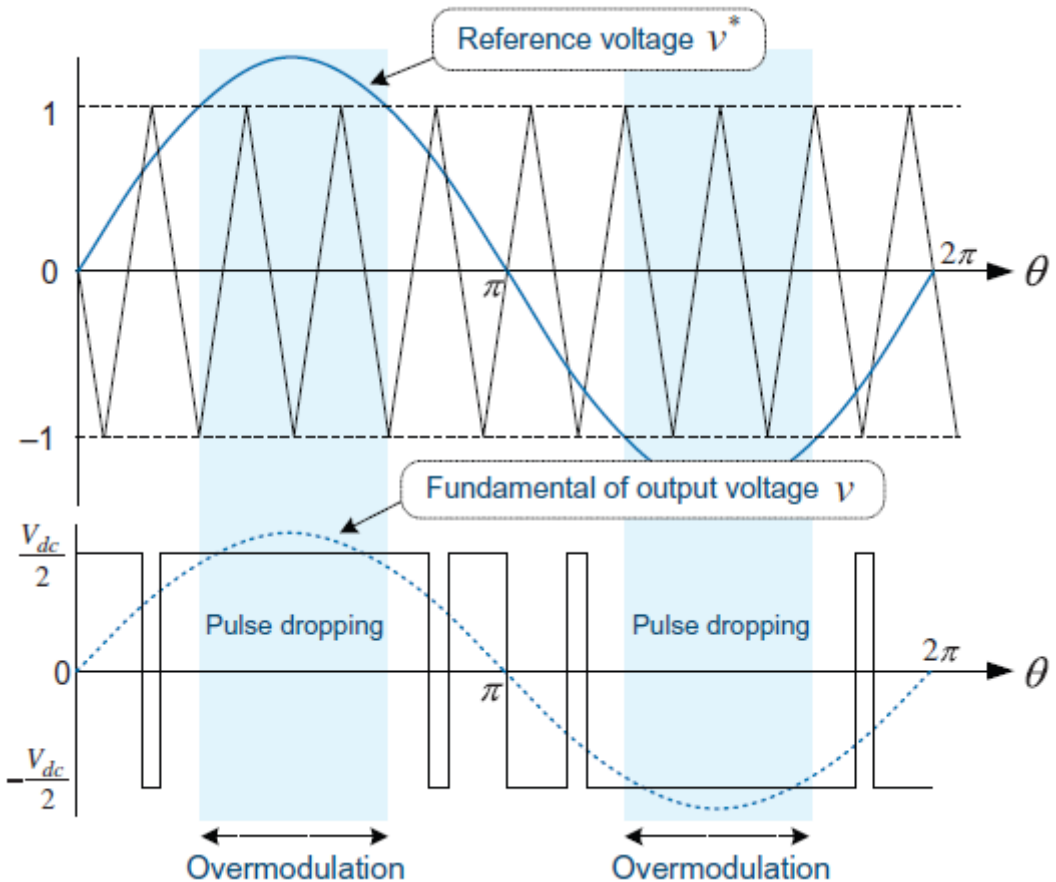


Figure 5.30: Over-modulation in the SPWM technique.[14]

The only effective voltage to a load is the fundamental component contained in the output voltage. Therefore, selecting a voltage reference with a fundamental

component that is greater than the triangle carrier's peak but not its own peak would possibly increase the linear modulation range. Adding a third harmonic to the voltage reference waveform can lead to improved performance. Adding a third harmonic to the voltage reference waveform results in a lower peak compared to the original waveform. The approach that employs this idea is third-harmonic injection pulse width modulation (THIPWM). THIPWM can increase the output voltage by 15.5% compared to conventional SPWM. This can be seen in Fig.5.31.

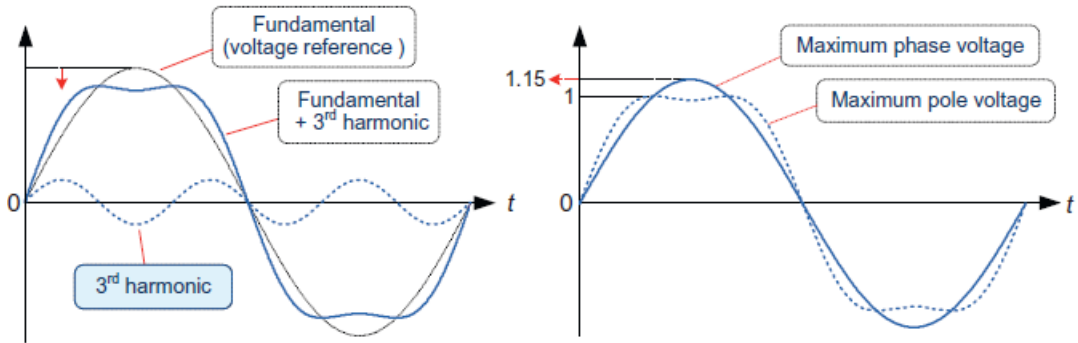


Figure 5.31: Principle of THIPWM.[14]

This intended third harmonic voltage is not present on the line-to-line and phase voltages for a three-phase load with a floating neutral point, such as AC motors. Thus, the injected third harmonic voltage does not cause any distortion on the line-to-line and phase voltages.

The THIPWM technique has a disadvantage in that the implementation complexity of the third harmonic and steady-state current harmonic characteristics are inferior to those of the SVPWM method. In addition to the third harmonic, there is another THIPWM technique that uses a higher order triple harmonic, such as the ninth harmonic.[14]

5.4.2.4 SPACE VECTOR PWM (SVPWM)

Space Vector Pulse Width Modulation (SVPWM) emerges as a innovative advancement in the domain of motor control, profoundly influencing the efficacy and precision of three-phase inverter operations. The previously stated PWM approaches modulate the three-phase voltage references independently. SVPWM, a PWM method based on space vectors, differs from other approaches. SVPWM introduces a sophisticated paradigm grounded in the concept of space vectors. The SVPWM technique uses a space vector v_{abc} in the complex plane to represent three-phase voltage references, which are then modulated by output voltage vectors from an inverter. The SVPWM technique is now widely used in many three-phase inverter applications because it produces fundamental output voltage 15.5% more than the one produced by the SPWM technique and gives less harmonic distortion of the load current, lower torque ripple in AC motors, and lower switching losses. To use this PWM technique, an inverter's output voltages have to be expressed as a space vector, as three-phase voltage references are. there are eight possible switching states in a three-phase inverter. The output voltage vectors, V_0-V_7 , corresponding

to the eight possible switching states. This can be seen in Fig.5.32.

Six of these vectors, V_1-V_6 , which are called active voltage vector, offer an effective voltage to the load. The magnitude of all active vectors is equal to $\frac{2}{3}V_{dc}$. However, they are 60° out of phase with each other. By contrast, the two vectors, V_0 and V_7 , are called zero voltage vector, which cannot yield an effective voltage to the load.[14]

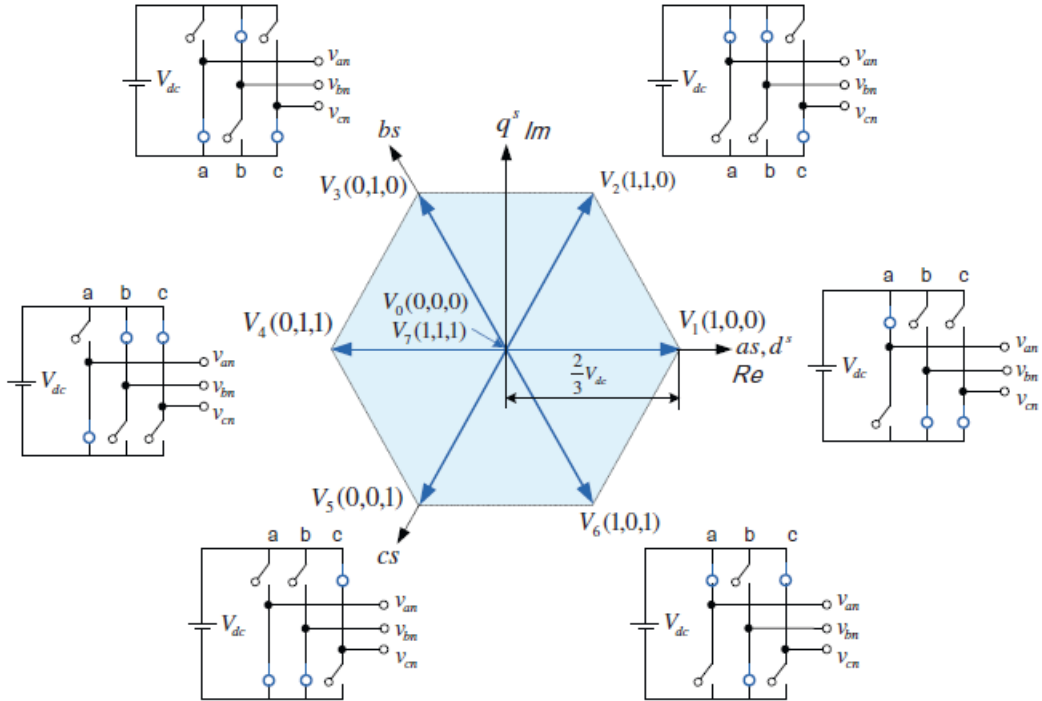


Figure 5.32: Output voltage vectors in the complex plane (or dq axes stationary frame).[14]

As the three-phase voltage references vary with time, the voltage reference vector V^* rotates in the counterclockwise direction in the complex plane. This vector completes one revolution per electrical period of the reference voltage. A voltage reference is given as a space vector of V^* and this voltage reference vector V^* is generated by using the output voltage vectors of a three-phase inverter. By using the two active voltage vectors adjacent to V^* and the zero vectors among the available eight voltage vectors, the SVPWM technique produces a voltage that has the same fundamental volt-second average as the given voltage reference vector V^* over a modulation period T_s .[14] The voltage reference vector V^* is assumed to be inside a hexagon, which is formed by six output voltage vectors of a three-phase inverter. Only when this condition is satisfied, the voltage reference vector can be modulated properly. For instance, consider a voltage reference vector V^* given in sector 1 of the six segments in the hexagon shown in Fig.5.33. The inverter cannot generate the required voltage reference vector directly because there is no inverter output vector that has the magnitude and the phase equal to those of the voltage reference vector. As an alternative, the two voltage vectors close to the voltage reference vector and the zero vectors are used to construct a voltage with the same fundamental volt-

second average as the voltage reference vector V^* . This modulation repeats each modulation period T_s depending on the switching frequency.

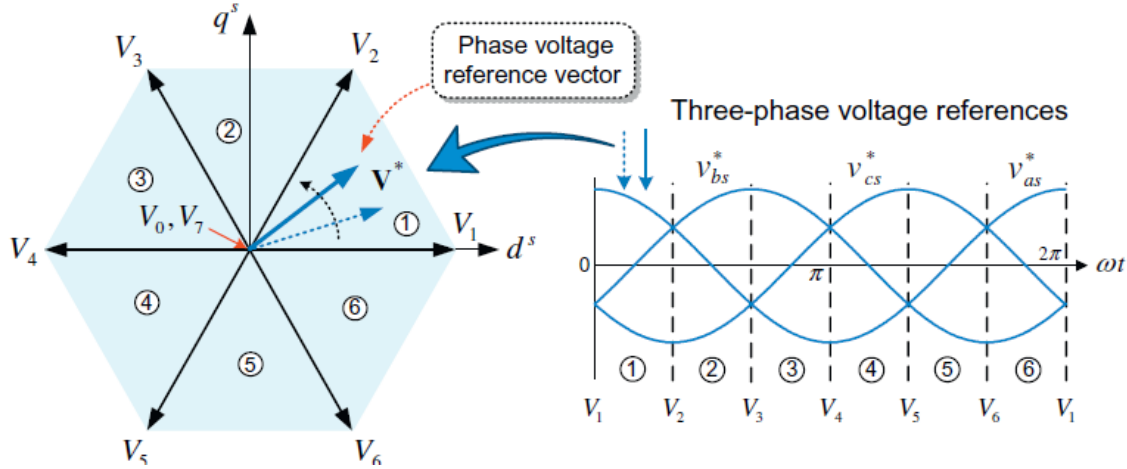


Figure 5.33: Rotation of voltage vector.[14]

In the first step, one of the two adjacent active voltage vectors, V_1 , is applied first during time T_1 . As a result, an output voltage is generated with the magnitude of $V_1 \cdot \left(\frac{T_1}{T_s}\right)$ in the direction of the vector V_1 . Next, another vector V_2 is applied during time T_2 to meet the magnitude and phase of the reference vector voltage V^* . Through these two steps, it is possible to generate the same output voltage as the reference voltage vector during the modulation period T_s . Lastly, if $T_1 + T_2 < T_s$, then one of the zero vectors, V_0 or V_7 , is applied during the remaining time $T_0 = (T_s - T_1 - T_2)$.[14]

The duration time (T_1 , T_2 and T_0) of each voltage vector for generating a given reference vector V^* be calculated as follows. The above modulation process can be expressed mathematically as

$$\int_0^{T_s} V^* dt = \int_0^{T_s} V_n dt + \int_{T_1}^{T_1+T_2} V_{n+1} dt + \int_{T_1+T_2}^{T_s} V_{0,7} dt \quad (5.82)$$

Taking a constant DC-link voltage during T_s into consideration. Thus,

$$V^*.T_s = V_n.T_1 + V_{n+1}.T_2 \quad (5.83)$$

As an example, if the voltage reference vector V^* is given in the first sector ($0 \leq \theta \leq 60^\circ$).[14] Therefore,

$$T_s \cdot |V^*| \cos(\theta) = T_1 \cdot \left(\frac{2}{3}V_{dc}\right) + T_2 \cdot \left(\frac{2}{3}V_{dc}\right) \cos(60) \quad (5.84)$$

$$T_s \cdot |V^*| \cos(\theta) = T_2 \cdot \left(\frac{2}{3}V_{dc}\right) \sin(60) \quad (5.85)$$

These equations yields

$$T_1 = T_s b \frac{\sin(60^\circ - \theta)}{\sin(60^\circ)} \quad (5.86)$$

$$T_2 = T_s b \frac{\sin(\theta)}{\sin(60^\circ)} \quad (5.87)$$

$$T_0 = T_s - (T_1 + T_2) \quad (5.88)$$

where

$$b = \frac{3}{2} \frac{|V^*|}{V_{dc}} \quad (5.89)$$

The duration times for the voltage reference vector in the other sectors 2 to 6 can be calculated in a similar manner.

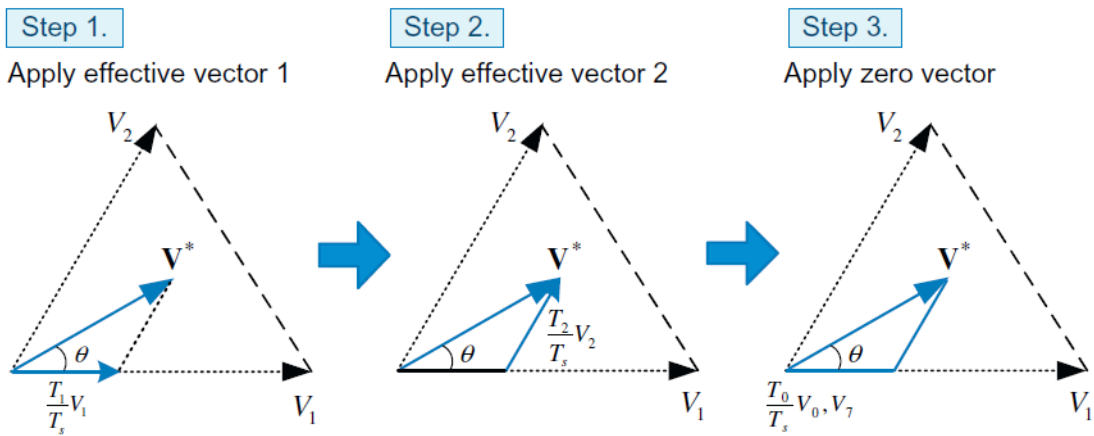


Figure 5.34: Modulation process for voltage generation.[14]

In the SVPWM technique, the sum of the duration times for the two active voltage vectors should not exceed the modulation period, i.e., $T_1 + T_2 \leq T_s$. The magnitude of the voltage reference to meet this requirement can be obtained as

$$T_1 + T_2 \leq T_s \rightarrow V^* \leq \frac{V_{dc}}{\sqrt{3}} \frac{1}{\sin(60^\circ + \theta)} \quad (5.90)$$

This equation indicates that the possible range of the reference voltage vector V^* is inside the hexagon formed by joining the extremities of the six active vectors. However, for a voltage reference vector over one electrical period, the range of the voltage reference vector should be inside the inscribed circle of the hexagon to obtain the equal magnitude. Therefore the radius of the inscribed circle, $\frac{V_{dc}}{\sqrt{3}}$, is the maximum fundamental phase voltage in the SVPWM technique. This value is about 15.5% larger than that of the SPWM technique and is equal to that of the THIPWM technique. The value corresponds to 90.7% of the output voltage in the six-step operation.[14] Fig.5.35 shows the reference voltage range for SVPWM.

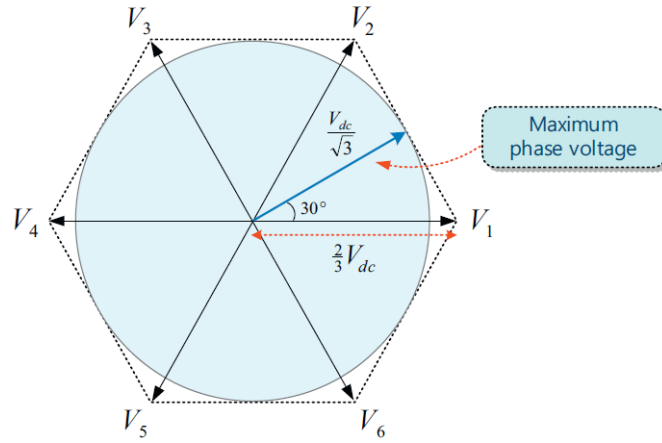


Figure 5.35: Possible range of the reference vector voltage in the SVPWM.[14]

Placing the effective voltage vectors in the centre of the modulation interval results in enhanced harmonic characteristics. The placement technique uses the symmetrical SVPWM method.[14] Centering can enhance the voltage modulation range by increasing the pulse width. The position of the zero-voltage vectors affects the effective voltage vectors throughout the modulation interval T_s . Thus, in the symmetrical SVPWM technique, the two zero vectors, V_0 and V_7 , during an equal time of $\frac{T_0}{2}$ are distributed at the beginning and the end of the modulation interval T_s . Moreover, under this circumstance, to obtain the minimum switching frequency, it is necessary to arrange the switching sequence in the order of $V_0(000) \rightarrow V_1(100) \rightarrow V_2(110) \rightarrow V_7(111)$. This can be seen in Fig.5.36.

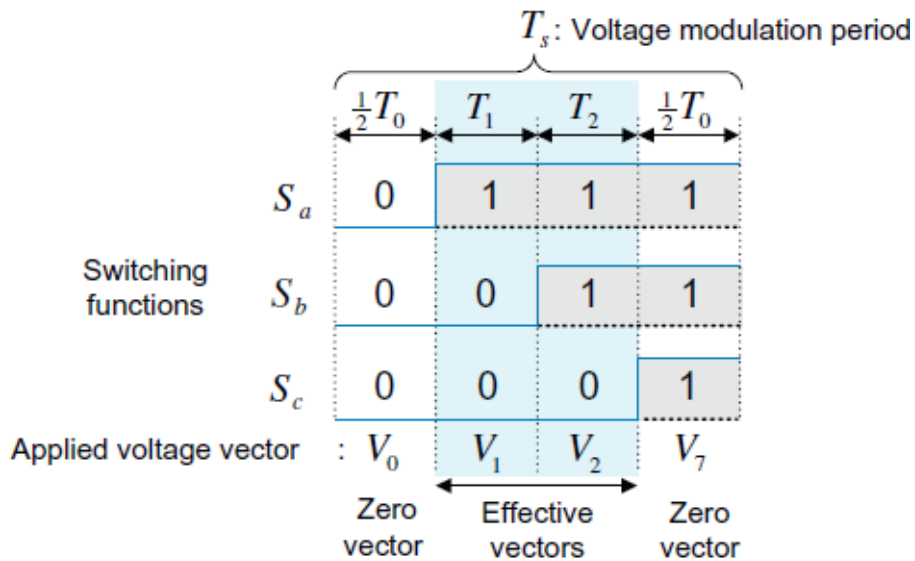


Figure 5.36: Switching sequence.[14]

The two zero vectors of V_0 and V_7 are used alternately in the interval T_s . In such a switching sequence, the transition from one vector to another vector can be performed by switching only one switch. In the next interval, the switching

sequence is reversed, i.e., $V_7 \rightarrow V_2 \rightarrow V_1 \rightarrow V_0$ as shown in Fig.5.37 Such alternating switching sequences at every modulation interval allow the switching frequency to be reduced.[14]

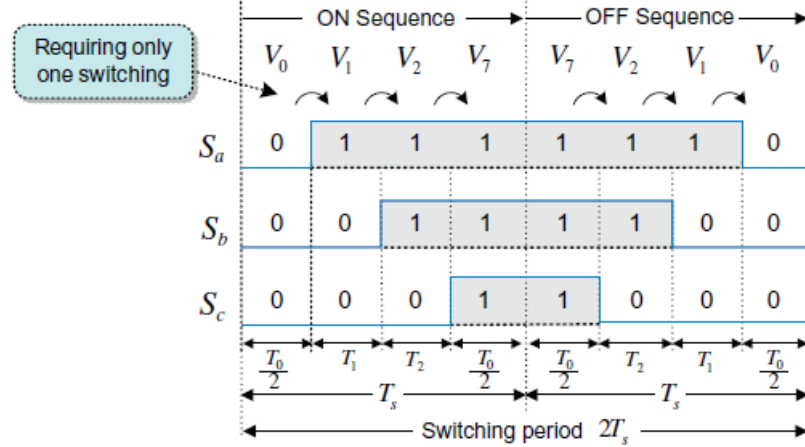


Figure 5.37: Alternate switching sequence.[14]

Fig.5.38 shows the switching sequences in all six sectors for the symmetrical SVPWM technique.

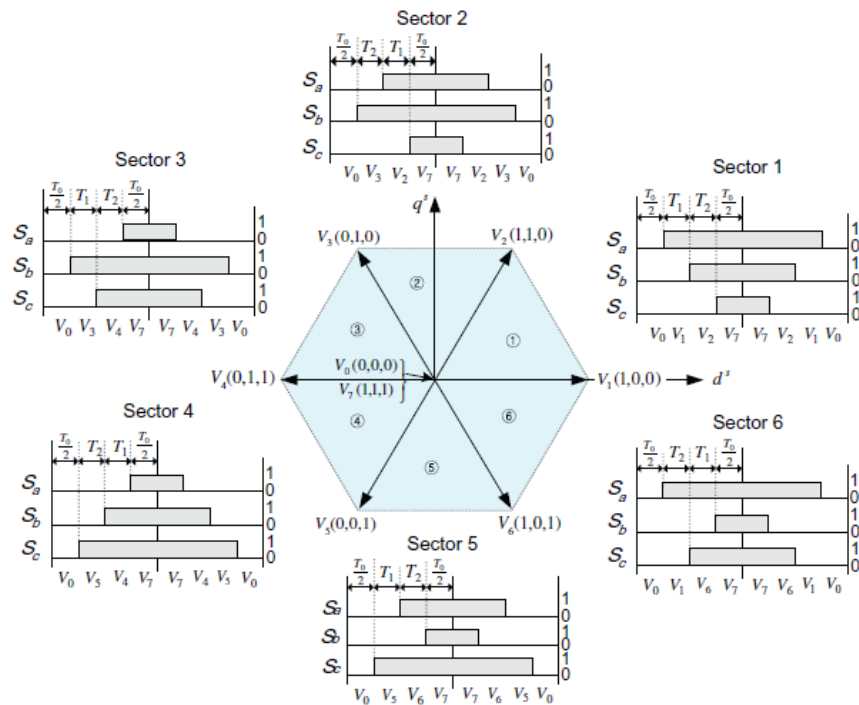


Figure 5.38: Switching sequences in six sectors.[14]

while offering significant advantages in motor control, presents several drawbacks. Firstly, its implementation entails a higher level of complexity, demanding more sophisticated control algorithms and computational resources. Additionally, SVPWM real-time calculations of space vector trajectories and modulation patterns can burden control hardware. However, nowadays, this method can be simply implemented by the carrier-based PWM technique using an offset voltage. The carrier-based PWM technique using an offset voltage is thoroughly discussed in [14].

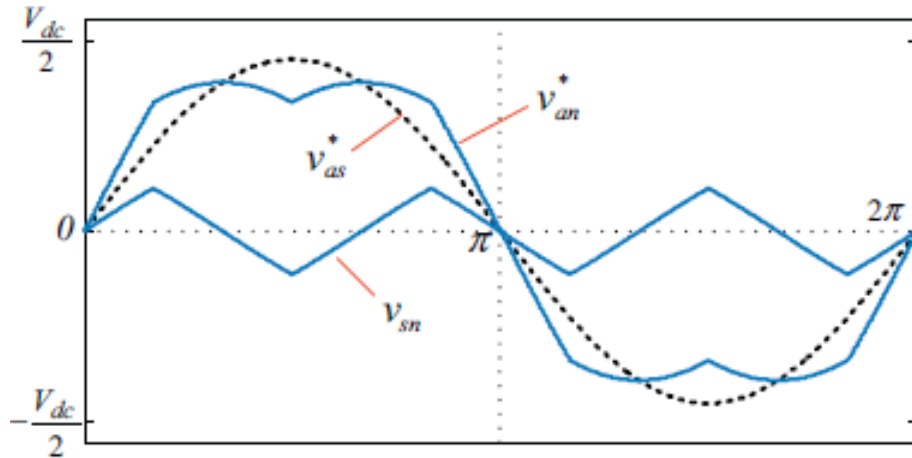


Figure 5.39: Voltages for equivalent SVPWM by using the offset voltage ($MI=0.9$).[14]

5.4.2.5 DISCONTINUOUS PWM (DPWM)

The PWM techniques discussed previously use continuous modulation in which the switching actions occur at all three poles of an inverter. In contrast, discontinuous modulation (also known as two-phase modulation) reduces the switching frequency by engaging only two of the three poles. Discontinuous modulation aims to lower switching frequency; however, its effects on switching losses, harmonics, and voltage linearity vary based on the placement of inactive switches (i.e., unmodulated sections). DPWM techniques could vary based on the location of the unmodulated section. There are several DPWM variations, as shown in Fig.5.40, and they are thoroughly discussed in [14] and [21].

- 60° DISCONTINUOUS PWM TECHNIQUE
- 60° ($\pm 30^\circ$) DISCONTINUOUS PWM TECHNIQUE
- $\pm 120^\circ$ DISCONTINUOUS PWM TECHNIQUE
- 30° DISCONTINUOUS PWM TECHNIQUE

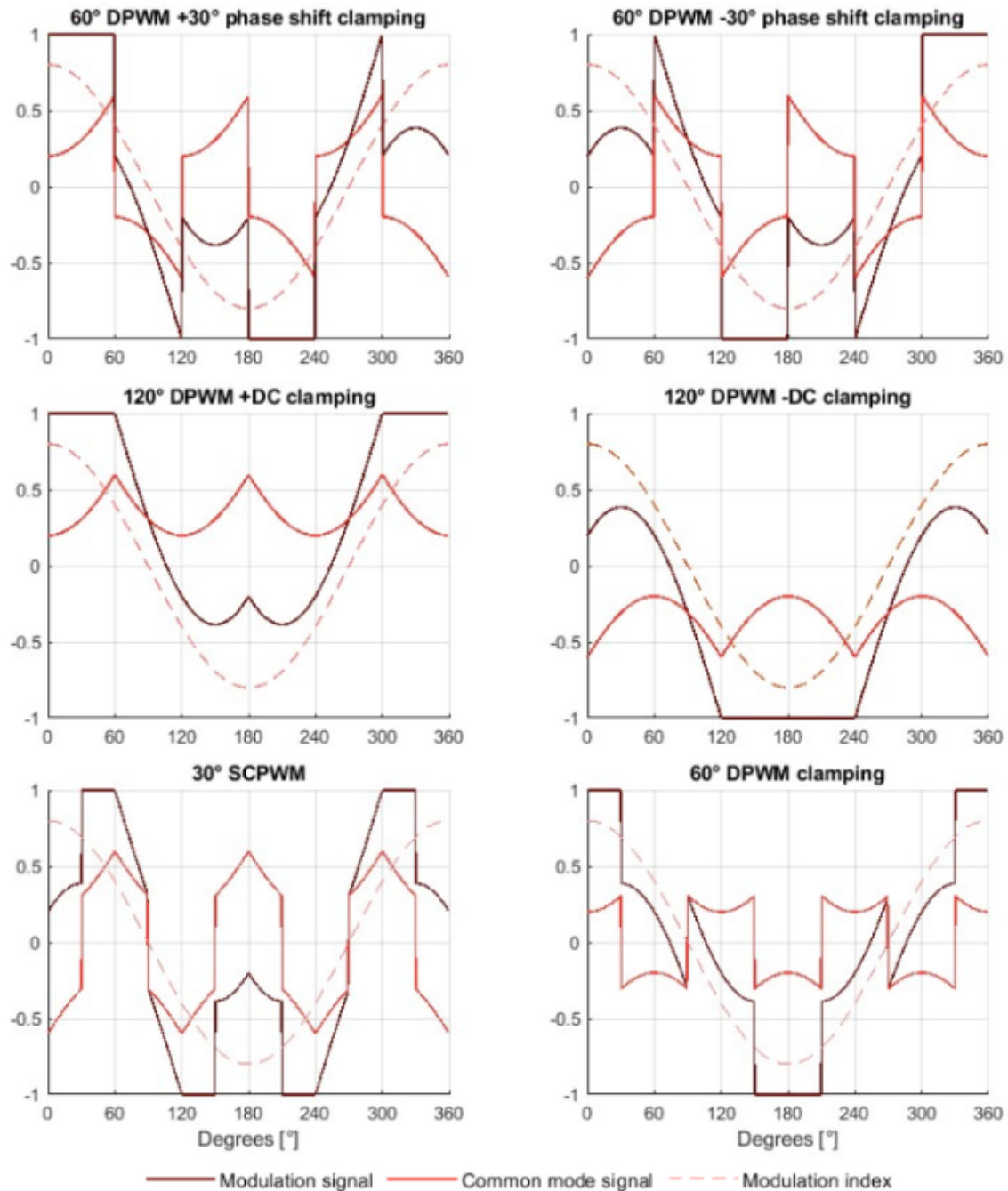


Figure 5.40: Modulation waveforms of popular Discontinuous PWM methods.[\[21\]](#)

Chapter 6

SIMULATIONS AND RESULTS

This chapter focuses on an extensive analysis of Field-Oriented Control (FOC) applied to Permanent Magnet Synchronous Motors (PMSM) using MATLAB/SIMULINK software. providing an essential analysis of the PMSM's open-loop performance, revealing fundamental insights into its behaviour in the absence of control intervention. Subsequently, the emphasis is then changed to evaluating the performance improvements achieved by FOC when applied to the motor using an ideal converter.

By meticulously assessing various aspects such as torque response, speed control, and efficiency. Furthermore, the chapter broadens its focus to include the impact of using inverters in combination with FOC, demonstrating the complexity brought about by various modulation approaches. highlighting the importance of selecting the modulation technique in motor performance indicators through comparison analysis.

Additionally, the chapter provides a thorough analysis of the impact of various tuning approaches for proportional-integral (PI) controllers inside the FOC framework. By methodically adjusting tuning parameters and assessing the subsequent motor responses, this section seeks to determine optimal tuning techniques favourable to reaching specified performance objectives. Through these numerous analyses, this chapter seeks to provide a comprehensive understanding of the intricate interaction between control strategies, converter configurations, and tuning methodologies to improve the operational efficiency and performance of the PMSM machine.

6.1 Open-loop Response

In this section, we take a close look at the open-loop response of our modeled machine employing the equations deduced in Chapter 4 and the Simulink model provided in the Simscape library. By comparing the results obtained from these two simulations, we aim to gain a comprehensive understanding of the machine's behavior under various operating conditions. This comparative analysis serves as a crucial foundation for further evaluations of control strategies and performance optimizations.

The simulation was performed using three phase voltage sources of peak voltage 200 **V** and frequency of 50 **Hz**. The machine parameters are shown in Table 6.1.

Parameters	Values (Units)
Phases	3
Rated Torque	111 (<i>N.m</i>)
Rated Speed	3000 (<i>RPM</i>)
Pole Pairs	4
Stator phase resistance (R_s)	0.05 (Ω <i>Ohms</i>)
d-axis Inductance (L_d)	0.635 (mH)
q-axis Inductance (L_q)	0.635 (mH)
Inertia (J)	0.011 ($kg.m^2$)
Viscous friction (B)	0.001889 ($N.m.s$)
Nominal DC voltage (V_{dc})	560 (V)
Rated Power	35 (KW)

Table 6.1: *Parameters of SM-PMSM*

6.1.1 No Load Torque Response

The following simulation response is for the two machines with no load torque to assess the machine's open-loop performance without load torque. From the parameters and the input values, we can deduce using the synchronous speed formula $N_s = \frac{120}{P}f$ that the synchronous speed $N_s = 750$ RPM.

Upon examination, it's clear that both machines perform similarly, showing similar torque fluctuations and speed inconsistencies during transient responses. However, they eventually stabilize under steady-state conditions. To improve their dynamic transient responses, a fine-tuned controller need to be introduced to enhance the dynamic response. the performance of both the simscape machine and modeled machine based on equations is shown in Fig.6.1 and Fig.6.2, respectively. in the next section, a load torque is to be added to both machine to evaluate their response.

6.1.2 With Load Torque Response

The following simulation response is for the two machines with load torque of 50*N.m* to assess the machine's open-loop performance load torque. From the parameters and the input values, we can deduce using the synchronous speed formula $N_s = \frac{120}{P}f$ that the synchronous speed $N_s = 750$ RPM. The parameters and inputs did not change.

Upon closer examination, it's clear that both machines perform similarly, showing some fluctuations in torque and speed during transient responses. However, they eventually stabilize in steady-state operation. To improve the dynamic transient response, we will need to implement a controller, as mentioned in the section above, which we will discuss in the next section. the performance of both is shown in Fig.6.3 and Fig.6.4 respectively.

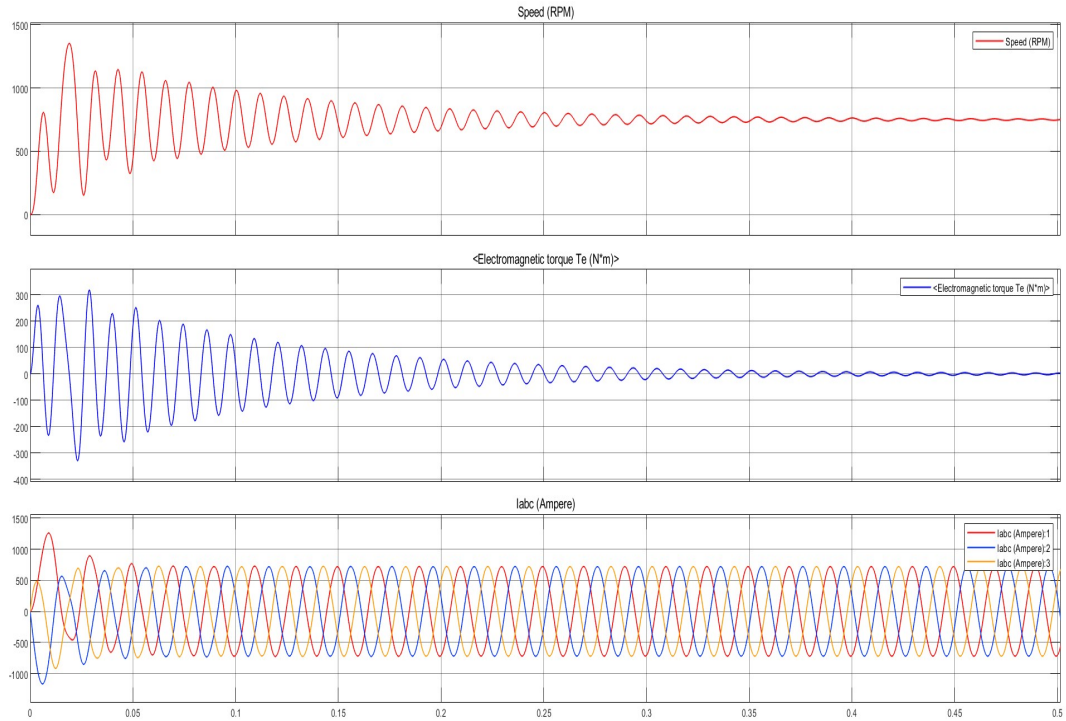


Figure 6.1: Open-loop response of Simscape machine with no load torque

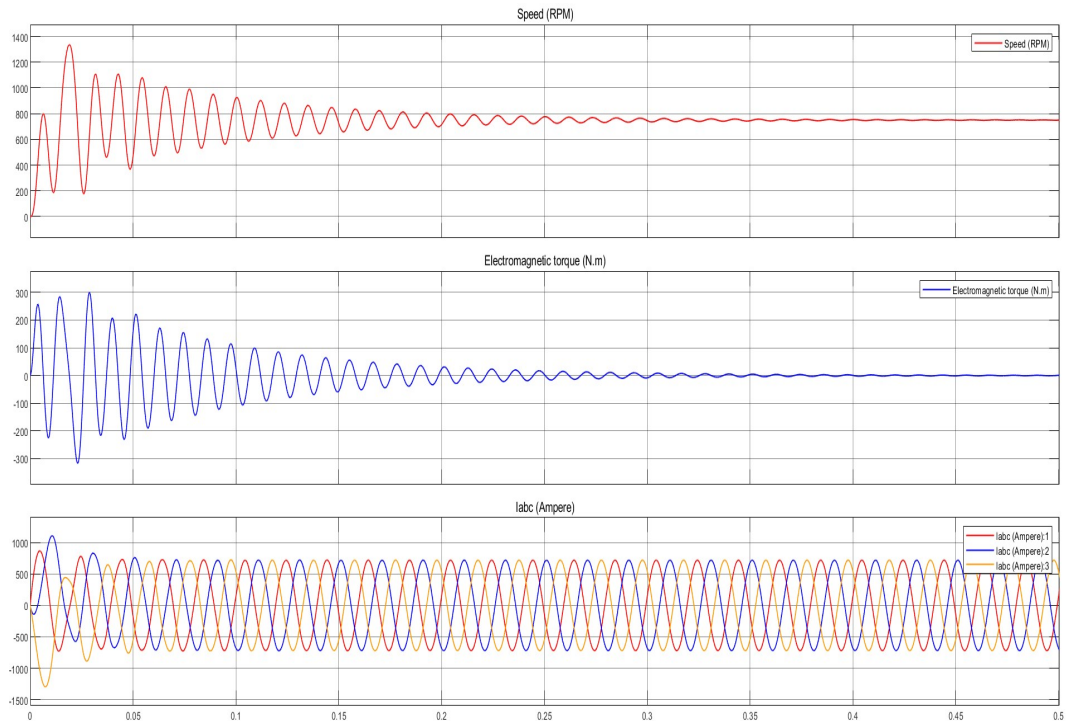


Figure 6.2: Open-loop response of Modeled machine based on equations with no load torque

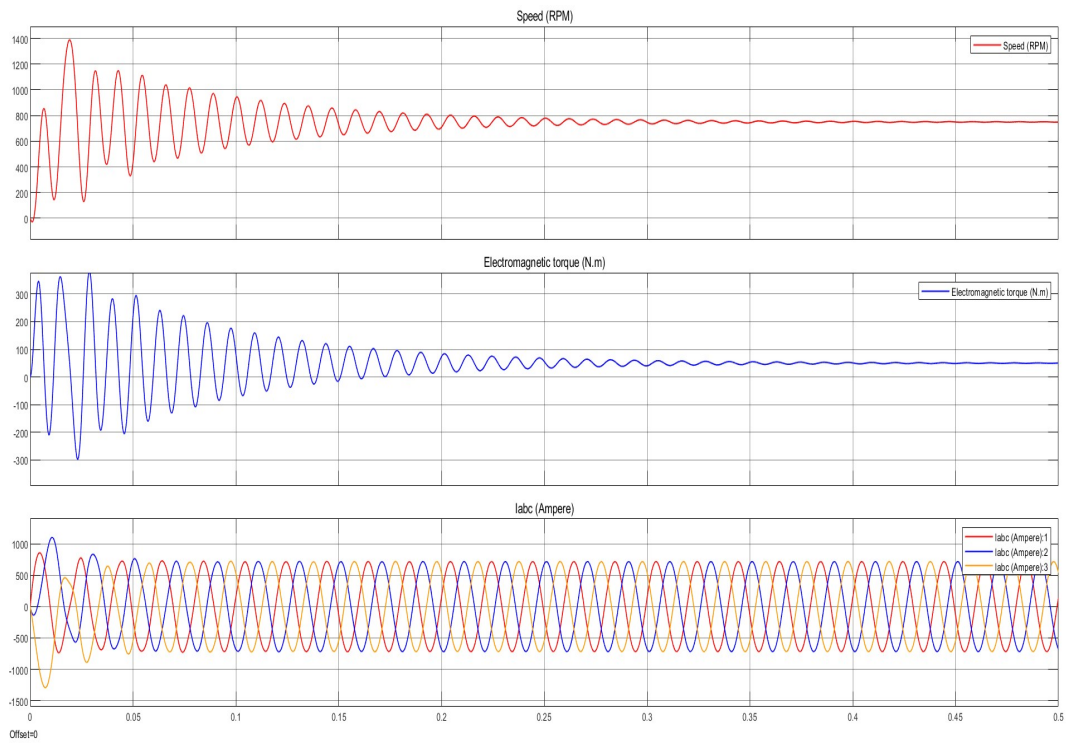


Figure 6.3: Open-loop response of simscape machine with load torque

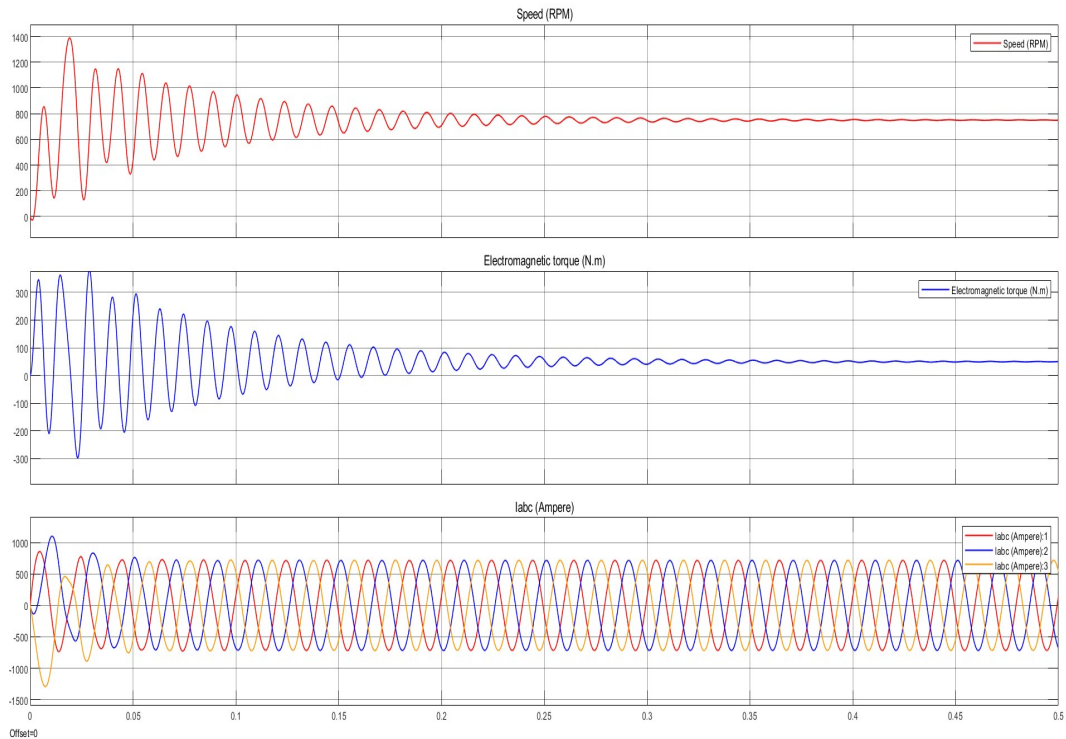


Figure 6.4: Open-loop response of Modeled machine based on equations with load torque

6.2 Closed-loop Response with FOC

In this section, we're diving into the closed-loop response of our modeled Permanent Magnet Synchronous Machine (PMSM). We're using both the PMSM equations we talked about in Chapter 4 and a Simulink model with Simscape, all under the Field-Oriented Control (FOC) setup. Our goal? To see how these two modeling approaches stack up under different conditions. We're throwing various scenarios at them to test their speed regulation, torque control, and overall stability. It is not just about comparing them; we want to understand how they perform and where they shine or fall short. This kind of hands-on comparison helps us fine-tune our control strategies and make sure that our PMSM system is primed for top-notch performance in real-world situations.

6.2.1 FOC Using Ideal Converter

In this section, the FOC is implemented using $i_d = 0$ as well as employing dynamic cross-axes decoupling and manual tuning for the PI controllers and the optimum controller design methods discussed in Chapter 5, where the magnitude optimum method is employed in the current controllers and the symmetrical optimum method is employed in the speed controller. In this section, the modulation techniques and the inverter are not employed, hence the name FOC Using Ideal Converter.

Current Controllers

Manual Tuning	Magnitude Optimum
$K_p = 0.5$	$K_p = 7.9735$
$K_i = 53$	$K_i = 625$

Table 6.2: Current Controllers parameters

Speed Controllers

Manual Tuning	Symmetrical Optimum
$K_p = 0.3283$	$K_p = 0.21653$
$K_i = 2.54$	$K_i = 2.124$

Table 6.3: Speed Controllers parameters

6.2.1.1 No Load Torque Response

The simulation response below is for the two machines with no load torque to Evaluate the machine's open-loop performance without load torque. One machine employs **Manual tuning** for the PI controllers, while the other employs **Magnitude Optimum criterion** and **Symmetrical Optimum criterion**.

6.2.1.1.1 Step Response of 1000 RPM.

The first test is a step response of 1000 RPM at $t = 0.2$ seconds with an initial value of **zero** for a simulation time of 1 second.

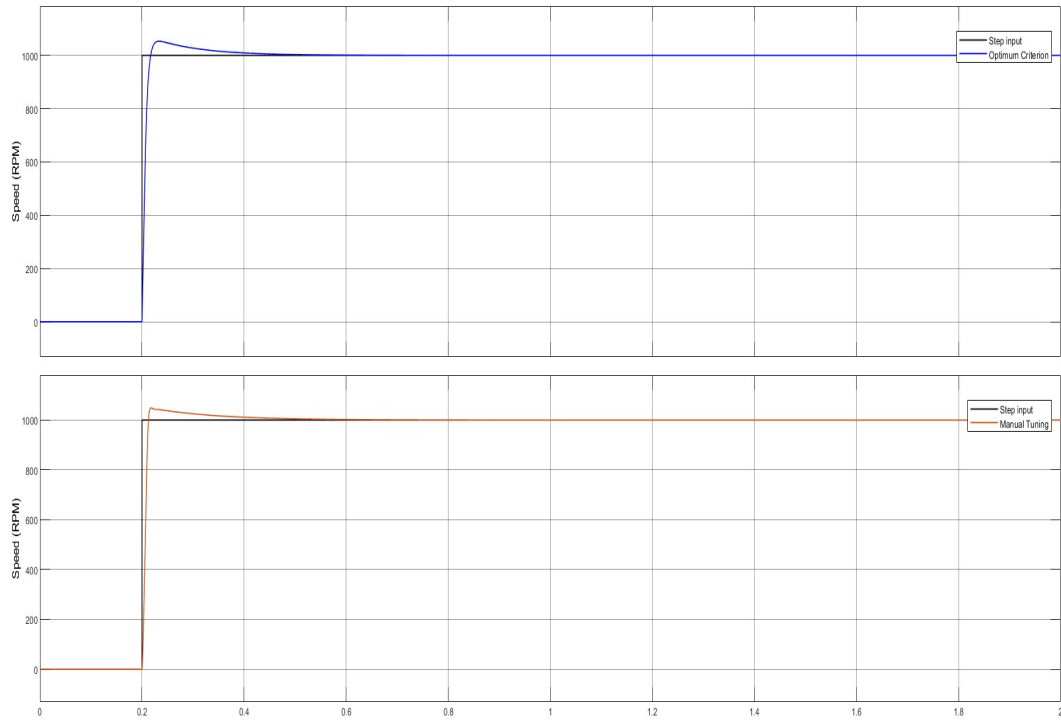


Figure 6.5: Step response of speed with Manual tuning and Optimum criterion

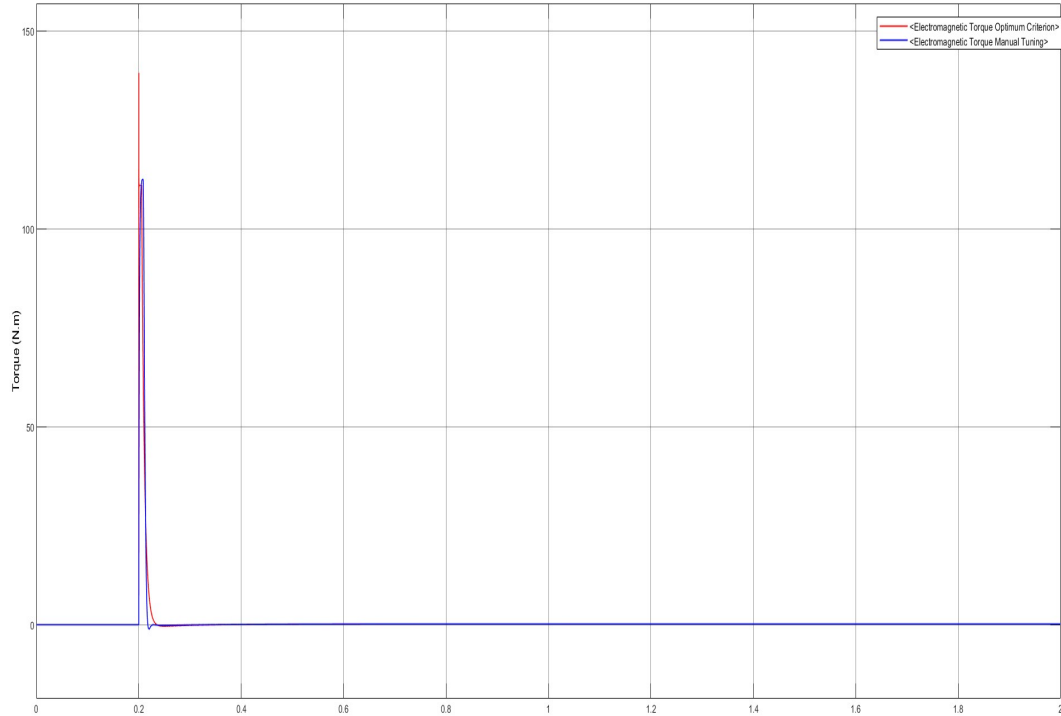
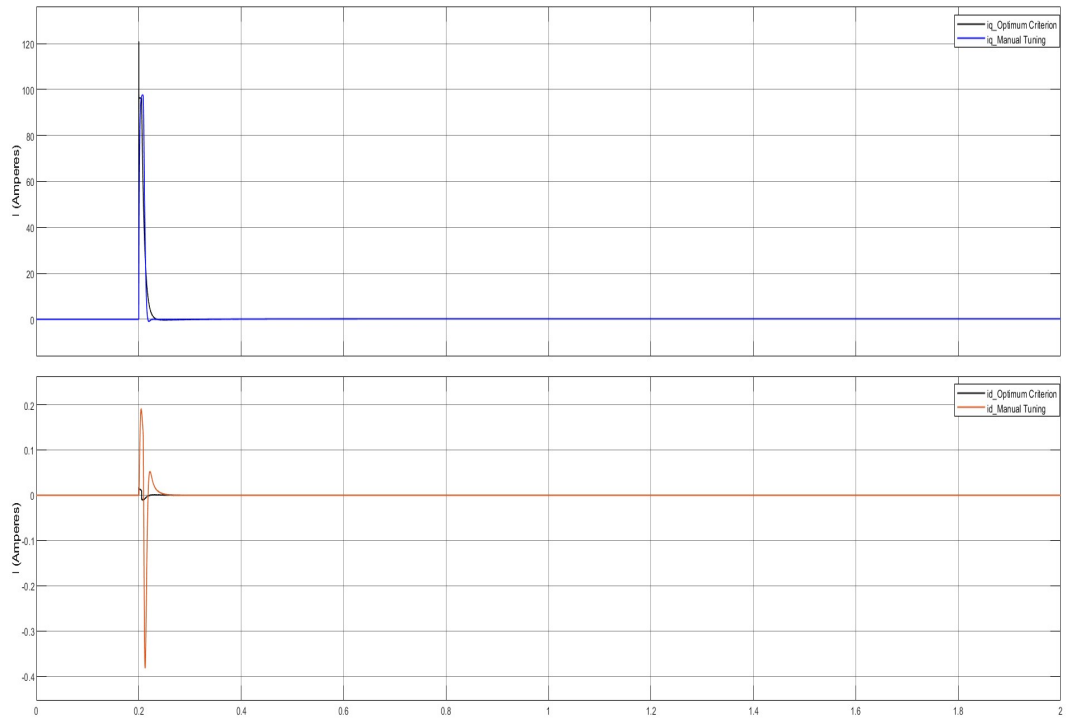


Figure 6.6: The response of torque with Manual tuning and Optimum criterion

**Figure 6.7:** The currents I_{dq} **Figure 6.8:** The currents I_{abc}

6.2.1.1.2 Step Response of 3000 RPM.

The second test is a step response of 3000 RPM at $t = 0.2$ seconds with an initial value of 1000 RPM for a simulation time of 1 second.

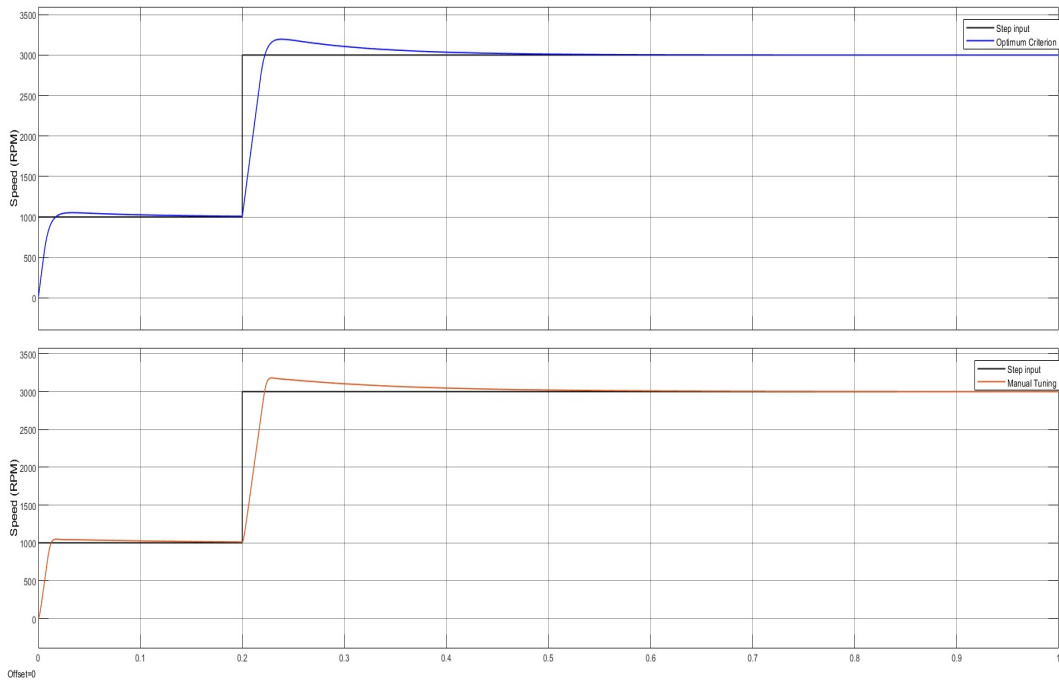


Figure 6.9: Step response of speed with Manual tuning and Optimum criterion

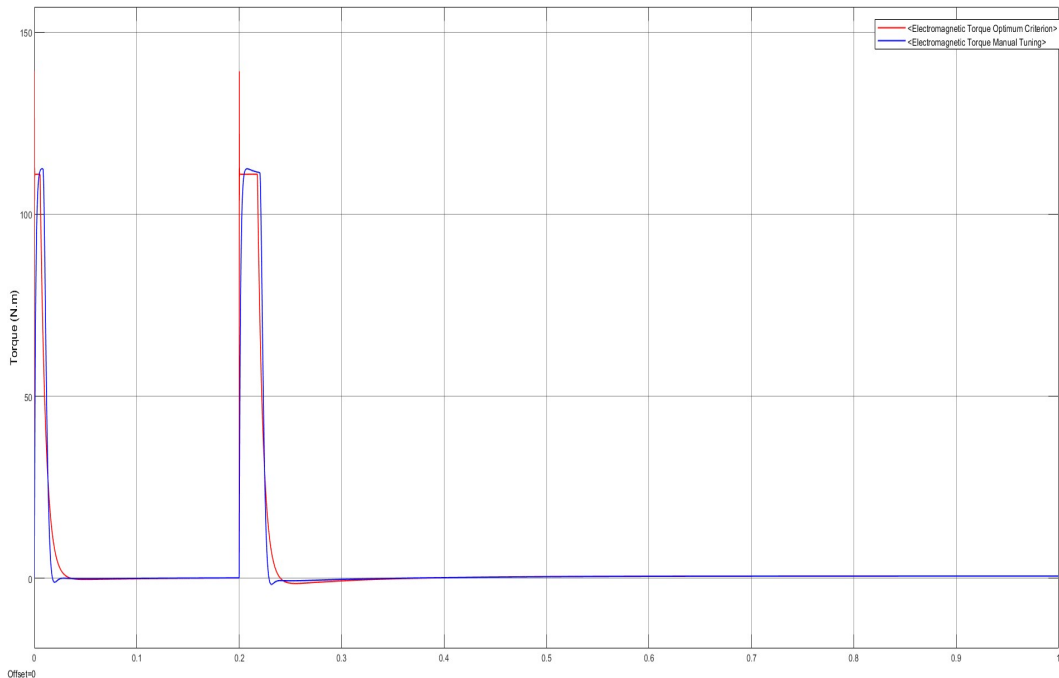
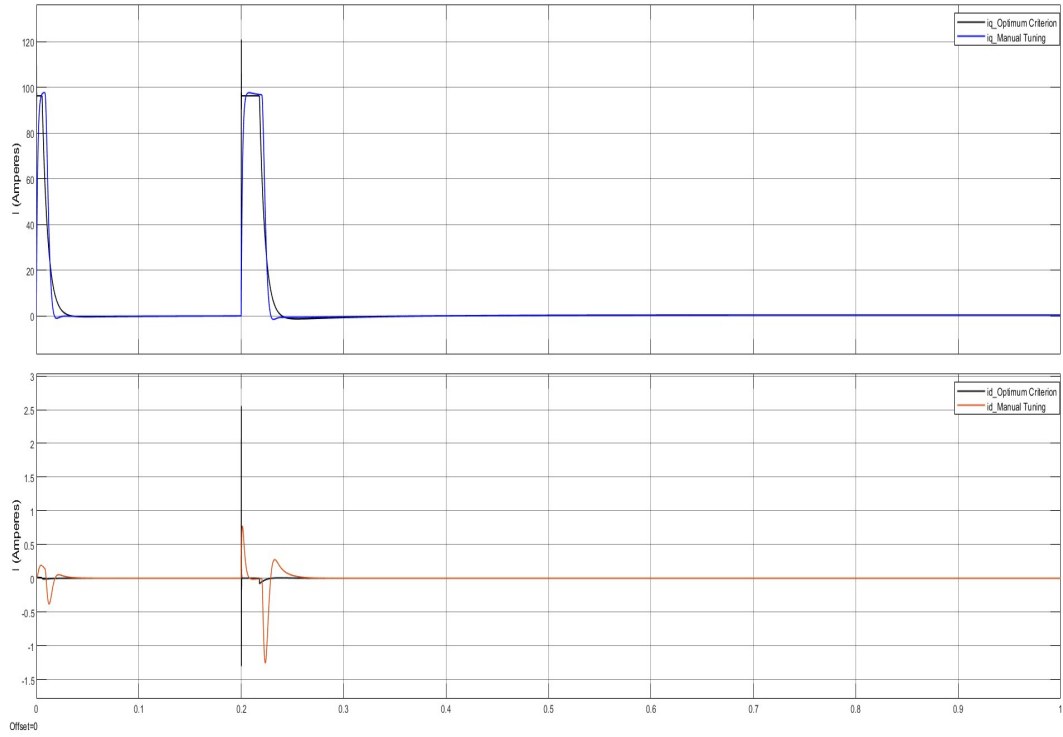
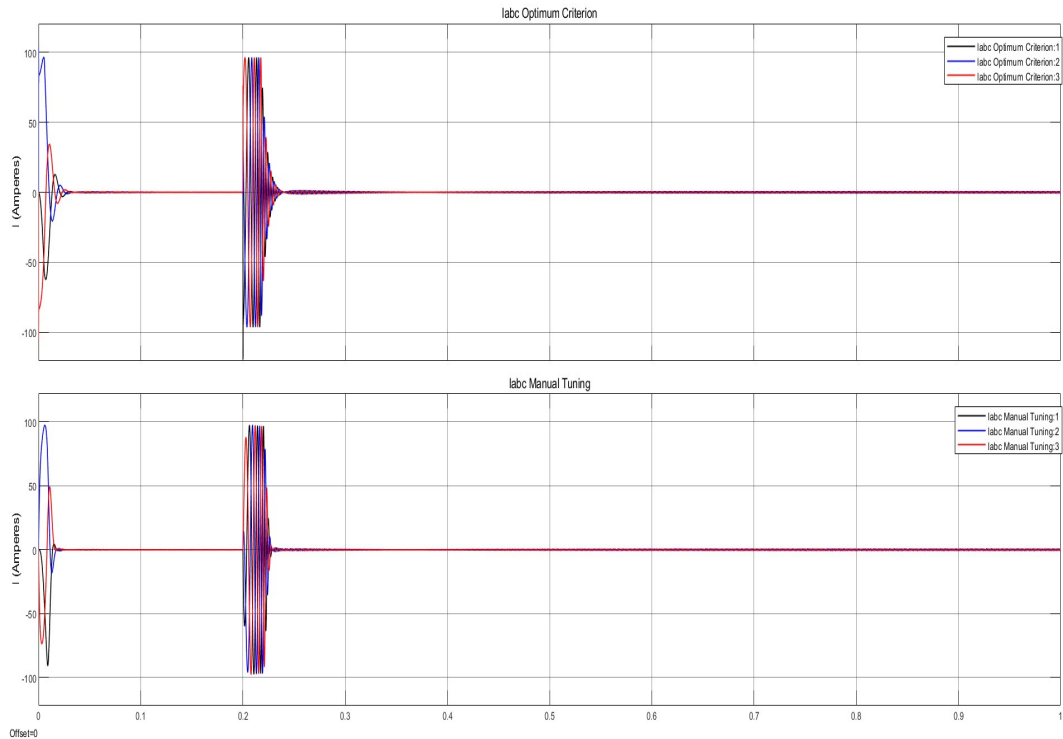


Figure 6.10: The response of torque with Manual tuning and Optimum criterion

**Figure 6.11:** The currents I_{dq} **Figure 6.12:** The currents I_{abc}

A detailed analysis of the simulations shown in Fig.6.5 to Fig.6.12 The comparison between both controllers demonstrates their capability to achieve the desired

speeds, albeit with subtle differences in their performance characteristics. Manual tuning results in a slight overshoot of approximately 9%, indicating responsiveness while maintaining reasonable deviations from the target speed. On the other hand, when employing the Magnitude Optimum and Symmetrical Optimum criteria, both controllers exhibit similar performance, with slight variations leading to speed overshoots of nearly 9% in certain simulated scenarios. The simulations show that the torque exceeds its limits. This is not due to any faults in the machine or errors in the modeling. Instead, it is caused by the nature of the input speed. A step input requires the speed to change instantaneously, resulting in an infinite rate of change. According to the equation for electromagnetic torque, the torque is directly proportional to the rate of change in angular speed. Therefore, this sudden change in speed explains the sudden increase in torque. To address this issue, the input speed should be gradually increased from one value to another, rather than changing instantaneously. However, as the motor approaches the target speed, the torque decreases and finally reaches zero under no-load conditions, but manual tuning performs better because it does not undershoot. Similarly, the behaviour of the i_q currents corresponds to that of the torque, suggesting a consistent reaction throughout the system components. These extensive observations provide clarification on the complex dynamics of the managed system and provide useful insights for fine-tuning control settings to reach desired performance goals.

6.2.1.2 With Load Torque Response

The simulation response below is for the two machines with load torque of **30 N.m** to Evaluate the machine's open-loop performance without load torque. One machine employs **Manual tuning** for the PI controllers, while the other employs **Magnitude Optimum criterion** and **Symmetrical Optimum criterion**. The test is a step in speed of 3000 RPM at $t = 0.2$ seconds with an initial value of 1000 RPM for a simulation time of 1 second. From the simulations in Fig.6.13 below, employing both manual tuning and the Magnitude Optimum and Symmetrical Optimum criteria for its controllers demonstrates a consistent outcome. The overshoot in speed is approximately 9.6% for both tuning methods. even though a load torque of $30N.m$ is added while the machine with manually tuned controllers appears to not be affected significantly by the load torque, the torque responses of both machines are almost the same in Fig6.14 . For the currents, it can be seen that i_q follows the same response as the torque and the stator three-phase currents are achieving almost the same values As can be seen, the frequency of the currents increased due to the increase in speed, as can be seen in Fig.6.15 and Fig.6.16. from this simulation, it can be seen that the manual tuning controller is slightly more robust and accurate than the Magnitude Optimum and Symmetrical Optimum criteria controller.

6.2.1.2.1 With Varying speed and Load Torque.

The simulation response below is for the two machines with step change in load torque from **10 N.m** to **35 N.m** at $t = 1$ second and step change in speed from **1000 RPM** to **2000 RPM** at $t = 0.3$ seconds The simulations are shown in

Fig.6.17 to Fig.6.20.

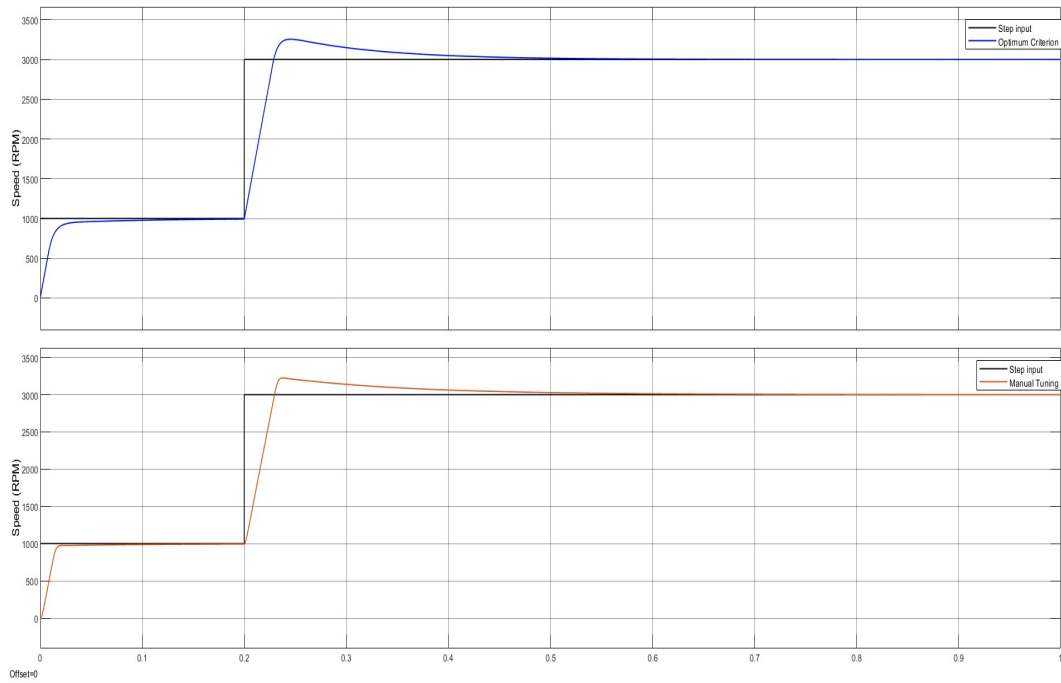


Figure 6.13: Step response of speed

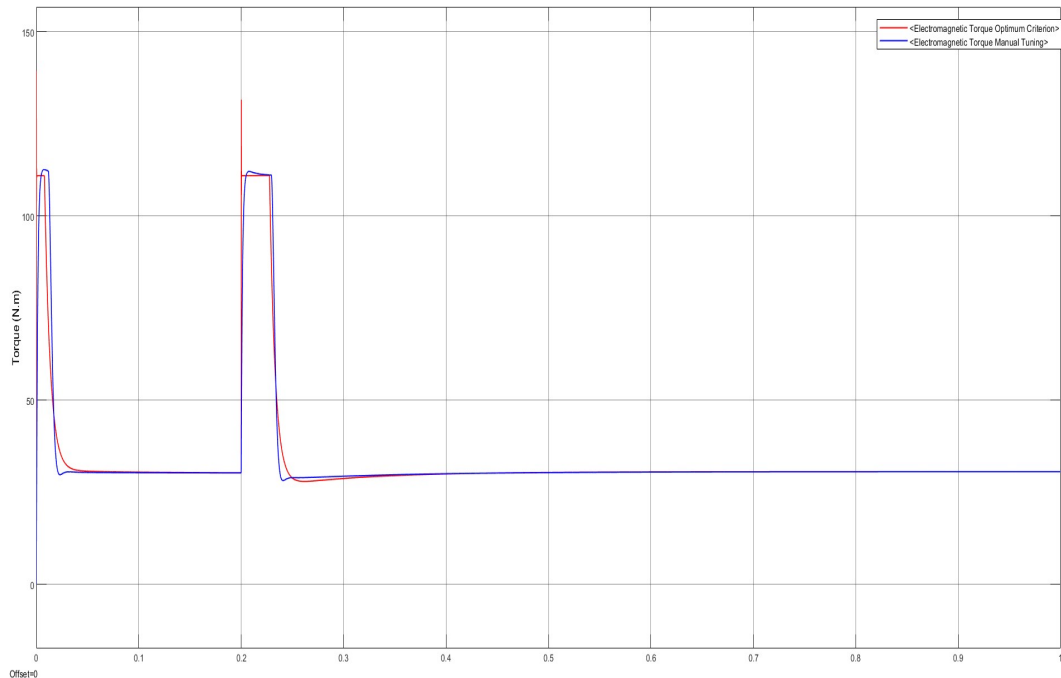
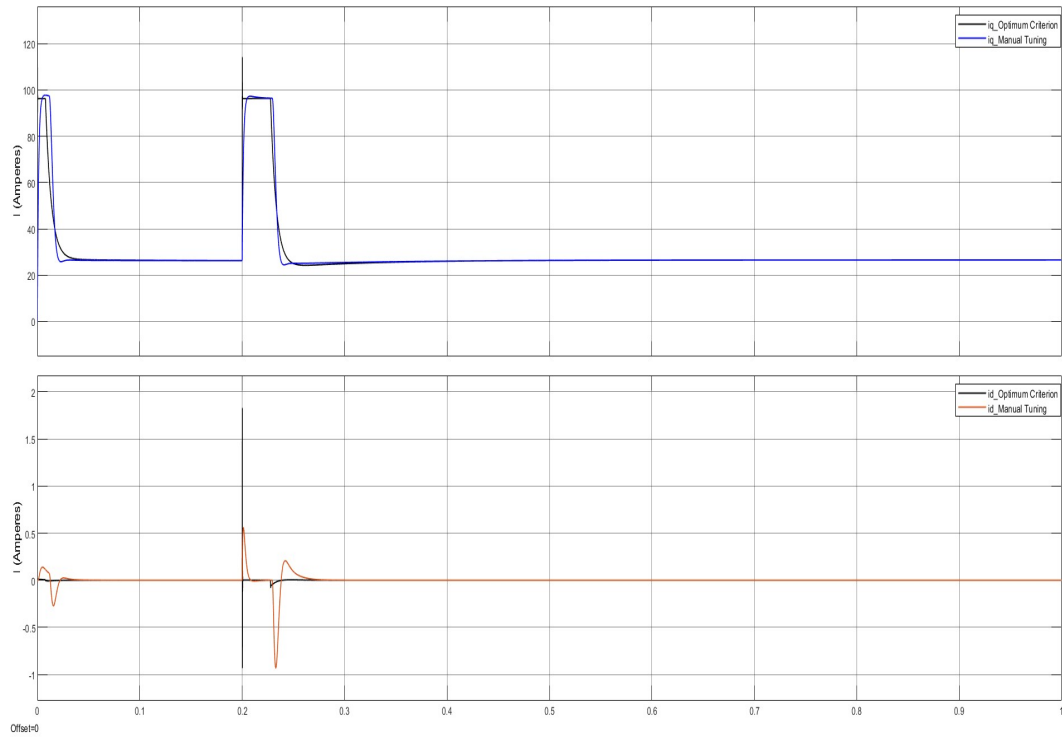
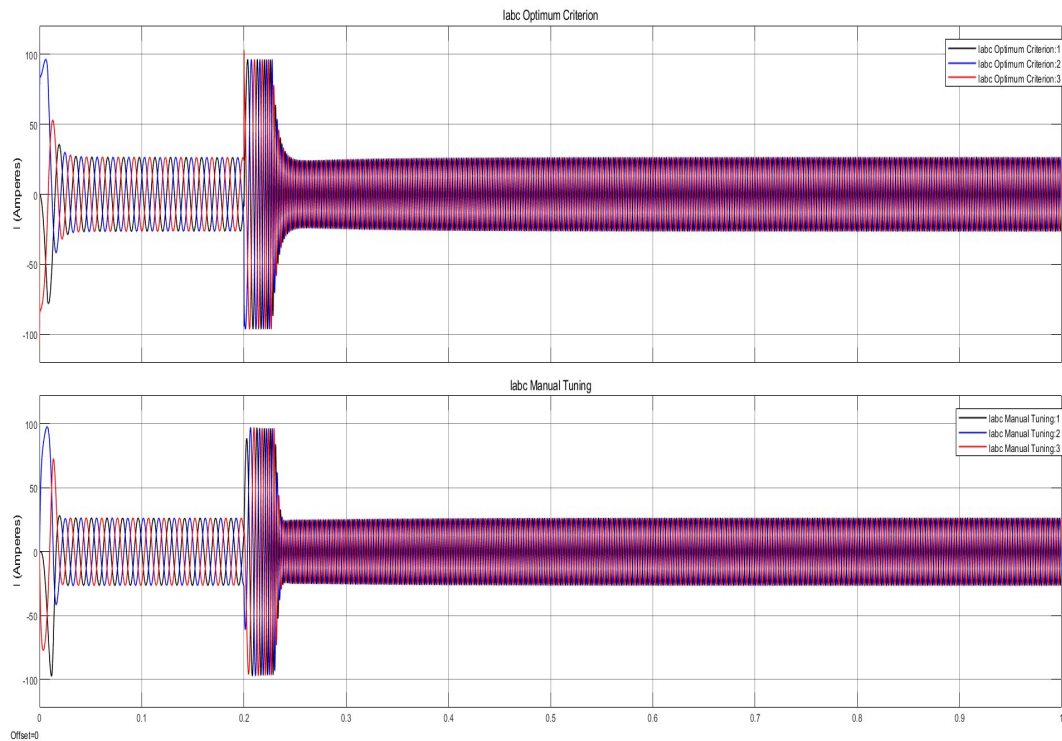


Figure 6.14: The response of torque

**Figure 6.15:** The currents I_{dq} **Figure 6.16:** The currents I_{abc}

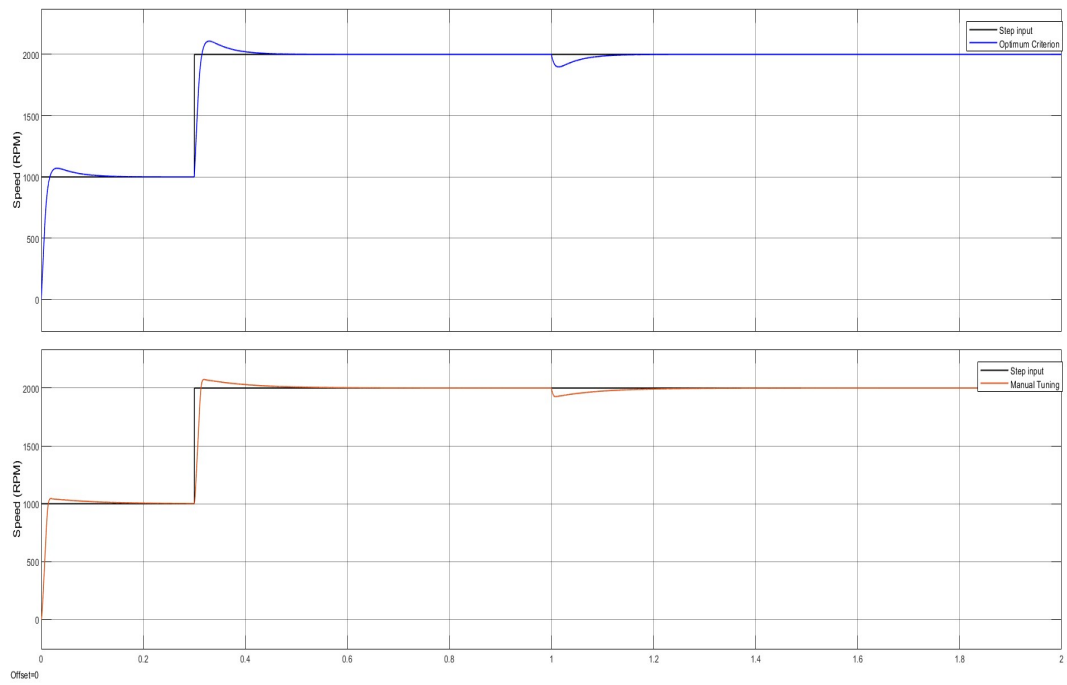


Figure 6.17: Step response of speed With Varying speed and Load Torque

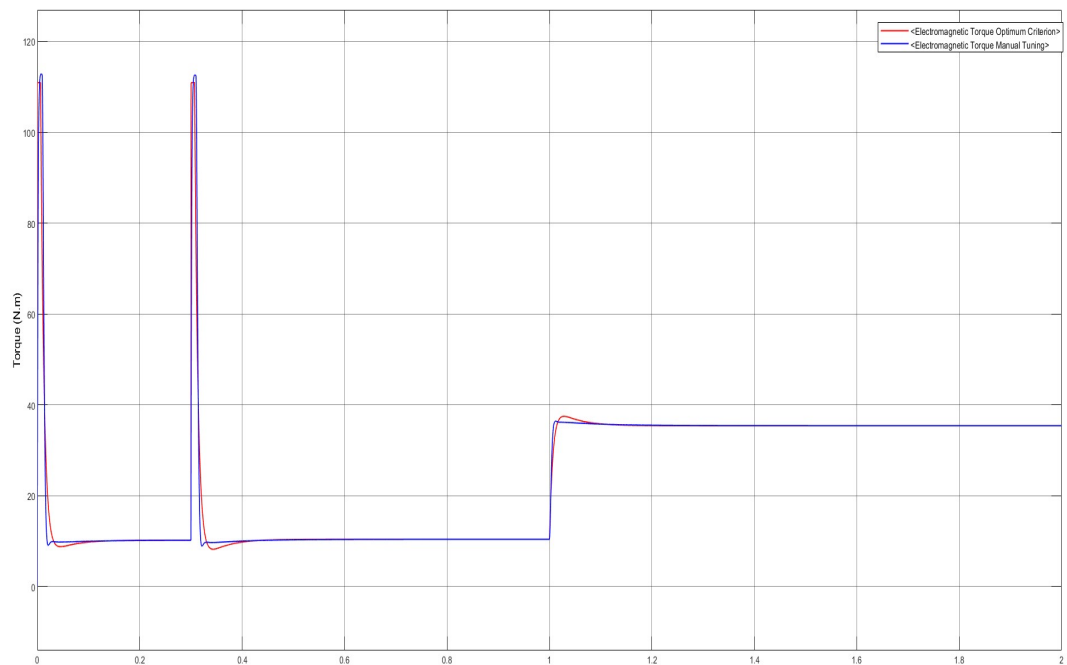


Figure 6.18: The response of torque With Varying speed and Load Torque

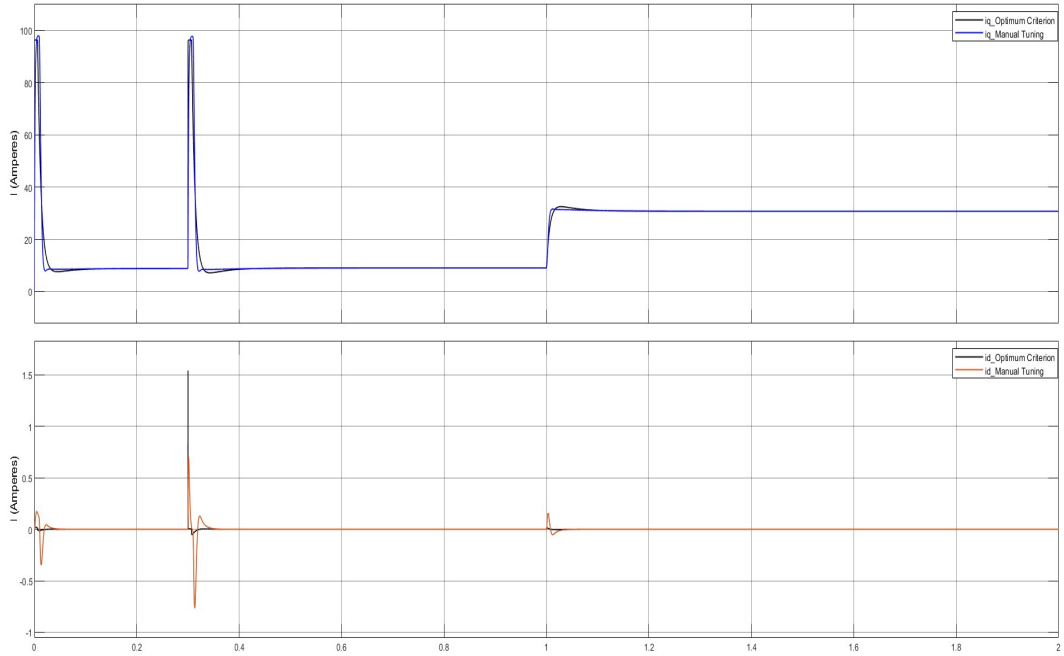


Figure 6.19: The currents I_{dq} With Varying speed and Load Torque

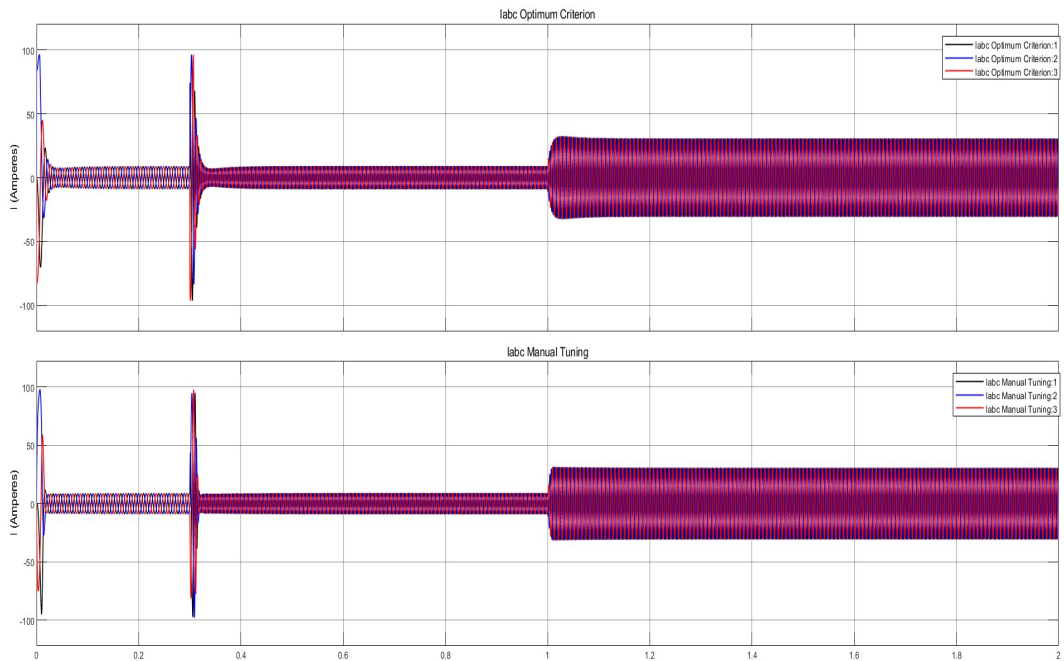


Figure 6.20: The currents I_{abc} With Varying speed and Load Torque

The simulations reveal that both controllers exhibit resilience in response to abrupt changes in torque, with slight differences observed between them. However, despite these variances, both controllers achieve the target speed and torque levels satisfactorily. This consistency underscores the robustness of the control strategies employed, highlighting their effectiveness in managing dynamic changes and ensuring stable motor operation. In general, the symmetrical optimum and magnitude

optimum criteria used to tune PI controllers exhibit precise and acceptable results. While manual tuning can also achieve satisfactory performance, the symmetrical optimum and magnitude optimum criteria offer a more scientific and systematic approach, reducing the reliance on trial and error inherent in manual tuning.

6.2.1.2.2 With Varying speed (Not Step Input) and Varying Load Torque.

The simulation response below is for the two machines with step change in load torque from **10 N.m** to **35 N.m** at $t = 1$ second and Speed gradually rising from **0 RPM** to **1000 RPM** from $t = 0$ to $t = 2$ then remaining constant at **1000 RPM** from $t = 2$ to $t = 2.1$ then increasing from **1000 RPM** to **2000 RPM** from $t = 2.1$ to $t = 4$ then remaining constant at **2000 RPM** from $t = 4$ to $t = 4.1$ then rising again to **3500 RPM** to $t = 6$ seconds then remains constant till $t = 6.5$ seconds then gradually decreasing till it reaches **0 RPM** at $t = 10$ seconds. This can be seen in Fig.6.21. The simulation results indicate that both controllers, one employing manual tuning and the other utilizing the Magnitude Optimum and Symmetrical Optimum criteria, exhibit comparable performance in speed response. They demonstrate minimal overshoot while effectively achieving precise speed control. while the electromagnetic torque is not overshooting much this is due to the input which have constant rate of change during the increase of speed and it similar for both controllers same goes for the I_{dq} currents.

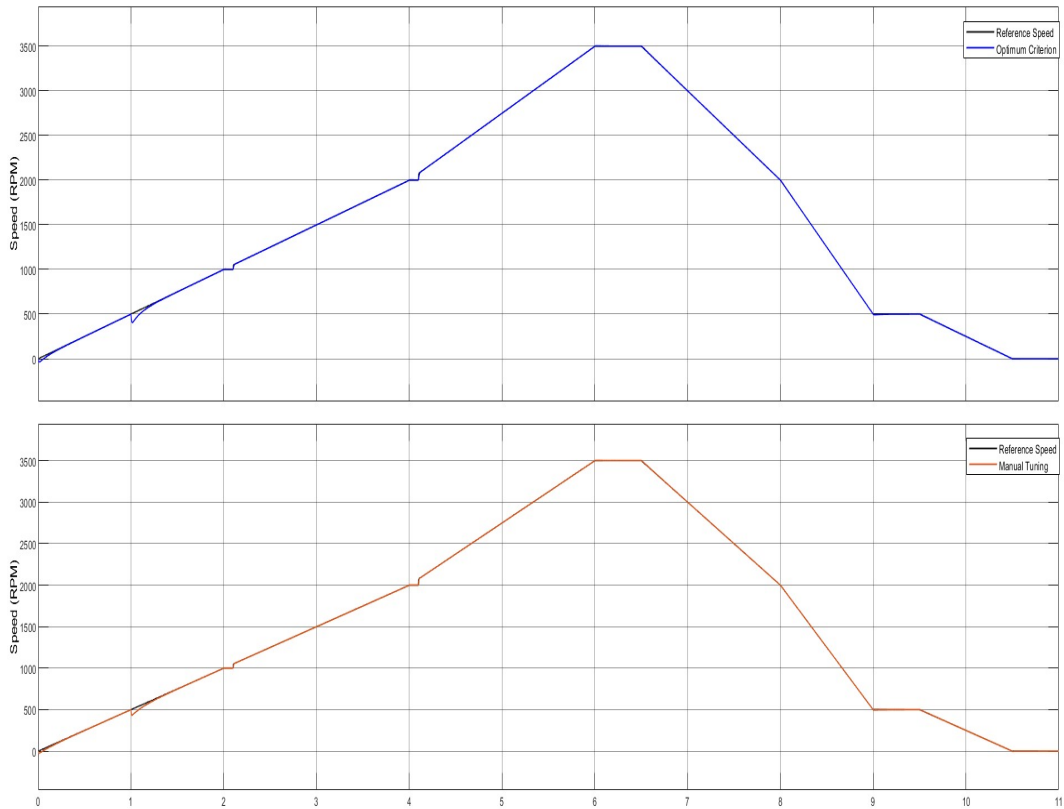


Figure 6.21: The Speed With Varying speed and Load Torque

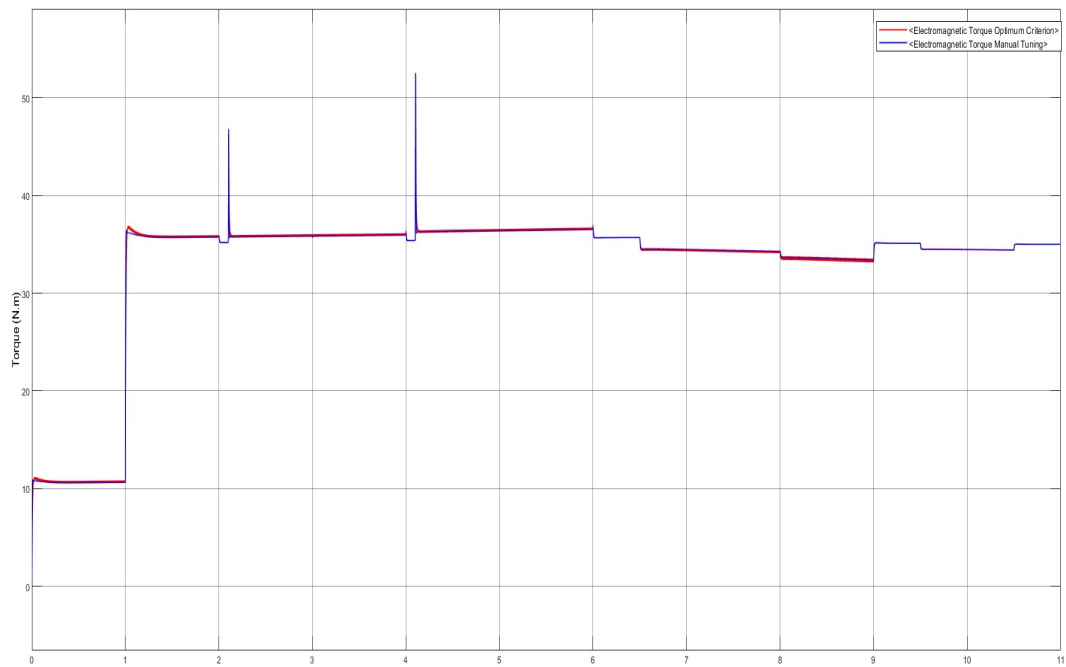


Figure 6.22: The torque With Varying speed and Load Torque

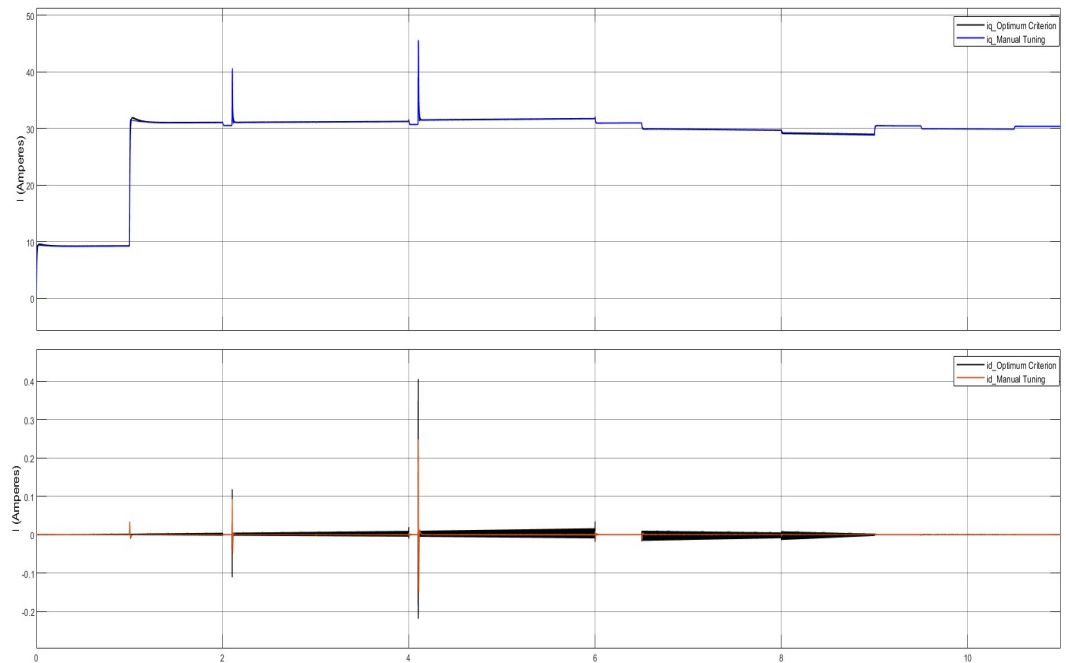


Figure 6.23: The I_{dq} currents With Varying speed and Load Torque

6.2.2 FOC Using Inverter

This section addresses the incorporation of Field-Oriented Control (FOC) with inverters, specifically the interplay of control strategies and modulation techniques in motor drive systems. The performance of FOC is evaluated using Simulink simulations across several modulation methods, ranging from traditional Sinusoidal Pulse Width Modulation (SPWM) to more complex techniques like space vector pulse width modulation (SVPWM). The goal is to investigate the effects of various approaches on crucial performance indicators such as torque ripple, current harmonics, and overall system efficiency. This section seeks to provide significant insight for optimizing motor drive systems across varied applications by delving into each modulation method within the FOC. In this section, the Simscape PMSM machine was used for compatibility with its power-electronics blocks.

6.2.2.1 FOC with SPWM

6.2.2.1.1 With No Load Torque Response.

In this simulation scenario, we explore the application of Field-Oriented Control (FOC) in conjunction with sinusoidal pulse width modulation (SPWM) and an inverter. The implemented carrier signal has a frequency of 50 kHz. The objective is to analyze the response of the system to a step input for speed, ranging from **500 to 2000 RPM**, under non-load torque conditions.

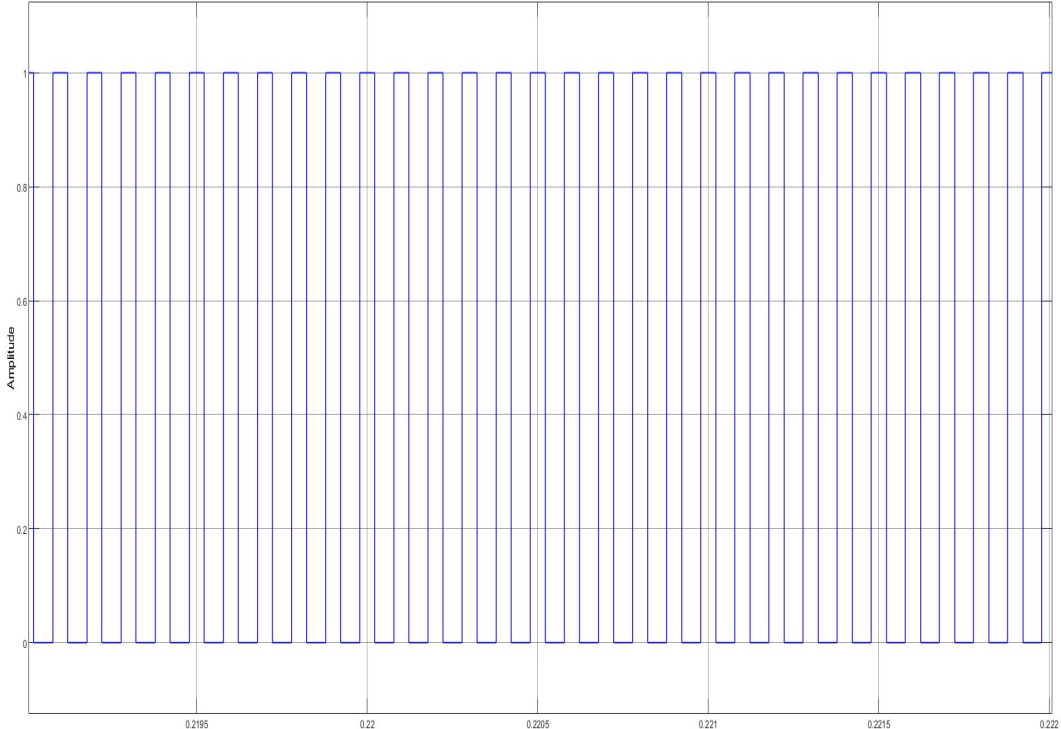


Figure 6.24: One of the sixth pulse signals generated from SPWM modulation

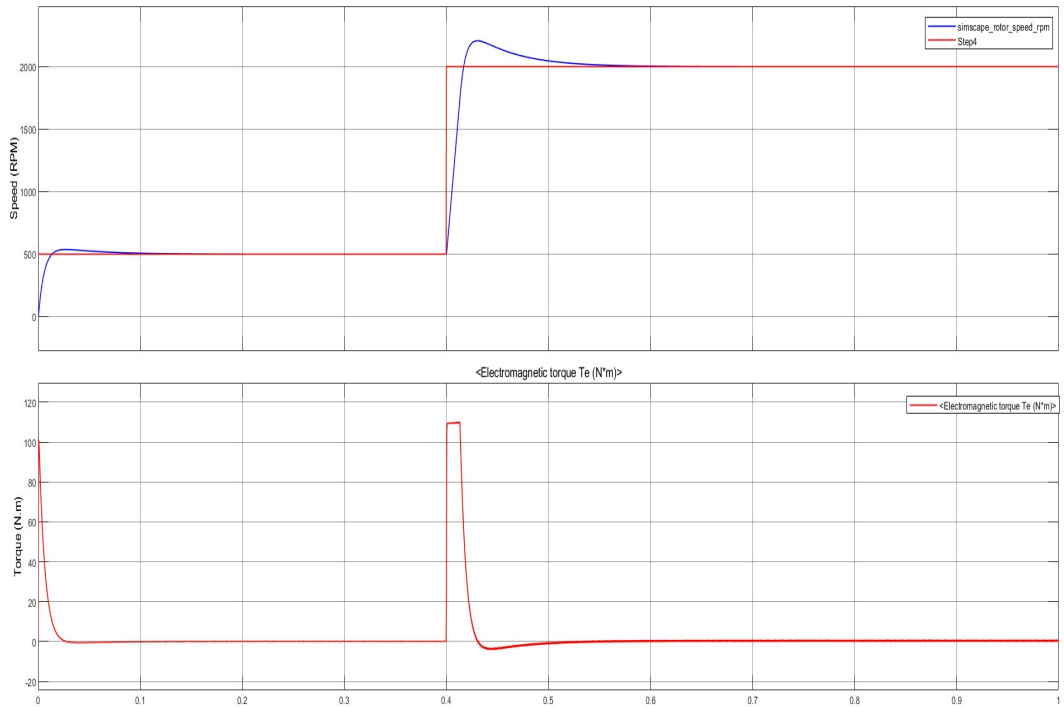


Figure 6.25: Speed and torque responses using SPWM with no load

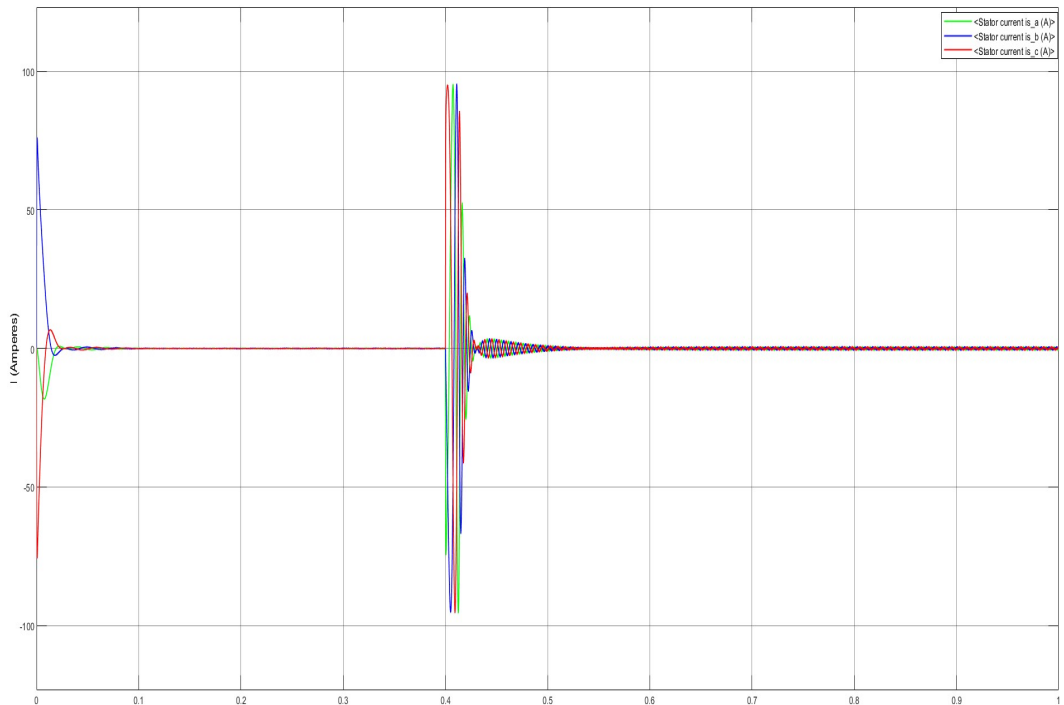


Figure 6.26: The three phase currents I_{abc} responses using SPWM with no load

The simulations of SPWM with no load torque reveal the presence of torque ripples, primarily stemming from the harmonics generated by the inverter and modulation technique. However, despite these fluctuations, it's noteworthy that the average torque remains zero. Interestingly, the motor demonstrates a commendable ability to accurately track the speed set. This indicates that while torque variations may occur due to the inherent characteristics of SPWM, the overall performance of the motor in terms of speed control remains precise and reliable.

6.2.2.1.2 With No Load Torque Response.

In this simulation scenario, Field-Oriented Control (FOC) in conjunction with sinusoidal pulse width modulation (SPWM) and an inverter is implemented. The objective is to analyze the response of the system to a step input for speed, ranging from **500 to 2000 RPM**, and a constant load torque of **30 N.m**.

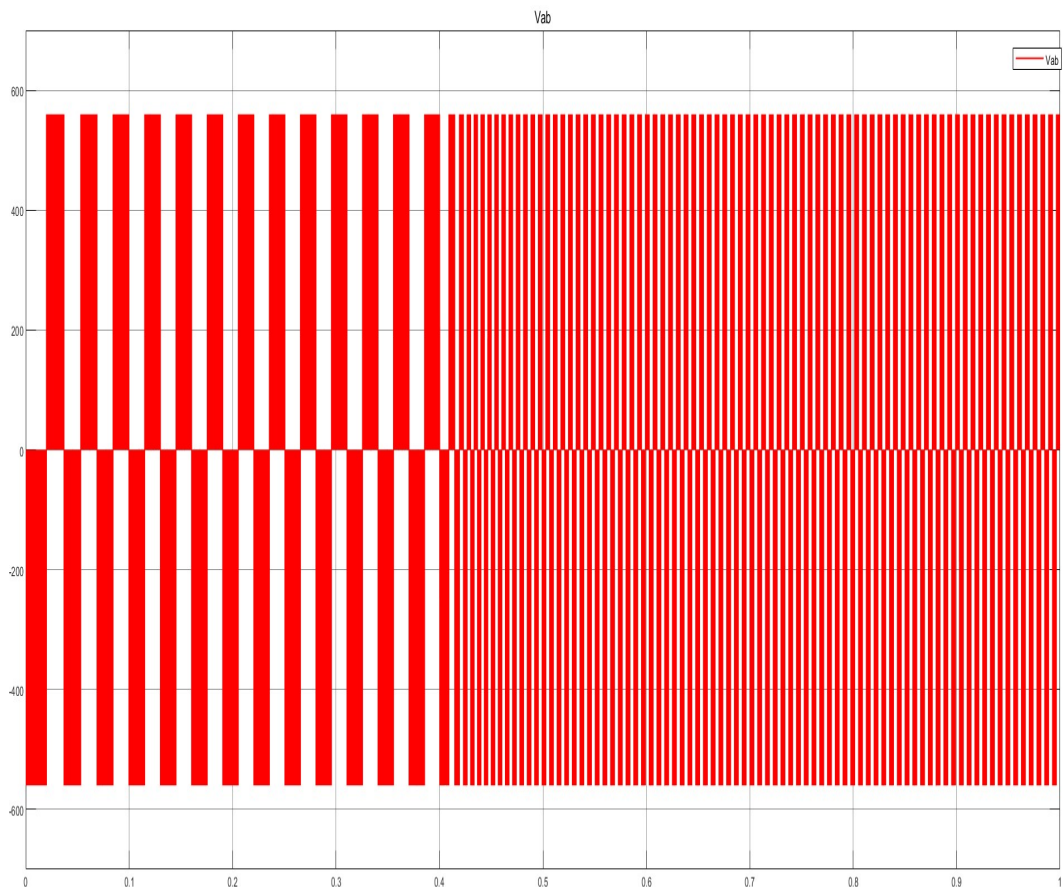


Figure 6.27: The Line to Line voltage V_{ab} produced from the inverter

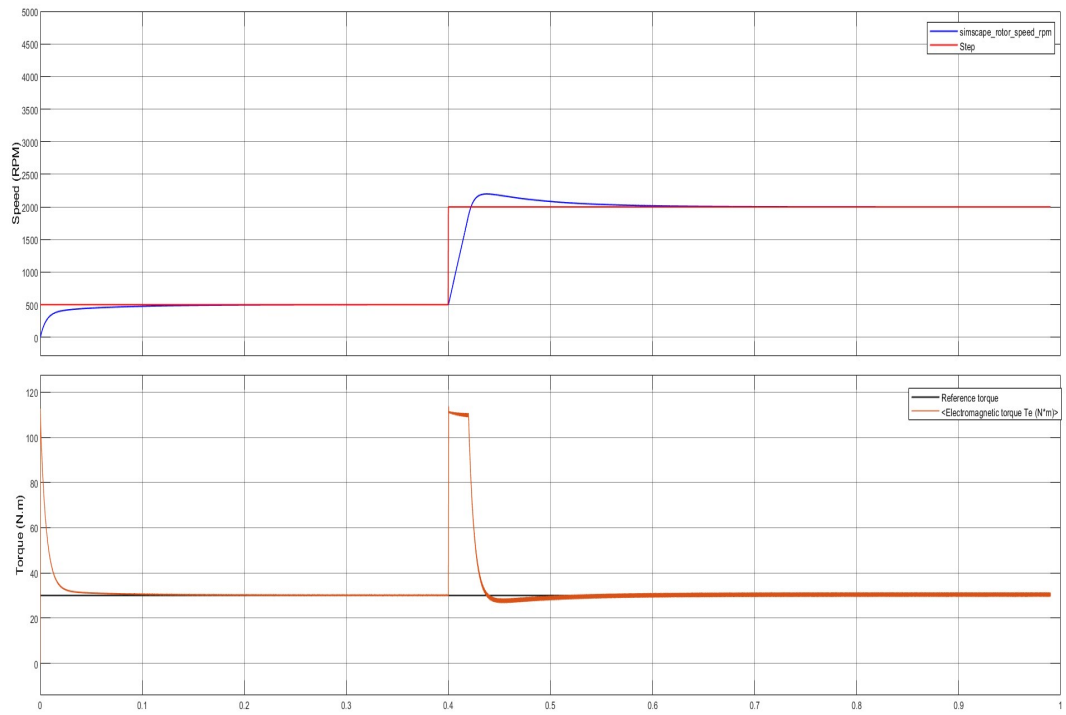


Figure 6.28: Speed and torque responses using SPWM with load torque of 30 N.m

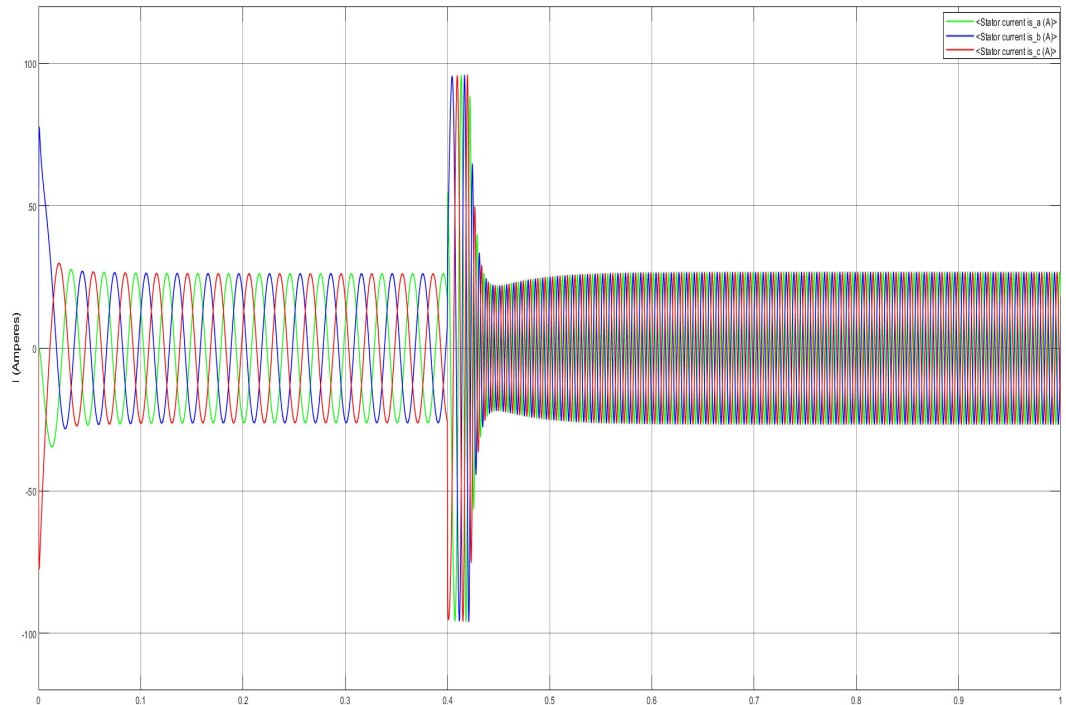


Figure 6.29: The three phase currents I_{abc} responses using SPWM with load torque of 30 N.m

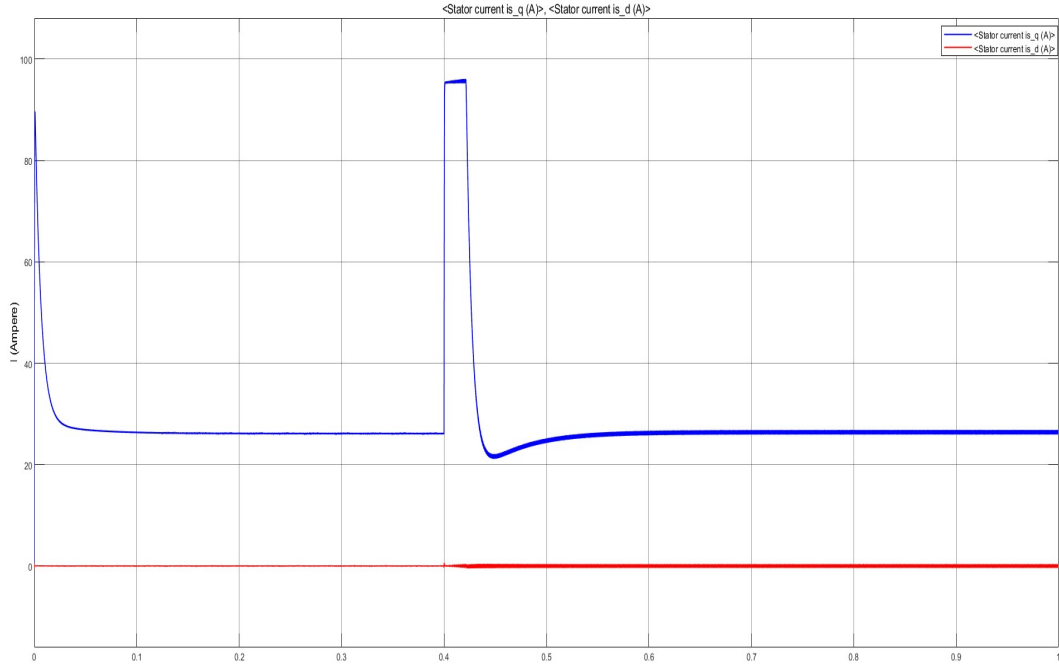


Figure 6.30: The I_{dq} responses using SPWM with load torque of 30 N.m

6.2.2.1.3 Varying speed and Load Torque.

In this simulation study, The performance of Field-Oriented Control (FOC) implemented with Sinusoidal Pulse Width Modulation (SPWM) inverter drive systems under varying input speeds and load torque conditions is analyzed. with the speed varying from **500 RPM** to **1000 RPM** to **2000 RPM** to **2500 RPM** and the torque varying from **10 N.m** to **30 N.m** to **80 N.m**.

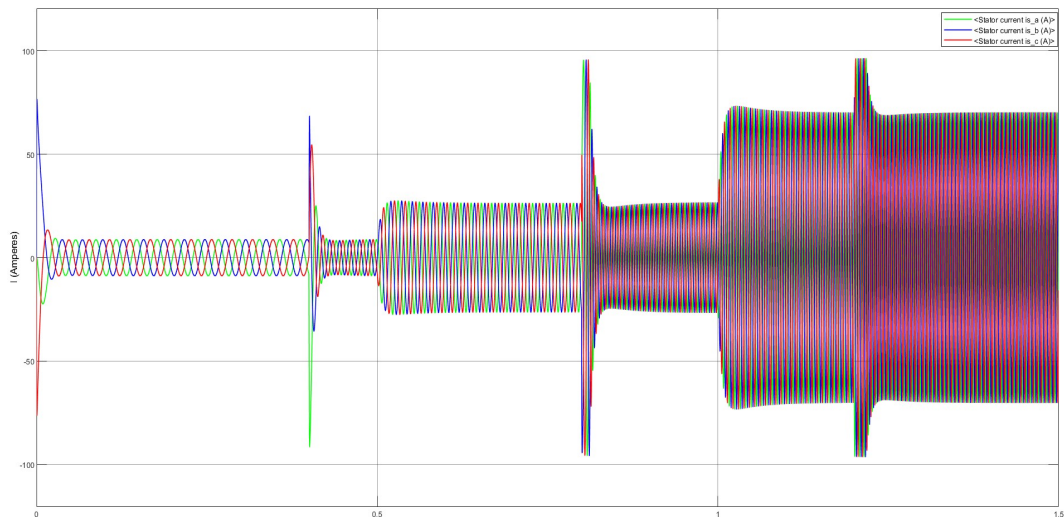


Figure 6.31: The I_{abc} responses using SPWM with varying speed and load torque

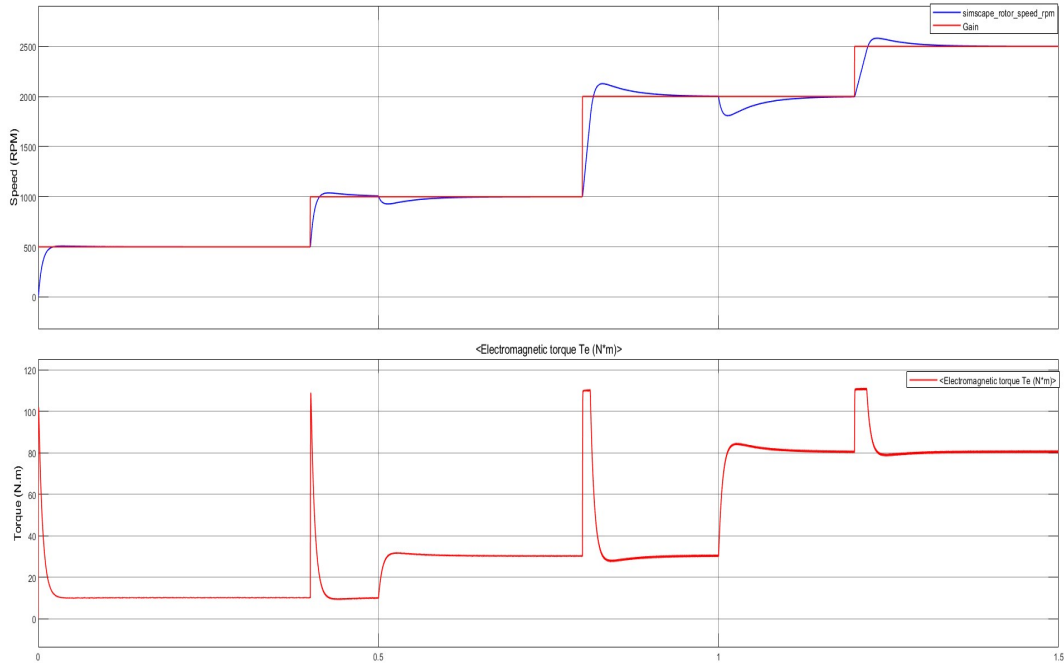


Figure 6.32: Speed and torque responses using SPWM with varying speed and load torque

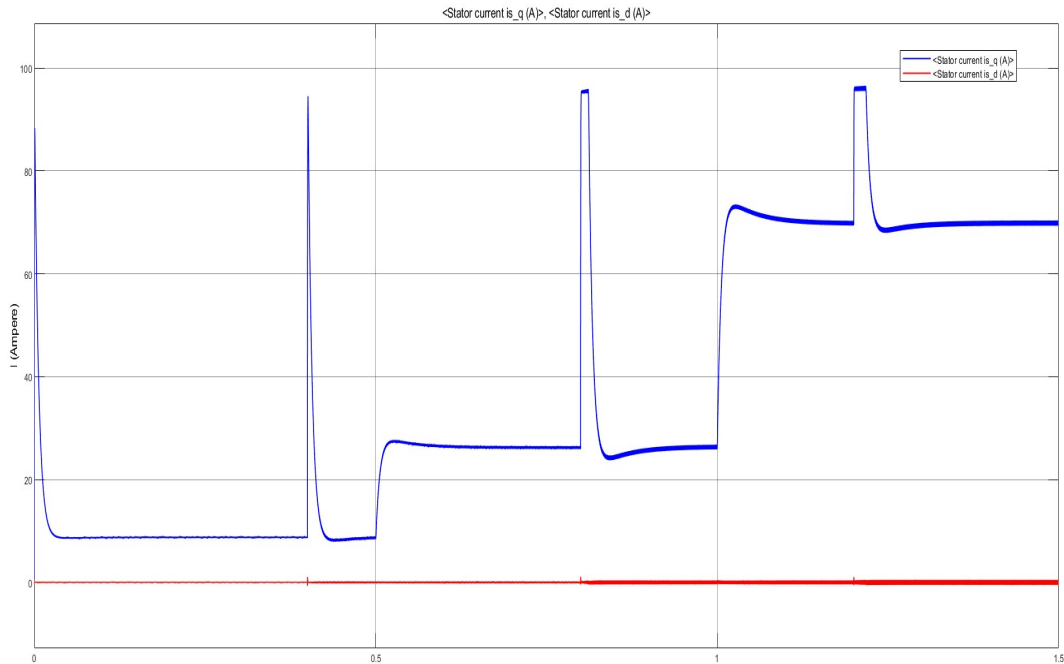


Figure 6.33: The I_{dq} responses using SPWM with varying speed and load torque

The simulations from Fig.6.31 to Fig.6.33 demonstrate that the motor's speed and torque closely track the specified inputs with precision, with slight overshoot in the speed that can be fixed through implementing much robust controller. However,

noticeable torque ripples are observed, attributed to the harmonics generated by the inverter. Additionally, the i_q current exhibits a similar behavior to the torque, while the i_d current remains consistently at zero. Furthermore, the frequencies of three-phase currents (I_{abc}) vary with changes in speed, while their amplitudes fluctuate in response to alterations in torque levels. This dynamic behavior underscores the intricate interplay between control inputs, motor response, and inverter operation in the simulated system.

6.2.2.2 FOC with SVPWM

6.2.2.2.1 With Load Torque Response.

In this simulation study, the performance of Field-Oriented Control (FOC) combined with Space Vector Pulse Width Modulation (SVPWM) and an inverter is investigated. The motor is subjected to a step-input speed transition from 500 RPM to 2000 RPM at a step time of 0.4 seconds while maintaining a constant load torque of 30 N.m. Through meticulous analysis of the motor response under these conditions, the effectiveness of FOC-SVPWM in regulating speed and torque in real-time scenarios is evaluated. As can be seen in the figure below, Fig.6.34 the line-to-line voltage V_{ab} produced from the inverter with SVPWM as modulation strategy, As shown in the figure, the voltage frequency and amplitude vary with the varying in the speed.

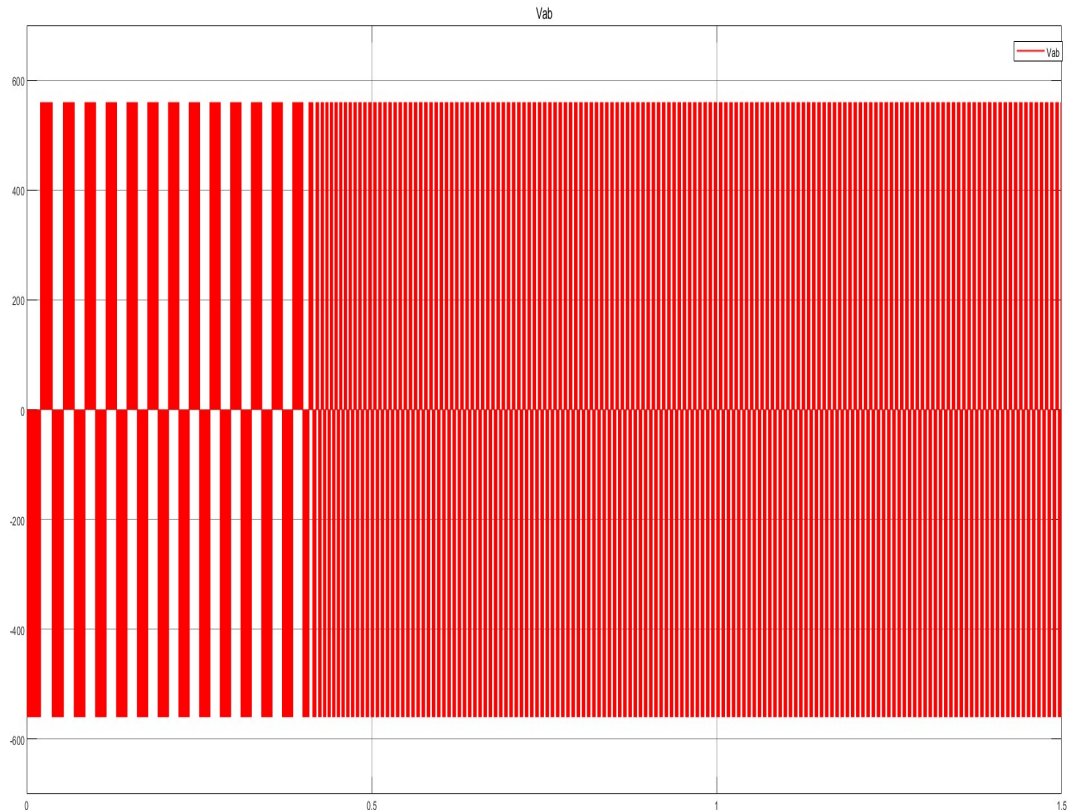


Figure 6.34: The line-to-line voltages V_{ab} using SVPWM

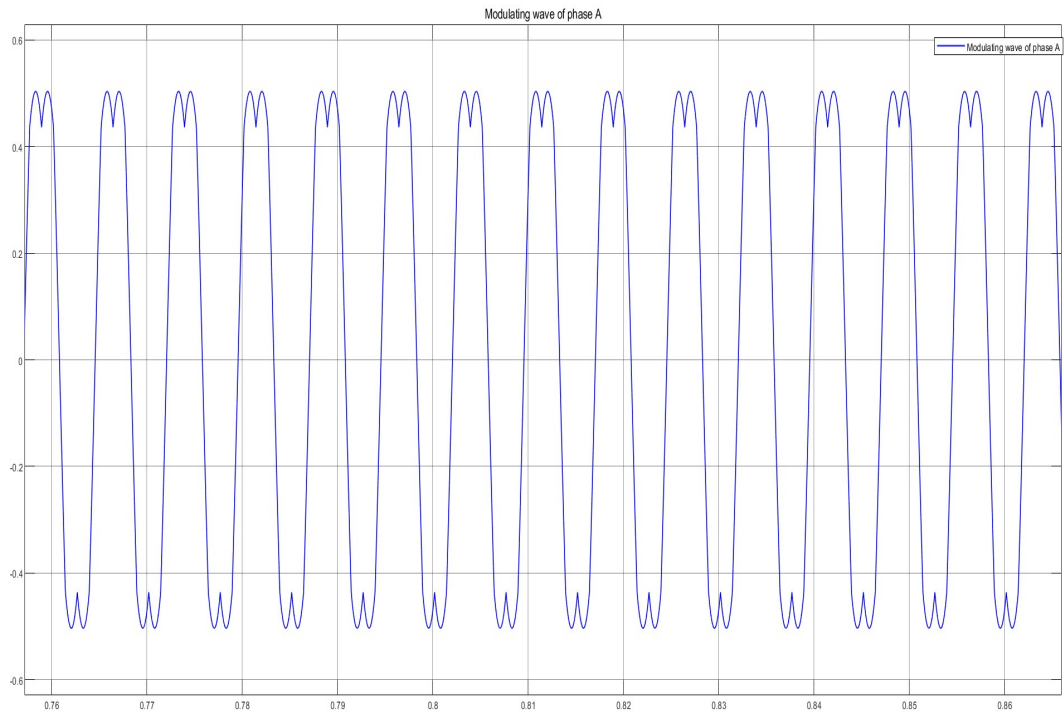


Figure 6.35: The modulating signal generated from SVPWM associated with phase A

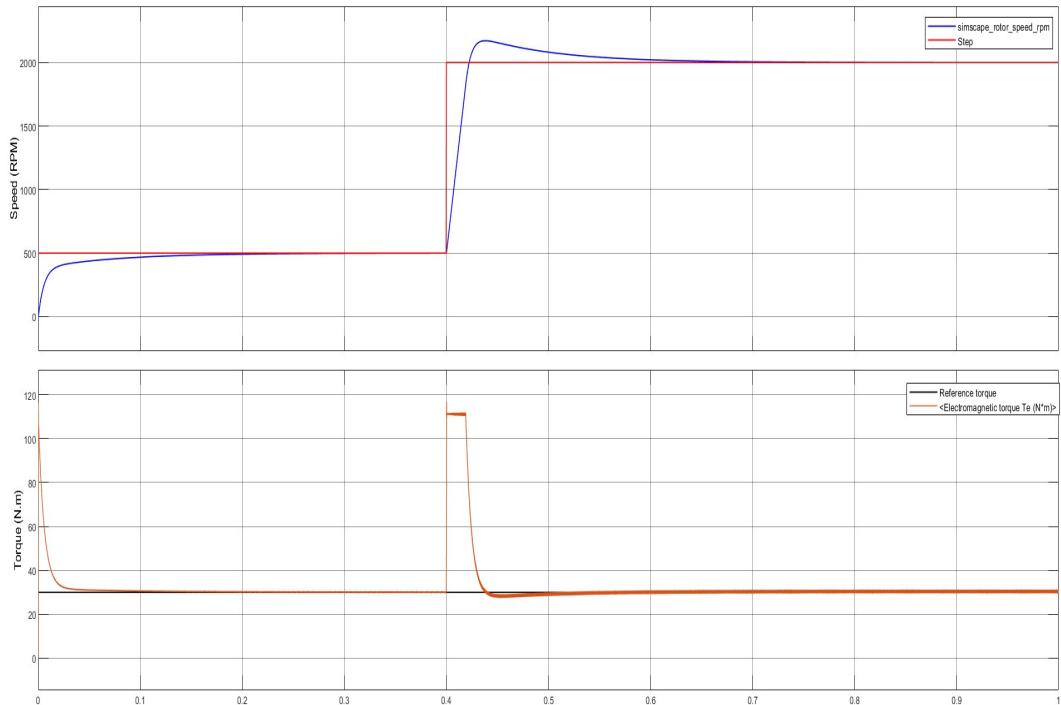


Figure 6.36: Speed and torque responses using SVPWM with load torque of 30 N.m

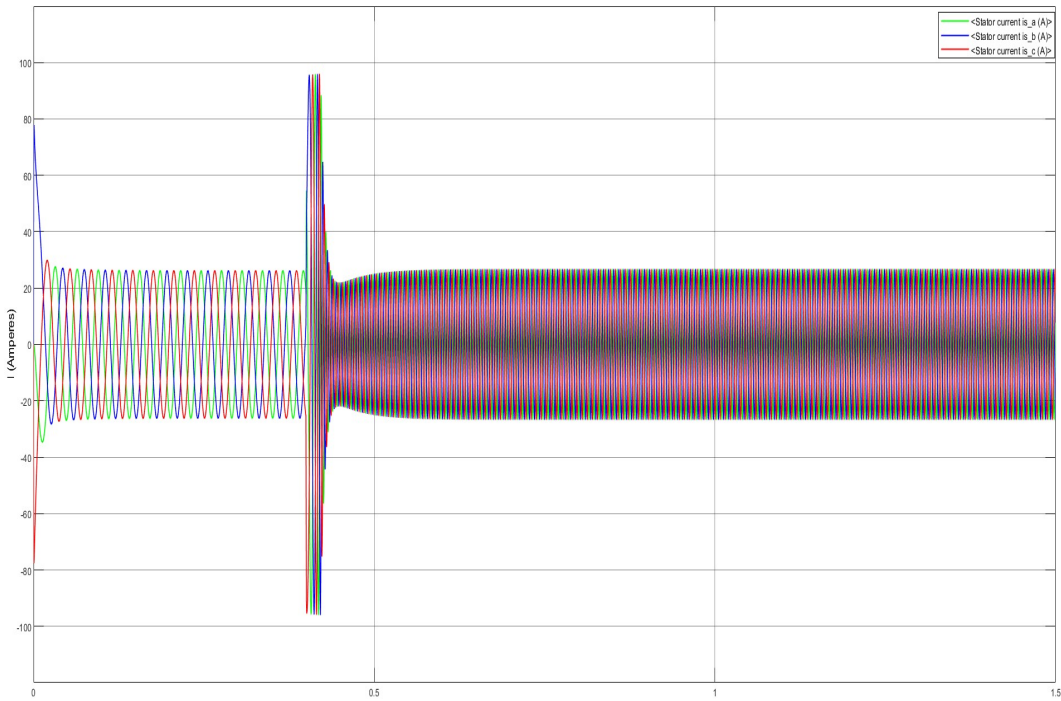


Figure 6.37: The three phase currents I_{abc} responses using SVPWM with load torque of 30 N.m

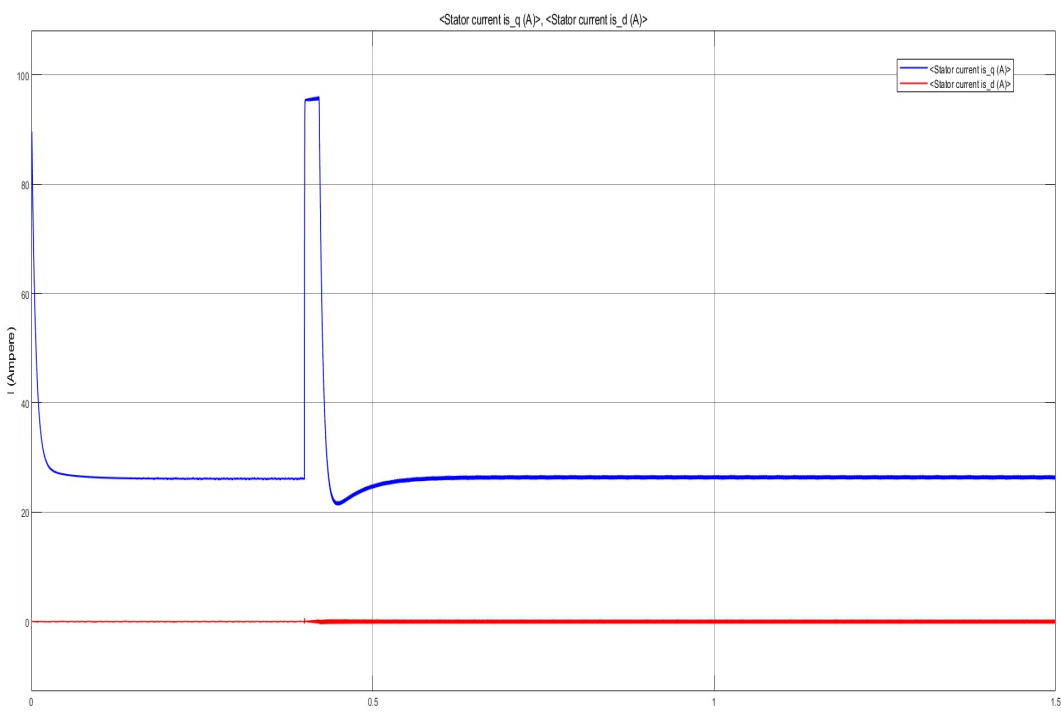


Figure 6.38: The I_{dq} responses using SVPWM with load torque of 30 N.m

The simulation from Fig.6.34 to Fig.6.38 outcomes closely resembled those observed with Sinusoidal Pulse Width Modulation (SPWM), exhibiting analogous performance characteristics. Notably, both control strategies demonstrated comparable abilities in governing speed and torque within the defined parameters. This alignment underscores the viability of integrating Field-Oriented Control (FOC) with Space Vector Pulse Width Modulation (SVPWM) as an effective means of motor drive regulation, particularly in scenarios necessitating swift speed transitions and precise torque modulation.

6.2.2.2 Varying speed and Load Torque.

In this simulation study, The performance of Field-Oriented Control (FOC) implemented with Space Vector Pulse Width Modulation (SVPWM) inverter drive systems under varying input speeds and load torque conditions is analyzed. with the speed varying from **500 RPM** to **1000 RPM** to **2000 RPM** to **2500 RPM** and the torque varying from **10 N.m** to **30 N.m** to **80 N.m**.

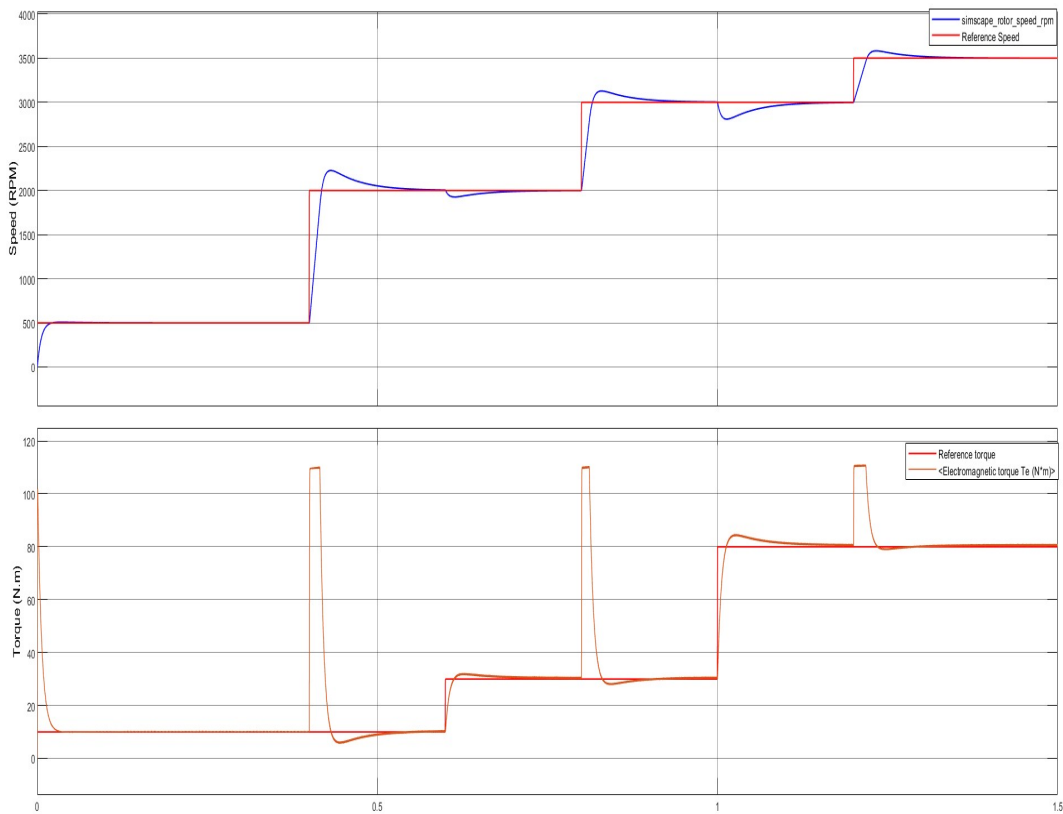


Figure 6.39: Speed and torque responses using SVPWM with varying speed and load torque

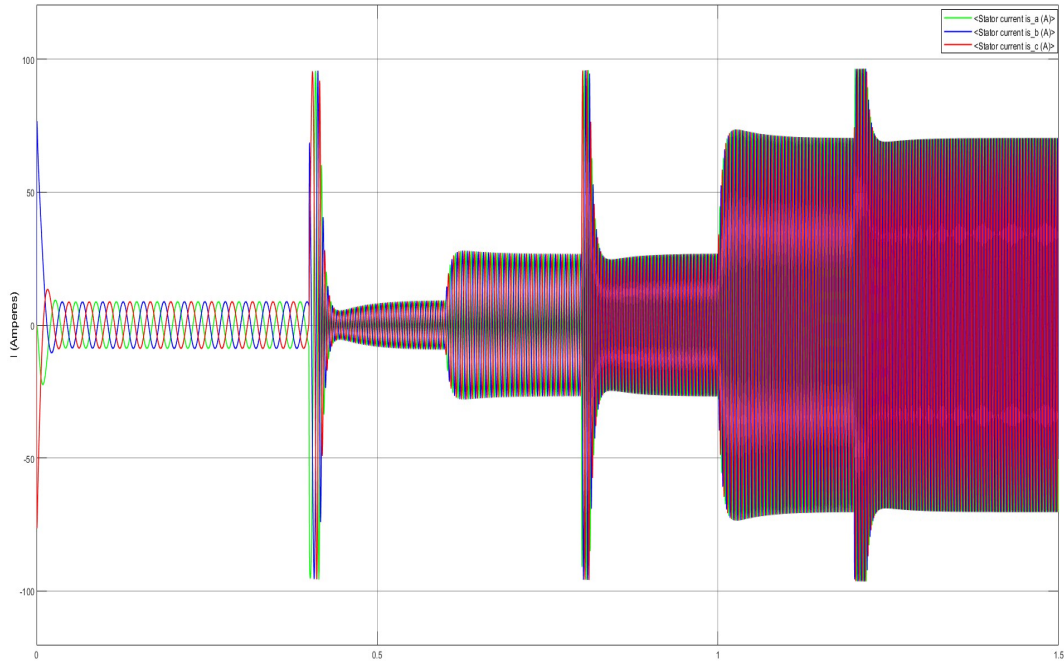


Figure 6.40: The three phase currents I_{abc} responses using SVPWM with varying speed and load torque

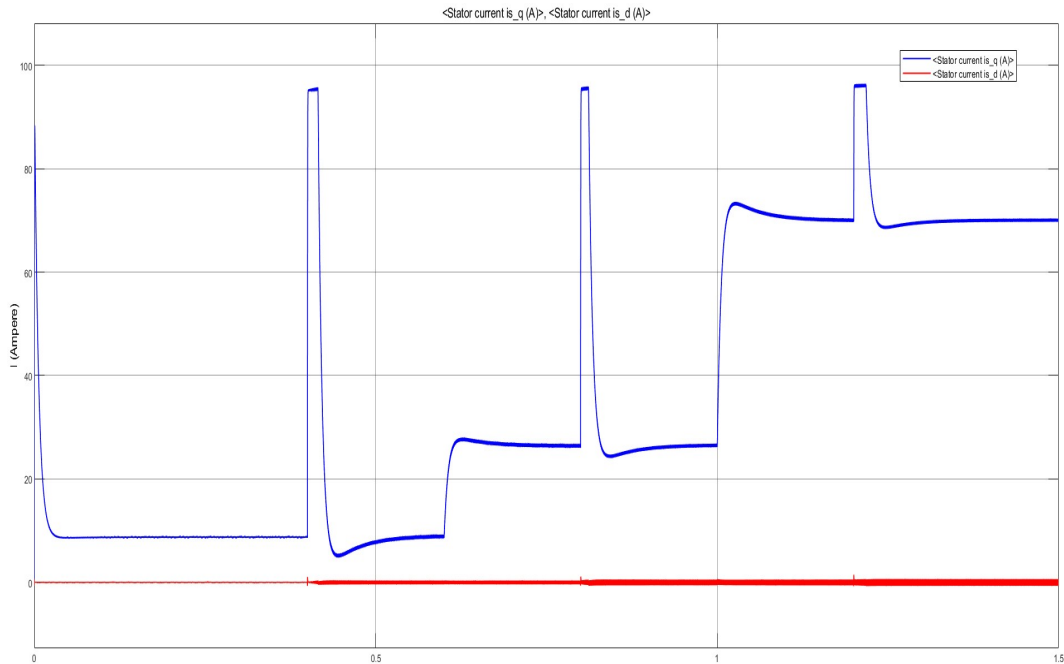


Figure 6.41: The I_{dq} responses using SVPWM with varying speed and load torque

The simulation results depicted in Figures 6.39 to 6.41 closely mirrored those obtained with Sinusoidal Pulse Width Modulation (SPWM), showcasing similar performance traits. In particular, both control methods exhibited comparable effi-

cacy in regulating speed and torque under the specified conditions. This consistency underscores the viability of integrating Field-Oriented Control (FOC) with Space Vector Pulse Width Modulation (SVPWM) as an effective approach to motor drive regulation, particularly in scenarios requiring swift speed transitions and precise torque modulation. In the next section, a fast Fourier transform (FFT) analyzer tool in Simulink is employed to measure the total harmonic distortion of both the SPWM and SVPWM.

6.2.2.2.3 Varying speed (Not Step) and Load Torque.

In this simulation study, The performance of Field-Oriented Control (FOC) implemented with Space Vector Pulse Width Modulation (SVPWM) inverter drive systems under varying input speeds and load torque conditions is analyzed.

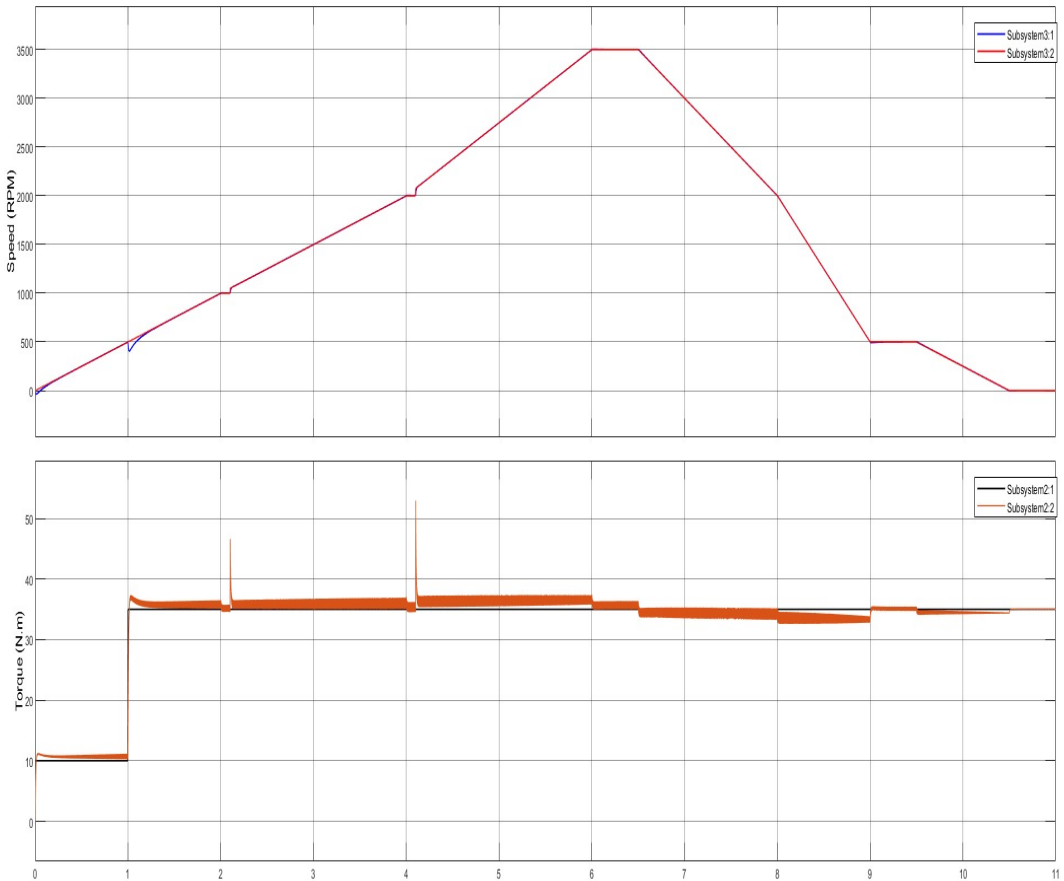


Figure 6.42: The speed and torque responses

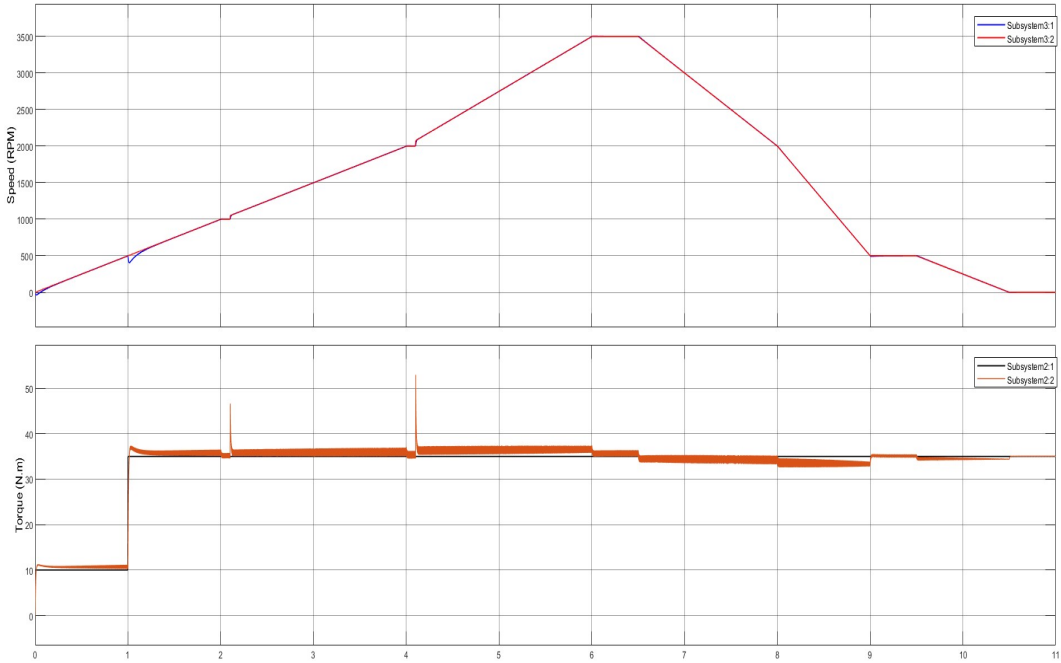


Figure 6.43: The I_{dq} currents

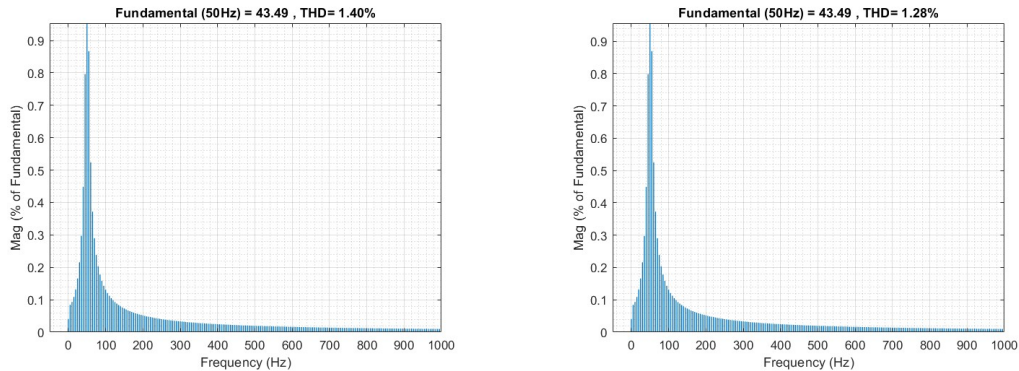
6.2.2.2.4 Comparing The THD of SPWM and SVPWM Within Base Speed.

In the evaluation of modulation techniques within the context of Field-Oriented Control (FOC) for Permanent Magnet Synchronous Motors (PMSMs), an examination of Total Harmonic Distortion (THD) between Sinusoidal Pulse Width Modulation (SPWM) and Space Vector Modulation (SVM) is essential. SPWM, despite its widespread use and relative simplicity in implementation, tends to exhibit higher THD levels compared to SVM. This is primarily attributed to SPWM's inherent limitations in precisely controlling inverter switching patterns, leading to increased harmonic content in the output voltage waveform. Conversely, SVM demonstrates superior harmonic suppression capabilities by optimizing voltage vector selection and switching patterns, resulting in reduced THD levels, enhanced motor performance.[3]

The initial assessment of Total Harmonic Distortion (THD) in the current is conducted utilizing the Simulink FFT analyzer tool. This analytical approach enables the determination of THD by analyzing the frequency spectrum of the current waveform. The motor was running at **750 RPM** and load torque attached was **50 N.m**.

The simulations reveal that the SVPWM has slightly less THD in the current waveform than the SPWM at fundamental frequency of **50Hz**.

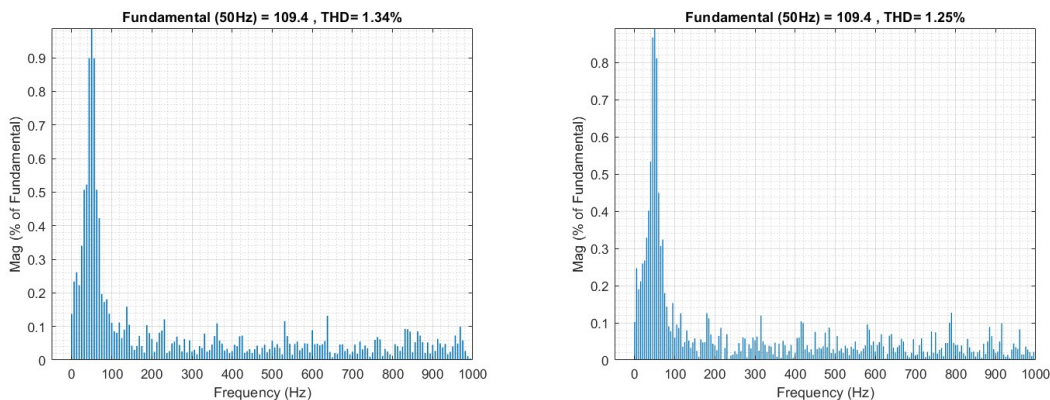
The second assessment of Total Harmonic Distortion (THD) in the line-to-line voltage V_{ab} is conducted utilizing the Simulink FFT Analyzer tool. This analytical strategy enables the determination of THD by analyzing the frequency spectrum



(a) The FFT analysis of SPWM current waveform-(b) The FFT analysis of SVPWM current waveform

Figure 6.44: The FFT analysis of the current waveforms

of the current waveform. The motor was running at **750 RPM** and load torque attached was **50 N.m**.6.45a and Fig.6.45b.



(a) The FFT analysis of SPWM current waveform-(b) The FFT analysis of SVPWM voltage waveform

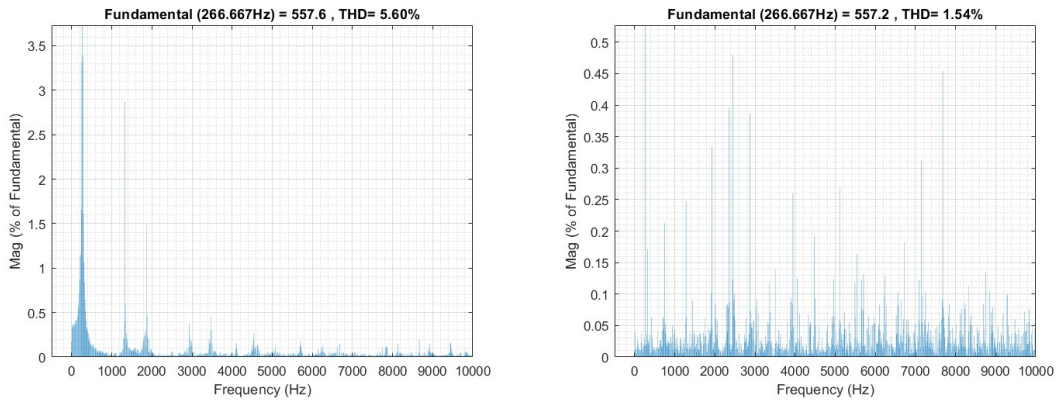
Figure 6.45: The FFT analysis of the voltage waveforms

The simulations reveal that the SVPWM has slightly less THD in the voltage waveform than the SPWM at fundamental frequency of **50Hz**.

6.2.2.2.5 Comparing The THD of SPWM and SVPWM Above Base Speed.

In this section, the comparison between Sinusoidal Pulse Width Modulation (SPWM) and Space Vector Pulse Width Modulation (SVPWM) when Permanent Magnet Synchronous Motors (PMSMs) operate above their base speed is explored. The focus lies on examining the Total Harmonic Distortion (THD) of both modulation techniques in overmodulation region. The motor was running at **4000 RPM** and zero load torque. as shown in Fig.6.46a and Fig.6.46b.

The simulations reveal that the SVPWM has less THD in the voltage waveform than the SPWM at fundamental frequency of **266.667 Hz**.



(a) The FFT analysis of SPWM current waveform (b) The FFT analysis of SVPWM voltage waveform

Figure 6.46: The FFT analysis of the voltage waveforms

Hence, opting for Space Vector Pulse Width Modulation (SVPWM) as the modulation technique for Field-Oriented Control (FOC) of Permanent Magnet Synchronous Motors (PMSMs) proves superior to Sinusoidal Pulse Width Modulation (SPWM). SVPWM demonstrates reduced Total Harmonic Distortion (THD) in both voltage and current waveforms while also yielding higher fundamental phase voltage compared to SPWM. Specifically, the fundamental phase voltage in SVPWM exceeds that of SPWM by approximately 15.5%, making it a more favorable choice for achieving enhanced motor performance and efficiency.

6.2.3 MTPA and Flux Weakening

In the simulations and results chapter, the focus is on the Maximum Torque per Ampere (MTPA) and flux weakening control strategies for Interior Permanent Magnet Synchronous Motors (IPMSM). Additionally, Space Vector Pulse Width Modulation (SVPWM) was used to enhance the performance of these control strategies.

MTPA is a critical control method designed to optimize the torque output relative to the current supplied to the motor. By maximizing the torque per unit of current, MTPA enhances the efficiency and performance of the IPMSM, making it a preferred choice for various high-performance applications.

Flux weakening, in contrast, is crucial for extending the operational speed range of the motor. At high speeds, the back electromotive force (EMF) increases, which can limit the current and thus the torque. Flux weakening reduces the magnetic flux in the motor to mitigate this issue, allowing the motor to achieve higher speeds without a significant drop in performance.

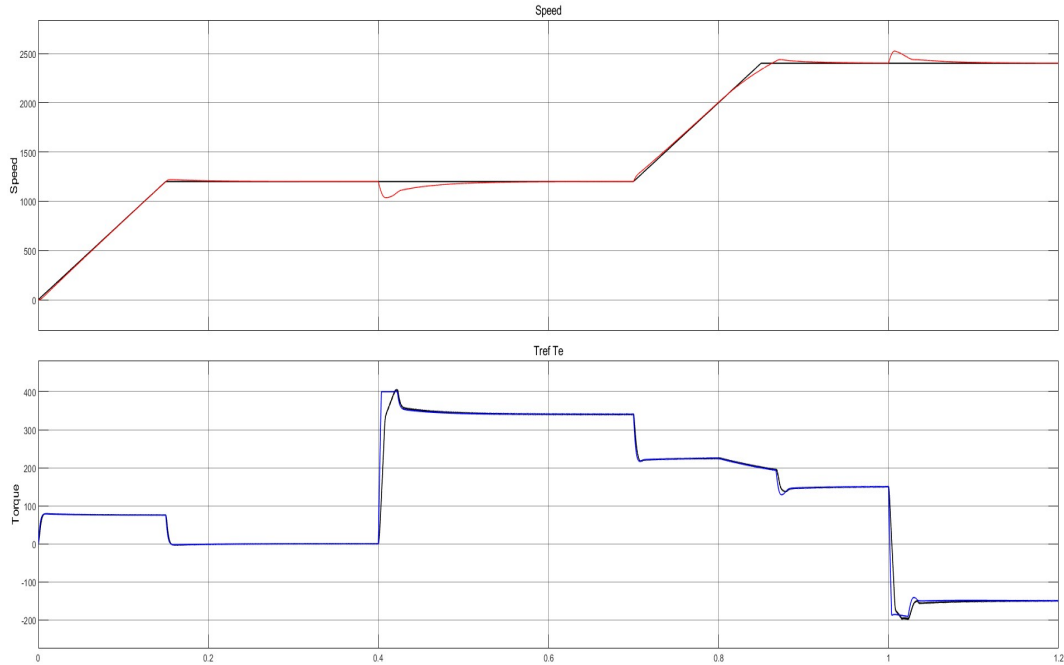
The IPMSM parameters used in these simulations, which form the basis for analyzing the effectiveness of MTPA and flux weakening, are detailed in Table 6.4.

Parameters	Values (Units)
Phases	3
Rated Torque	400 ($N.m$)
Rated Speed	1200 (RPM)
Pole Pairs	4
Stator phase resistance (R_s)	6.5 ($m\Omega$)
d-axis Inductance (L_d)	1.597 (mH)
q-axis Inductance (L_q)	2.057 (mH)
Inertia (J)	0.09 ($kg.m^2$)
Viscous friction (B)	0.002 ($N.m.s$)
Nominal DC voltage (V_{dc})	550 (V)
Rated Power	50 (KW)

Table 6.4: Parameters of IPMSM

6.2.3.1 Motor performance: different speed and load torque

This section demonstrates the motor performance across different speeds and load torques. The speed ranges from the base speed to overspeed, while the torque varies from 0 to nearly its maximum and also in the reverse direction. This can be seen in Fig.6.47.

**Figure 6.47:** The speed and torque response

6.2.3.2 MTPA

This section demonstrates the effect of the MTPA on the motor currents at a speed of **1000 RPM** and changing load torque. This can be seen in the figures from Fig.6.48. to Fig.6.50.

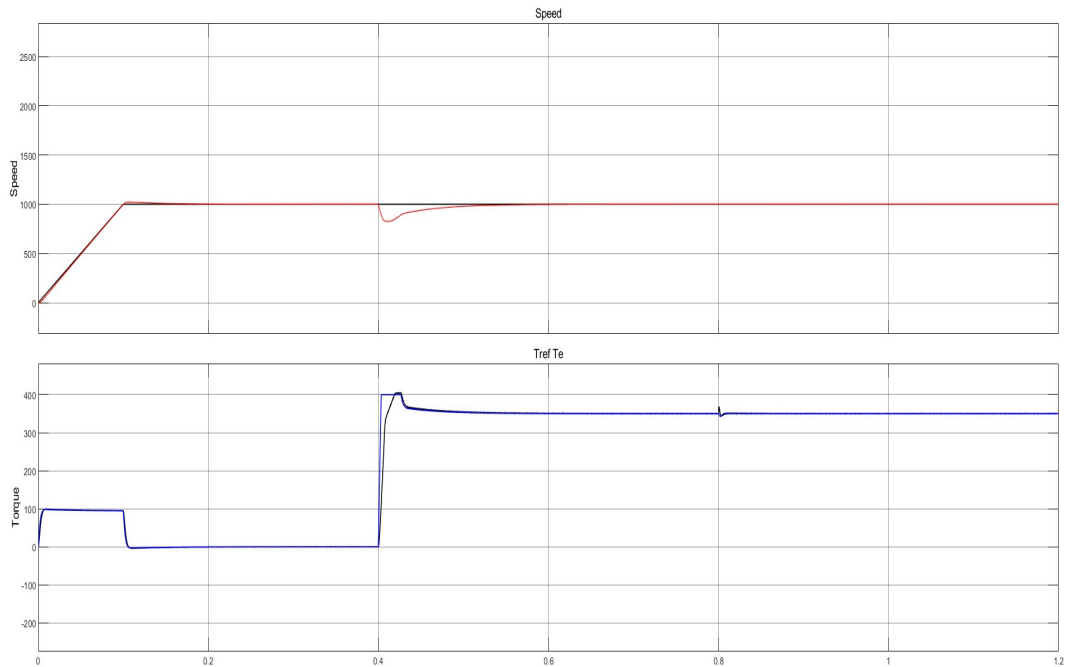


Figure 6.48: The speed and torque response

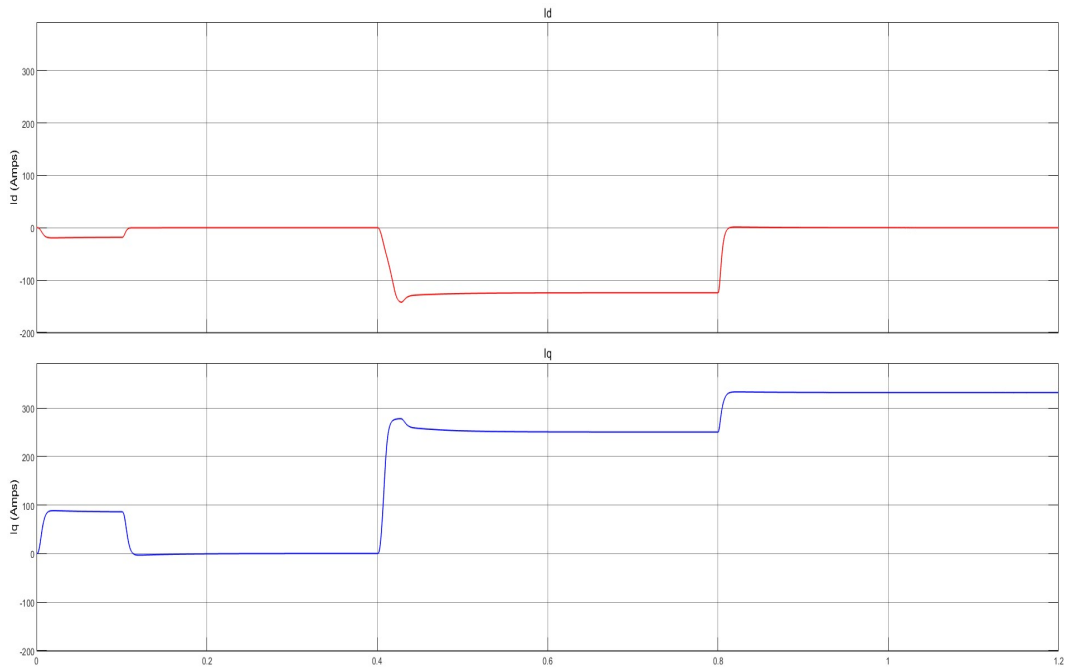


Figure 6.49: The I_{dq} currents

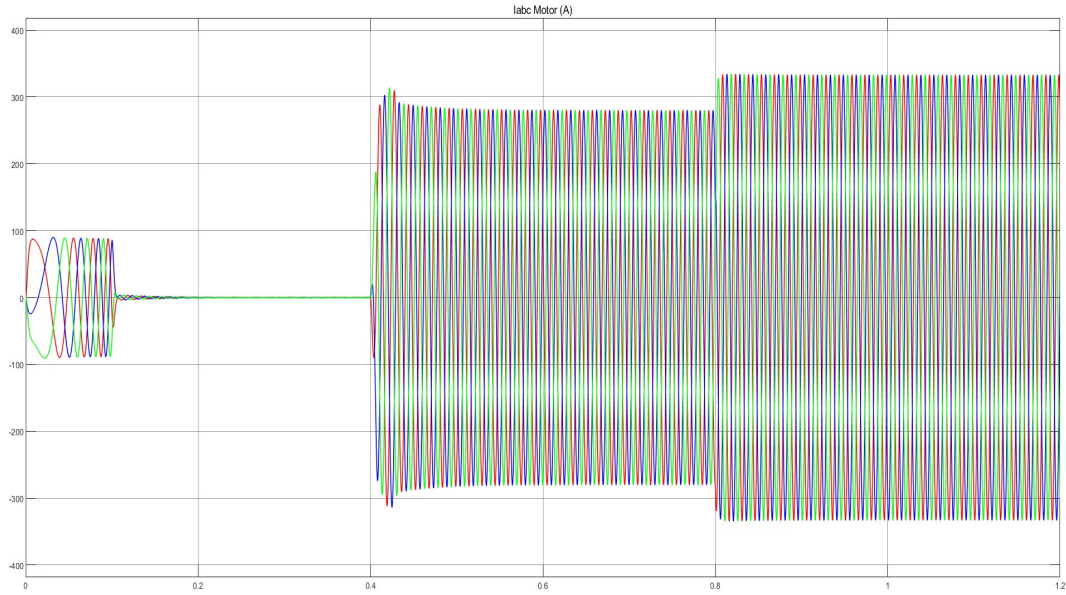


Figure 6.50: The I_{abc} currents

6.2.3.3 Flux Weakening

Flux weakening is particularly important for achieving wide-speed operation in IPMSM motors. This simulation illustrates the motor's performance across a broad speed range, from 0 rpm to 6000 rpm, demonstrating the effectiveness of flux weakening in maintaining performance at high speeds.

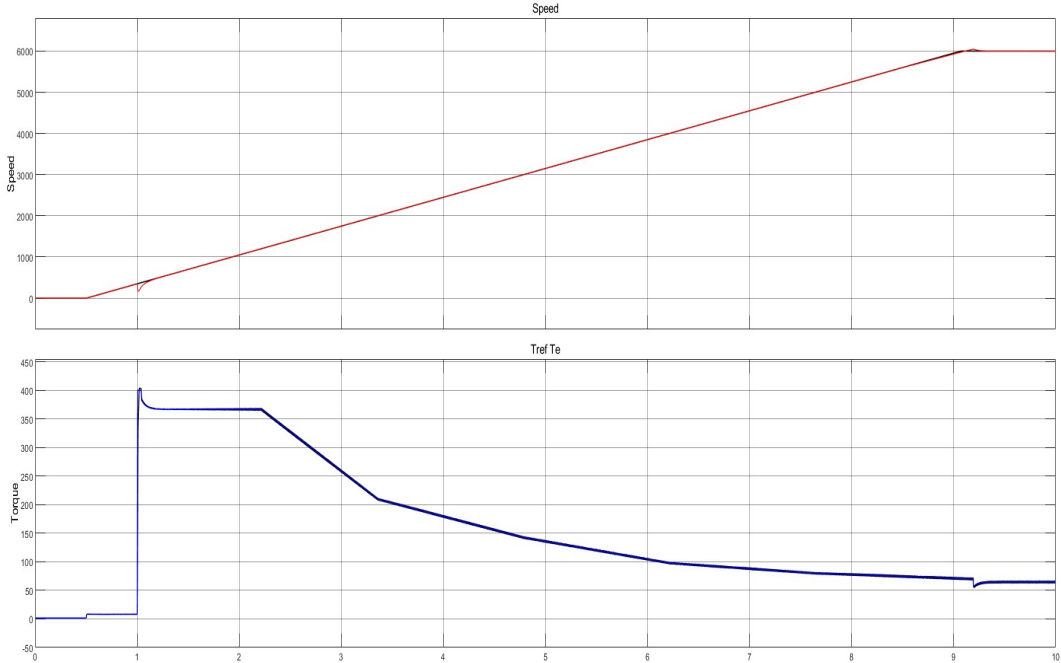


Figure 6.51: The speed and torque response

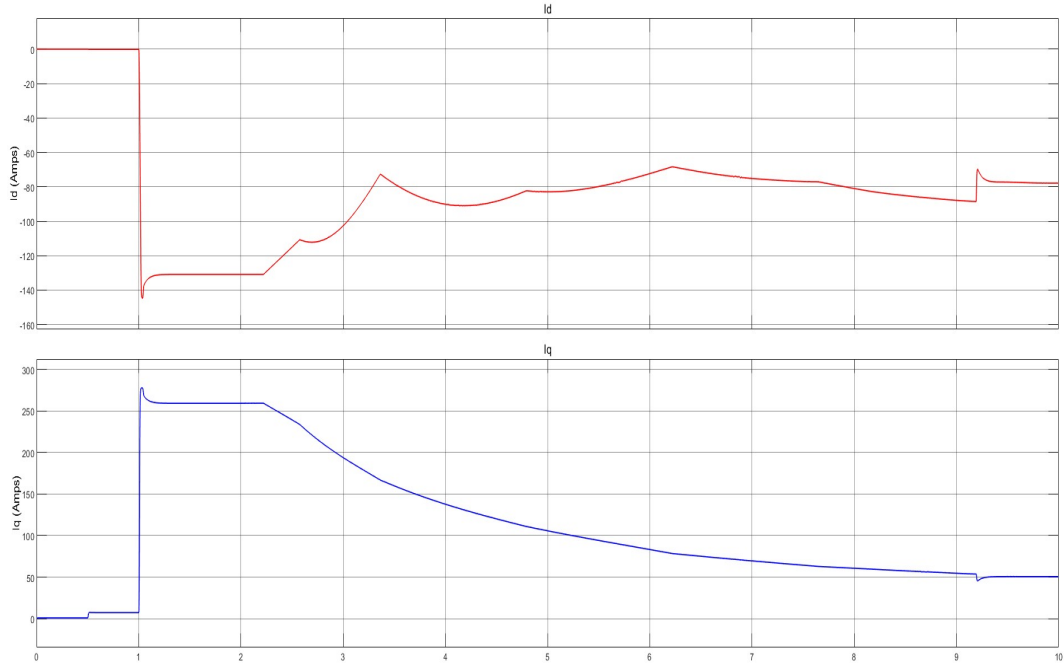


Figure 6.52: The I_{dq} currents

The simulations of MTPA and flux weakening demonstrated that both control strategies achieved the speed and torque references with high precision while maintaining their core functionality. The MTPA control method effectively maximized torque output for a given current level, ensuring efficient motor operation. Meanwhile, the flux weakening strategy successfully extended the motor's operational speed range up to 6000 rpm, mitigating the effects of increased back electromotive force at high speeds. Together, these simulations validate the robustness and reliability of MTPA and flux weakening in optimizing the performance of Interior Permanent Magnet Synchronous Motors (IPMSM) across a wide range of speeds and torque demands.

Chapter 7

Conclusion and Future Work

7.1 Conclusion

This thesis focused on field-oriented control (FOC) of Permanent Magnet Synchronous Motors (PMSMs). The modeled motor based on the derived mathematical equations was compared with the Simscape model of PMSM. Different methods were compared to control the PI and the effectiveness of various modulation techniques was evaluated.

Through simulations of the open-loop response of the modeled motor based on the derived mathematical equations, the Simscape model of PMSM produces the same results. Thus, verifying the equations on which the motor was based on.

Simulations showed that manually adjusting the PI controllers produced results very similar to those achieved using the symmetric and magnitude optimum methods. This indicates that while these methods can be helpful, manual tuning can be just as effective when performed correctly.

The comparison between Space Vector Pulse Width Modulation (SVPWM) and Sinusoidal Pulse Width Modulation (SPWM) revealed that SVPWM is superior. SVPWM handles harmonics better and makes better use of the DC voltage, leading to more efficient motor operation.

7.2 Future Work

1. **Hardware Implementation:** The FOC and PI tuning methods should be tested on real hardware to validate the simulation results. This would provide a more comprehensive understanding of their practical applicability and performance.
2. **Advanced Control Strategies:** Future research should explore more advanced control methods, such as Model Predictive Control (MPC) or Sliding Mode Control (SMC) or adaptive control, which have the potential to further enhance the performance of PMSMs.

3. **Optimization Algorithms:** Investigating automatic tuning methods for PI controllers is essential to reduce reliance on manual adjustments. This could improve the consistency and reliability of controller performance.
4. **Harmonic Reduction Techniques:** Advanced methods to further reduce harmonics in motor drives should be researched. This would contribute to the overall efficiency and longevity of PMSMs.
5. **Energy Efficiency:** It is important to study the impact of different control and modulation techniques on the energy efficiency of motor drive systems, especially under varying load conditions. This could lead to more sustainable and cost-effective motor operations.
6. **Advanced Modulation Techniques:** Implementing and testing more advanced modulation techniques, such as Discontinuous pulse width modulation (DPWM) or predictive modulation methods, could further improve the performance of PMSMs by enhancing torque control accuracy and reducing switching losses.

Bibliography

- [1] Q. Al azze. Field-oriented control of permanent magnet synchronous motors based on dsp controller, 2015.
- [2] F. Blaschke. The principle of field orientation as applied to the new transvector closed-loop control system for rotating-field machines. *Siemens Review*, 1982.
- [3] B. K. Bose. *Modern Power Electronics and AC Drives*. Prentice Hall, 2006.
- [4] M. Caruso, A. O. Di Tommaso, R. Miceli, C. Nevoloso, C. Spataro, and M. Trapanese. Maximum torque per ampere control algorithm for low saliency ratio interior permanent magnet synchronous motors. *IEEE*, December 2017.
- [5] K. T. Chau. *Electric Vehicle Machines and Drives: Design, Analysis, and Application*. Wiley, 2015.
- [6] J. Cheema, M. & Fletcher. *Advanced Direct Thrust Force Control of Linear Permanent Magnet Synchronous Motor*. Springer, 2020.
- [7] H. B. Ertan, M. Y. Üçtuğ, R. Colyer, and A. Consoli. *Modern Electrical Drives*. Springer, 2000.
- [8] Dorrell D. G. and James L. R. *Control of Electric Machine Drive Systems*. Wiley-IEEE Press., 2014.
- [9] Zhang G., Wang G., Zhao N., and Xu D. *Permanent Magnet Synchronous Motor Drives for Gearless Traction Elevators*. Springer, 2022.
- [10] Bhag S. Guru and Hüseyin R. Hiziroglu. *Electric Machinery and Transformers*. Oxford University Press, 2001.
- [11] M. Ibrahim and P. Pillay. Aligning the reluctance and magnet torque in permanent magnet synchronous motors for improved performance. *IEEE*, June 2018.
- [12] Y. Jiang, W. Xu, and Ch. Mu. Robust sliding mode speed control with adaptive torque observer for high performance pmsm. *IEEE*, 2016.
- [13] J. G. Kassakian, M. F. Schlecht, and G. C. Verghese. *Principles of Power Electronics*. Addison-Wesley. Addison-Wesley., 2011.
- [14] S. H. Kim. *Electric Motor Control*. ELSEVIER, 2017.

- [15] R. Krishnan. *Electric Motor Drives: Modeling, Analysis, and Control*. Prentice Hall, 2001.
- [16] R. Krishnan. *Permanent Magnet Synchronous and Brushless DC Motor Drives*. CRC Press, 2010.
- [17] J. Li, J. Yu, and Z. Chen. A review of control strategies for permanent magnet synchronous motor used in electric vehicles. *Applied Mechanics and Materials*, 321-324(6):1679–1685, June 2013.
- [18] S. E. Lyshevski. *Electromechanical Systems and Devices*. CRC Press, 2008.
- [19] Morari M. and Zafriou E. *Robust Process Control*. Prentice Hall., 1989.
- [20] H. Mehta, A. Apte, S. Pawar, and V. Joshi. Vector control of pmsm using ti's launchpadf28069 and matlab embedded coder with incremental build approach. *IEEE*, June 2018.
- [21] Blardone D.and Cherix N., Stampbach A., Fernandez G., and S. Strobl. Discontinuous pwm (dpwm) - imperix technical notes., February 2024.
- [22] Mohan N., Undeland T. M., and Robbins W. P. *Power Electronics: Converters, Applications, and Design*. Wiley., 2003.
- [23] Assoc Prof.Dr. W. H. Omran. Lecture notes in electric machines, 2023.
- [24] Assoc Prof.Dr. W. H. Omran. Lecture notes in power electronics, 2023.
- [25] Krause P., Wasynczuk O., Sudhoff S., and S. Pekarek. *Analysis of Elecric Machinery and Drive Systems*. IEEE, 2013.
- [26] K. G. Papadopoulos. *PID Controller Tuning Using the Magnitude Optimum Criterion*. Springer, 2015.
- [27] R. H. PARK. Two reaction theory of synchronous machines: A generalized method of analysis-part i. *IEEE*, 1929.
- [28] M. H. Rashid. *Power Electronics Handbook: Devices, Circuits, and Applications*. ACADEMIC PRESS, 2014.
- [29] M. H. Rashid. *Microelectronic Circuits: Analysis and Design*. Cengage Learning., 2017.
- [30] A. Tolba. Development of a simulation environment to investigate the control behaviour of a permanent magnet synchronous motor, 2014.
- [31] J. Tripathi, K. Sharma, and J.N. Rai. Speed control analysis of brushless dc motor using pi, pid and fuzzy-pi controllers. *FOREX*, August 2022.
- [32] J.W. Umland and M. Safiuddin. Magnitude and symmetric optimum criterion for the design of linear control systems: What is it and how does it compare with the others? *IEEE*, MAY 1990.

- [33] P. Vas. *Sensorless Vector and Direct Torque Control*. Oxford University Press., 2000.

Appendices

Appendix A

SIMULINK Models

Open Loop Model

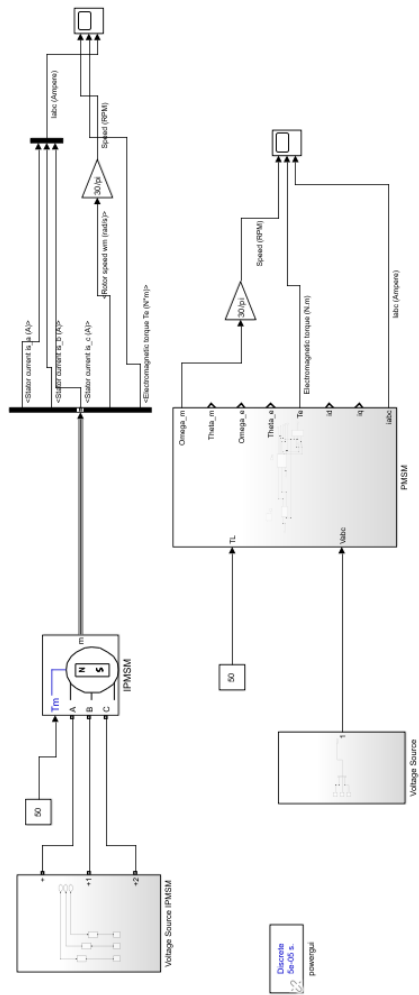


Figure A.1: Open-loop response of Modeled machine based on equations with load torque

PMSM Dynamic Model

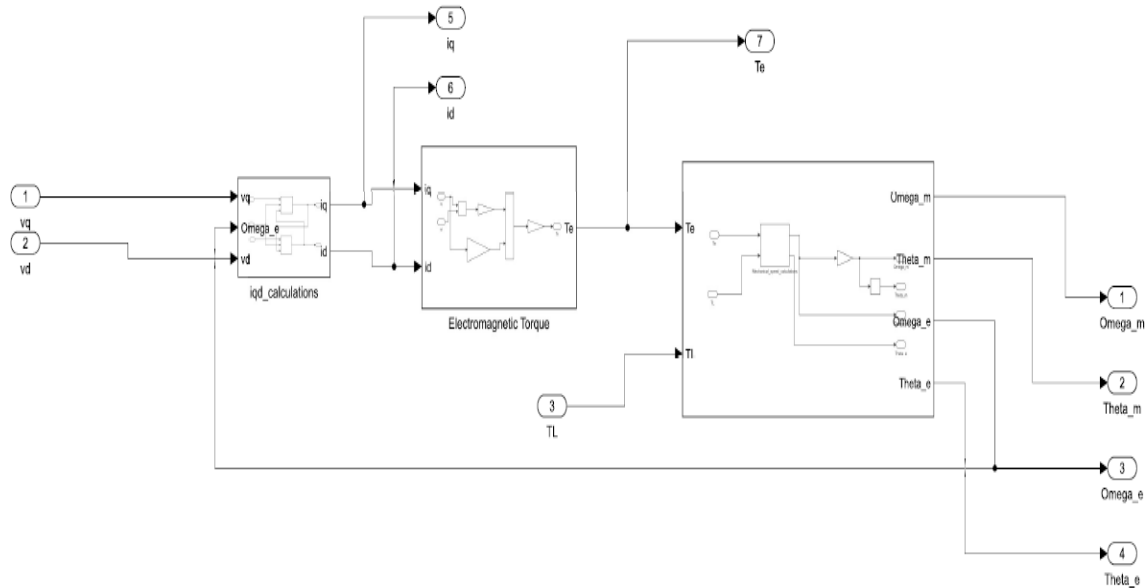


Figure A.2: PMSM Dynamic Model in SIMULINK

PMSM Mechanical System

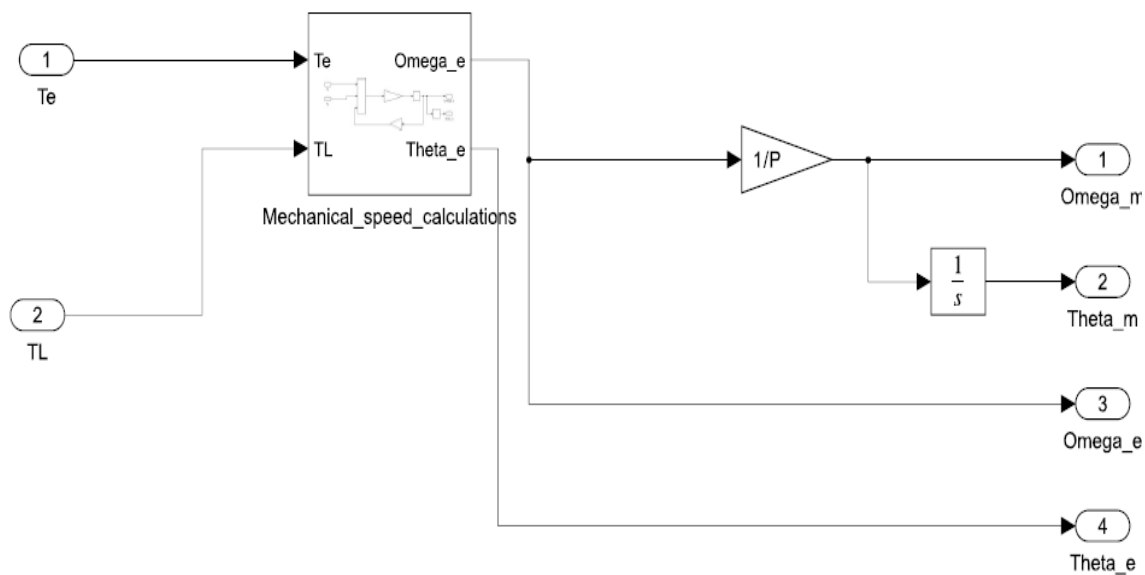


Figure A.3: PMSM Mechanical System

Mechanical Equation

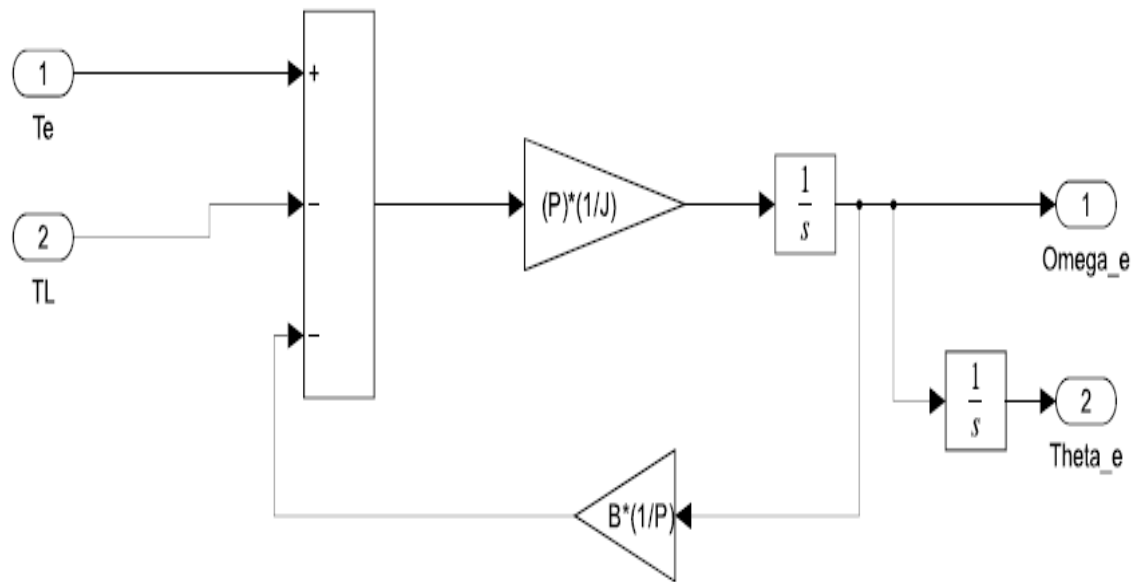


Figure A.4: PMSM Mechanical Equation

Electrical Equations

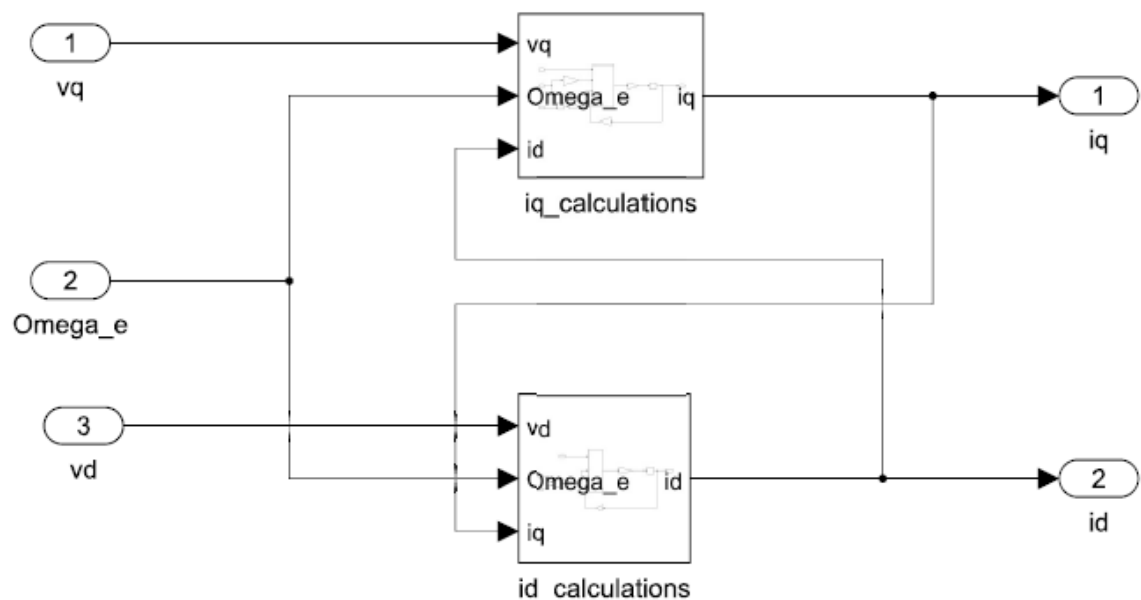
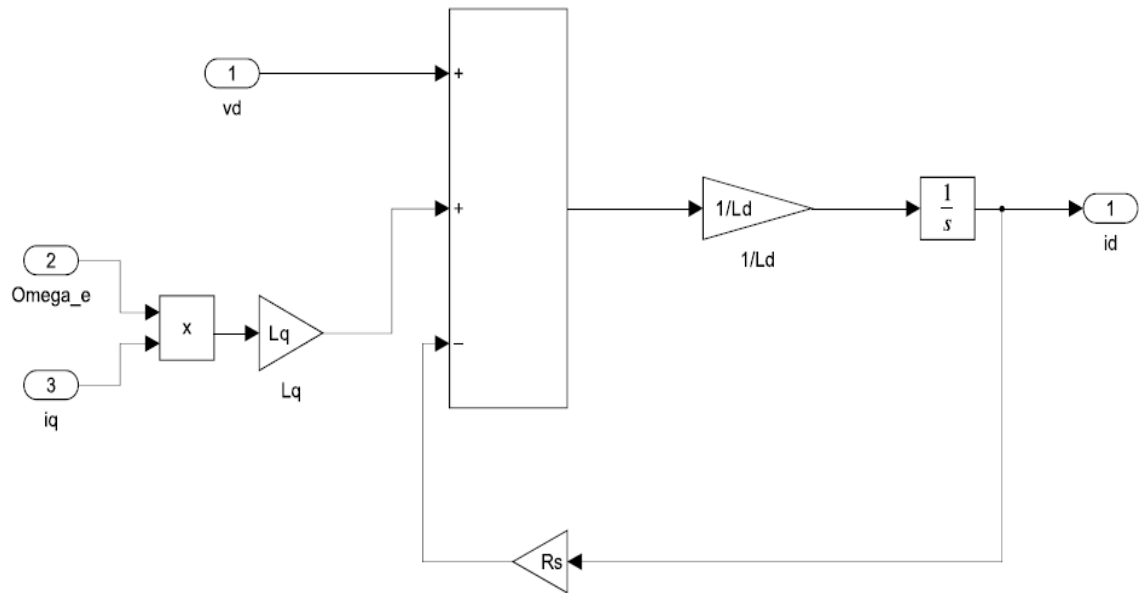
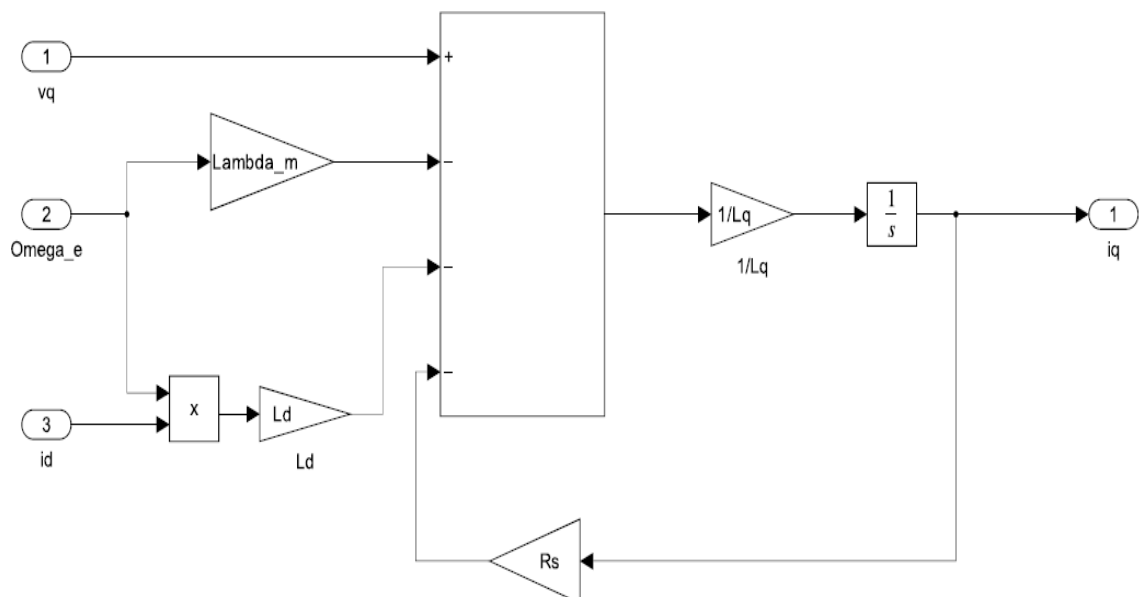


Figure A.5: PMSM Electrical Equations

I_d Equation**Figure A.6:** I_d Equation **I_q Equation****Figure A.7:** I_q Equation

Torque Equation

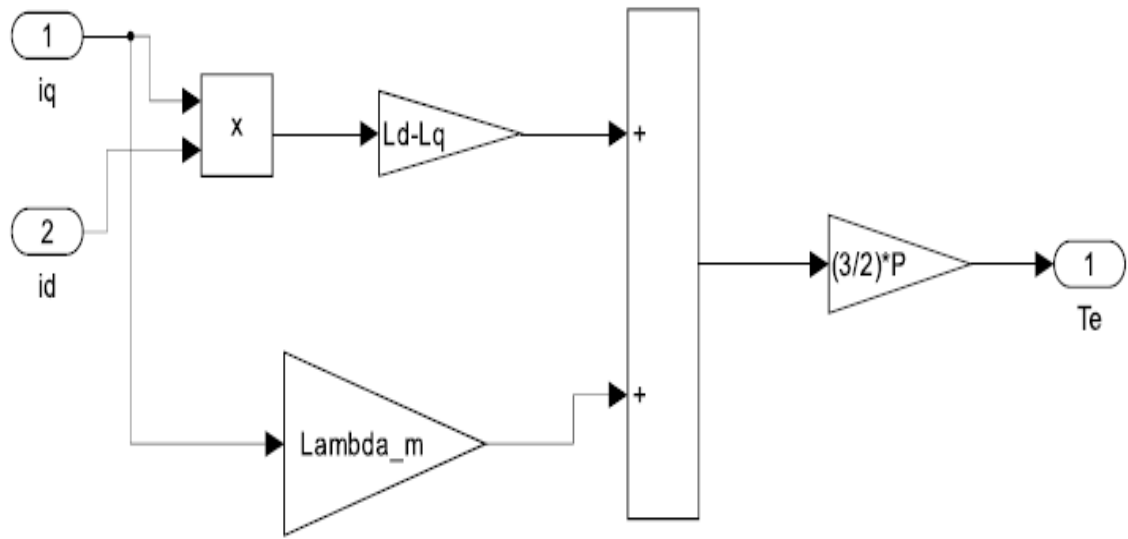


Figure A.8: *Torque Equation*

Cross-axes Dynamic Decoupling Control

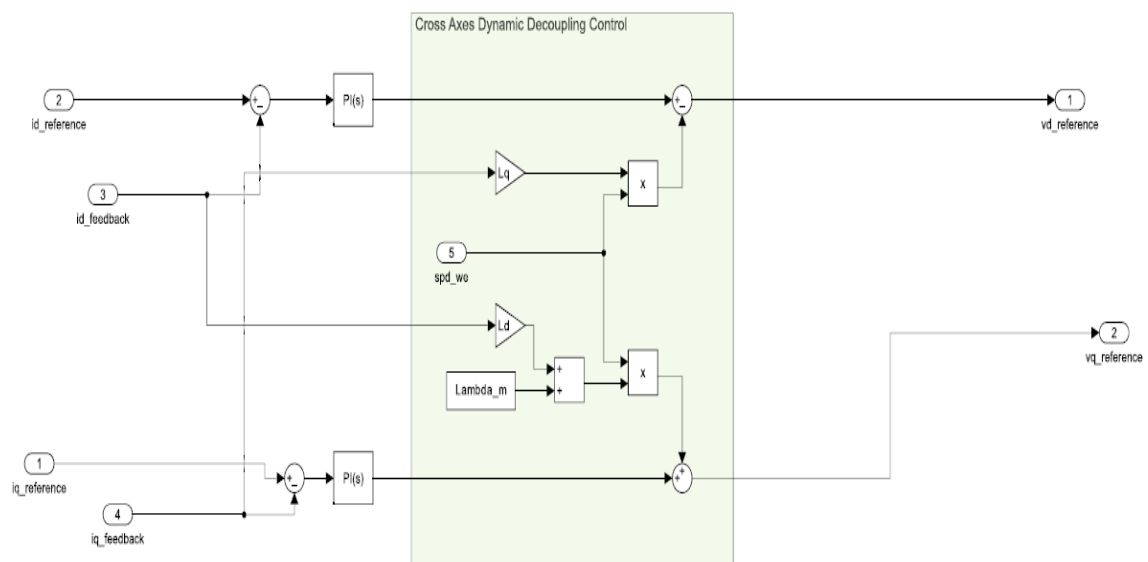


Figure A.9: *Cross-axes Dynamic Decoupling Control*

FOC comparison "Ideal Converter"

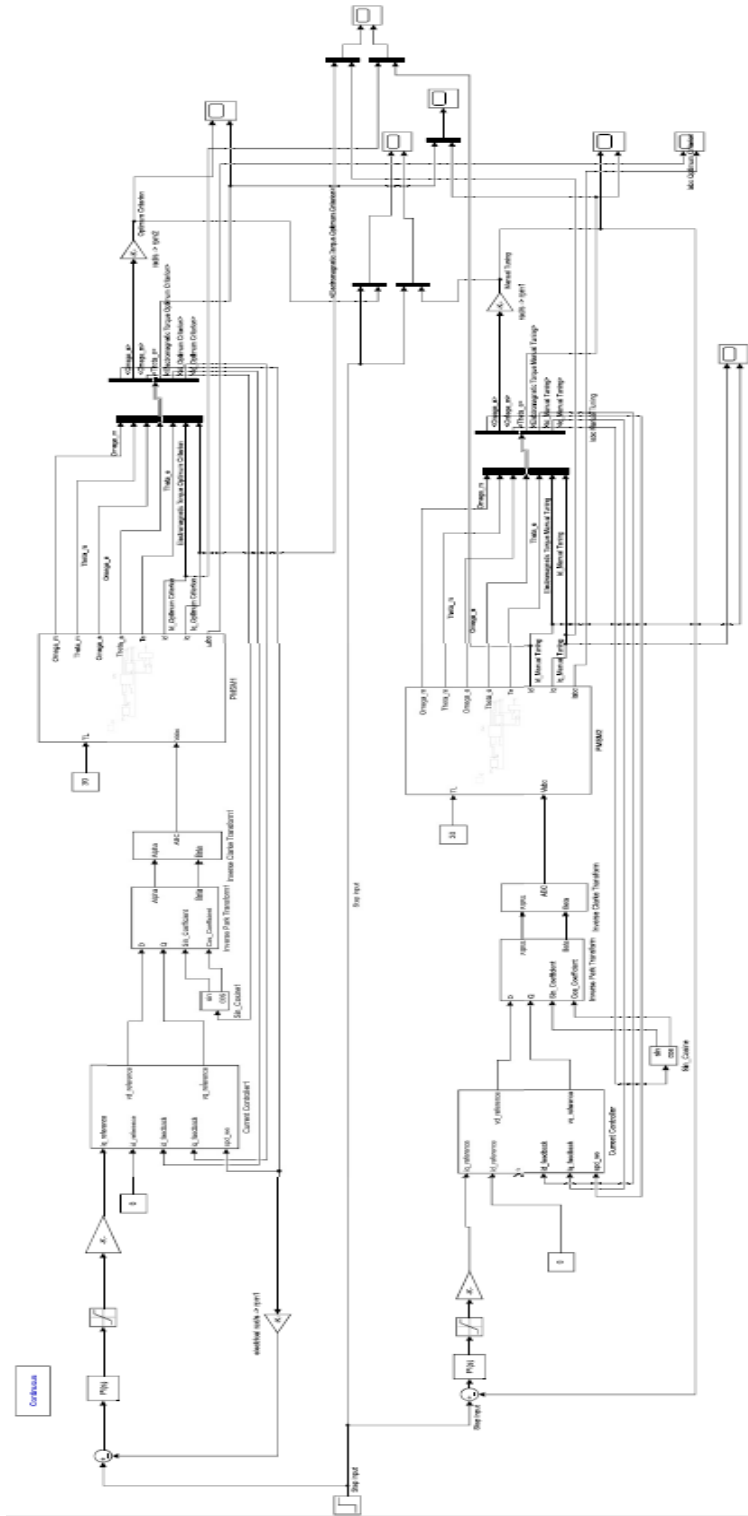


Figure A.10: FOC comparison of the manual tuning and Optimum Criteria methods

FOC "SPWM"

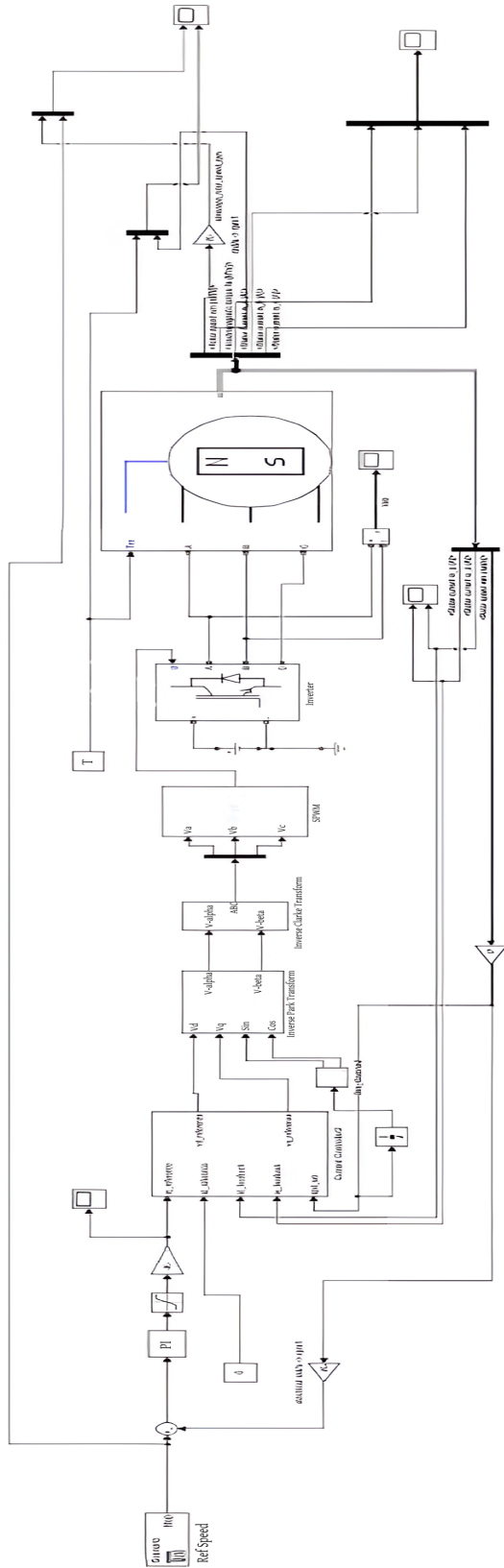


Figure A.11: FOC with SPWM modulation technique and Inverter

FOC "SVPWM"

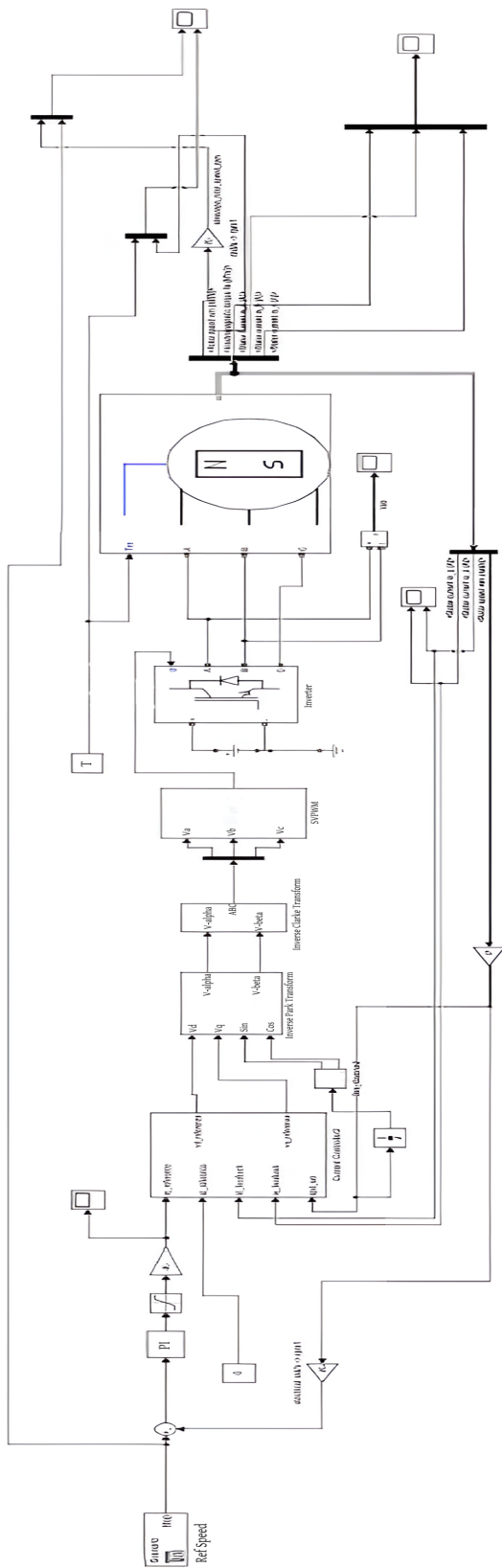


Figure A.12: FOC with SVPWM modulation technique and Inverter

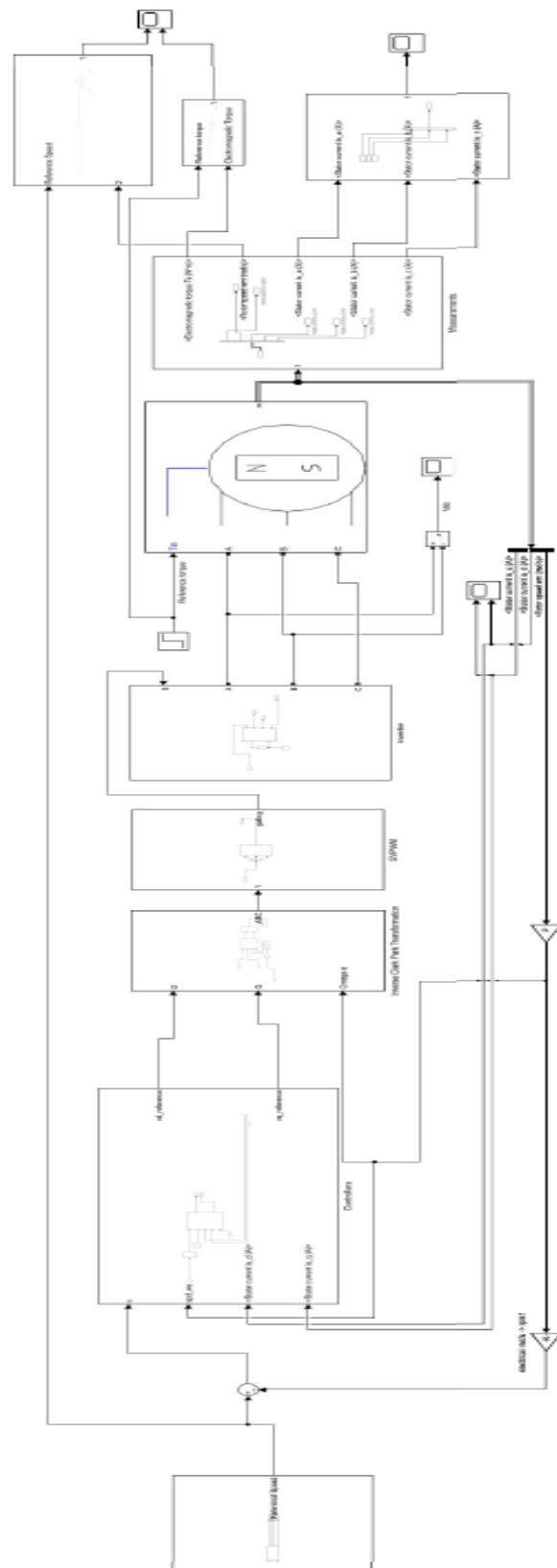


Figure A.13: FOC with SVPWM

Appendix B

MATLAB Codes

Current Controller Magnitude Optimum criterion

```
R = 0.05; %stator resistance
L = 0.000635; %stator inductance
t_s = L/R; %stator time constant
V_s = 1/R;
t_o = 0.00004; %total delay time
Kp = 7.9375;
T_n = t_s;
G_c = Kp*tf([T_n 1],[T_n 0]); %transfer function of the
control
G_s = V_s*tf(tf(1,[t_s 1])*tf(1,[t_o 1]),1); %transfer
function of the plant
L_s = G_c*G_s; %transfer function of the system
gamma = (t_o/t_s)*V_s*Kp;
L_s = gamma*(tf(1,[t_o 0])*tf(1,[t_o 1]));
T_Ls = feedback(L_s,1);
W_o = (sqrt(gamma)/t_o);
d = 1/(2*sqrt(gamma));
figure
step(G_c)
grid on
figure
step(T_Ls)
figure
bode(T_Ls)
```

Speed Controller Symmetrical Optimum criterion

```
J = 0.011; % rotor inertia
B = 0.001889;
R = 0.05; %stator resistance
L = 0.000635; %stator inductance
K = (3/2)*0.191*4;
P = 4;
Lambda_m = 0.191;
t_s = L/R; %stator time constant
Te = 0.02544; %Total time delay
Tn = 4*Te;
Kp = J/(2*Te);
G = tf(1,[Te 1])*tf(1,[J B])*K
C = tf([Kp*Tn Kp],[Tn 0])
T = feedback(C*G,1)
figure
step(T);grid on;
```